ELECTROSPUN FIBERS FROM BOTH SOLUTION AND MELT: PROCESSING, STRUCTURE AND PROPERTY

A Dissertation

Presented to the Faculty of the Graduate School

of Cornell University

In Partial Fulfillment of the Requirements for the Degree of

Doctor of Philosophy

by

Huajun Zhou

January 2007

ELECTROSPUN FIBERS FROM BOTH SOLUTION AND MELT: PROCESSING, STRUCTURE AND PROPERTY

Huajun Zhou, Ph. D.

Cornell University 2007

Electrospinning, in which a droplet of polymer liquid is elongated by the action of a strong electrical field, is an effective method to produce submicron scale fibers. The resulting nanofibers are collected as non-woven mats with large surface area to volume ratios which can be used in filtration, catalysis, tissue engineering and reinforced composites. Studies on electrospinning, however, have been limited to relatively simple polymeric systems and researchers have just begun to scratch at the surface of the structure and morphology of various sub-micron scale fibers.

To achieve a fundamental understanding of material-processing-structure relation during nanofiber formation, the following three systems have been investigated experimentally. First, the formation of nanofibers from polylactic acid (PLA) and its nanocomposite solutions has been studied to investigate the effects of inclusion of silica nanoclays. It is observed that the inclusion of nanoclays gives rise to strong cold crystallization, formation of beta crystals and structural orientation in PLA fibers. Electrospun PLA nanocomposite fibers also exhibit improved mechanical properties due to the preservation of intercalated structures and further alignment of nanoclays throughout the entire fiber. We further studied the effect of inclusion of polyethylene oxide (PEO) on PLA fibers. The mechanical properties of PLA are greatly affected by the addition of PEO. Electrospun PLA/PEO blend fibers with less than 10wt% of PEO exhibit increased elongational modulus, yield strength and breaking strain.

Secondly, we have created a unique route to nanofibers directly from the melt which eliminates the organic solvents present in solution electrospinning. This new solvent-free approach not only allows us to investigate a rich array of experimental studies to develop novel nanofibers directly from polymer melts and composites but also opens the door to theoretical routes to model nanofiber formation without the complications associated with solvent evaporation. Sub-micron PLA fibers have successfully been electrospun from its melt by investigating the effects of a series of processing parameters on fiber diameter. The degradation during melt electrospinning has also been studied.

The third system is an extension from melt electrospinning, which is heated solution electrospinning of polyolefin. We explored the possibilities of electrospinning sub-micron polyolefin fibers directly from their solutions and investigated the effects of processing parameters on fiber morphologies and properties.

BIOGRAPHICAL SKETCH

Huajun Zhou was born in a small town named Huabu which is located in a eastern province, Zhejiang of People's Republic of China. He finished the elementary education and junior high school education in the town and then moved to Quzhou city for the senior high school education where he was exposed to a more open environment. He has been interested in studying materials since then. It is deeply believed by him that materials play fundamental role in the development of technologies and human society.

Then it was 1996 when he entered the famous research-oriented University of Science and Technology of China (USTC) to continue his dream in the material world. He survived from the competitive environment and was constantly a top five student among sixty-three in the class. He completed the study with a thesis titled with 'Synthesis and photocatalytic properties of TiO_2 nanoparticles'. After five years' study in material physics and a B.S. degree, he felt it was time to dig deeper into the subject by entering world-famous Cornell University. There is an interesting anecdote in his application to department of material science & engineering at Cornell University. He did not apply to Cornell until late March which was beyond the application deadline. He wrote an email asking if he could still apply. He was lucky enough to get a positive response from a secretary of MS&E and an overnight fedex including application materials. His life was then turned to Cornell after the late unprepared inquiry.

At Cornell, he was both brave and lucky enough to be supervised by a young professor in school of chemical and biomolecular engineering. His research topic moved from synthesis of inorganic nanoparticles to fabrication of nanofibers from electrospinning. He invented and patented a melt electrospinning apparatus with his advisor. And then he patented another finding in nanocomposite fibers. Both of them are supported and licensed by a filtration company. When studying at Cornell, he was

closely affiliated with Cornell Center of Material Research (CCMR) where he participated in various CCMR outreach programs such as Research Experience for Undergraduate (REU) and Research Experience for Teachers (RET). He also participated in the image contest of CCMR and got an honorable mention award.

Besides the intensive researches, he enjoyed greatly the life in Ithaca. He frequently went wine-tasting in fingerlake wineries and acquired considerable knowledge on wines. He also benefited from the active participation of soccer games organized by CSSA dragon club and badminton exercises in Helen Newman Hall.

Through the long-run in the academia, he has extended both his research interests and personal interests. At this point, he will be finishing up his Ph.D. study and pursue an application-oriented industrial job.

I dedicate my dissertation work to my beloved parents: Mr. Meixian Zhou and Ms. Rongxiang Qiu. Although they lack of strong educational background, they are so supportive to my studies. In many moments when I need to make a critical decision, my parents always stand by my side and offer their experiential suggestion. Their open minds are a big source of inspiration to me. Without their support and understand, this work is hard to come to a completion.

This work is also dedicated to my younger brother: Guojun Zhou and many of my friends. Their encouragement and joyful accompany during my study pulls me through the dark night and come to the completion of this work.

ACKNOWLEDGMENTS

I would like to gratefully and sincerely thank Dr. Yong Lak Joo for his guidance, understanding, patience, and most importantly, his friendship during my graduate studies at Cornell. As one of his first two Ph.D. students, I received the most patient and insightful instructions on my researches. He was willing to share his life experiences as an international student studying in the US. His optimistic view on problems and shining ideas always inspired and propelled me towards more progress. He encouraged me to not only grow as an experimentalist but also as an instructor and an independent thinker. It was his encouragement and inspiration that led me into the wonderful polymer world. With his help and the assistance of CCMR at Cornell, I was able to have the opportunity to work with several bright undergraduate students and develop my mentoring skills. I would like to thank my undergraduate assistants: Tania Berges from Univ. Puerto Rico, Kathleen Baron from MIT, Debra Audus at Cornell, Geoffrey C.H. Tang at Cornell, Derrick Tang at Cornell for their diligent and productive work. Debra has been working with me on the heated solution electrospinning of polyolefin for over one year and I benefited from her organizational skills. Derrick Tang and Geoffrey Tang worked with me on the electrospinning of PLA-PEO blend system and had been really thoughtful on the topic. I would also like to thank Choo-won Kim and Timur Ivanikov for giving me humor and entertainment in what could have otherwise been a somewhat stressful laboratory environment. I would also like to thank Colman Carroll and Edward Zhmayev for providing me their unique understanding on the theory of electrospinning. All other Joo research group members are also appreciated for their help in either experiments or technical solutions.

Due to the inherent interdisciplinary attributes of our research, we have many inner and outer collaborators. I would like to thank Dr. Emmanuel Giannelis and Dr. Kyoung-woo Kim for their support in my study of polymer nanocomposite. And I would also like to thank a number of CCMR facility managers: Dr. Maura Wheathers for XRD characterizations, Anthony Condo for characterization of thermal properties, John Hunt for SEM assistance, John Grazul for TEM assistance, John Sinnott for compression molding support and Jonathan Shu for AFM assistance. I would also like to thank the National Science Foundation for funding this work through a CAREER Award, Grant no. CTS-0448270 to Dr. Joo. This work was supported in part by Clarcor Corporation. We would also like to thank E.I. du Pont de Nemours and Company for funding through a DuPont Young Professor Grant to Dr. Joo. Their generous funding is critical to the completion of this work.

TABLE OF CONTENTS

LIST OF FIGURES

LIST OF TABLES

CHAPTER 1
INTRODUCTION

Nanoscale fibers are defined as fibers with diameter between 50 nm to 500 nm. It is their small size, their large surface area to volume ratio as a consequence, that intrigued many of us. Potential applications can be found in the fields of catalytic development, water/air filtration, biomedical engineering and sensoring technology et al. Since the first patent on applying electrostatic force on making fibers in 1930s, electrospinning process has been proved to be an effective way to produce nanofibers or sub-micron fibers for over fifty materials including organic, inorganic and hydrid materials [1].

In typical electrospinning, a charged solution or melt droplet is stretched and accelerated by a strong electrical field instead of mechanical force in conventional spinning. The charged jet undergoes a straight jet stage and/or a whipping motion before being collected as non-woven fiber mats. At the same time, jet solidifies quickly due to the fast evaporation of solvent or temperature gradient in the spinning region. Although the electrospinning is straightforward in regards to the process itself, the underlying mechanism involved in the electrospinning process are still pending for solutions.

1.1 History of Electrospinning

The term “Electrospinning” derives from electrostatic spinning and first used around 1994. Electrospinning roots from the earliest electrospray used for painting in early nineteenth century. The milestone for this technique should be marked by a series of patents filed by Formhals during 1934 and 1944 [2-6]. He designed an electrospinning setup to produce polymer fibers which were much larger than so

called nanofibers. His contributions other than this setup also included producing fibers of polymer blend system and aligning fibers in a parallel way.

Since then, electrospinning has seemed to be dormant until 1966 when a new apparatus was designed by Simons [7]. In his patent, he demonstrated that production of ultra thin and light non-woven fabrics were feasible through electrospinning and found that less viscous solutions could produce shorter and finer fibers while more viscous solutions produce thicker and relatively continuous fibers.

During the same period, Taylor [8-10] studied the shape of initial charged droplet in an electrospinning. In his studies, he found that the solution droplet starts to become cone-shaped when the needle potential increases. The critical angle for the stable cone is at $\varphi=49.3^{o}$. Beyond this angle, a jet will break through which is due to the maximum instability of the fluid surface induced by the electrical field. The deformed droplet at the tip of the needle was later called "Taylor Cone".

Taylor's theory later was proved by the production of sub-micron fibers by Baumgarten in 1971 [11]. When the critical voltage was reached, the relative viscous solution (1.7-215 Poise in his experiments) did not breaks into droplet instead a fluid stream broke out. And he found that the diameter of the resulting fibers was determined by the solution viscosity by a power law of ~0.5.

In the 1980's Larrondo and Manley devised the first melt electrospinning setup [12-14]. They studied the jet formation from polyethylene/paraffin solution and more importantly molten polyethylene. His studies greatly extended the application of electrospinning. However, due to the lack of temperature control in spinning region, only 50 μm fibers were able to be produced. Nevertheless, he demonstrated that controlling the temperature of the spinneret and spinning voltage could affect the fiber diameters.

Reneker and coworkers re-explored this processes and hence contributed greatly to the development of this field [15-20]. Numerous experiments and a number of theoretical works have been carried out to better understand the process and search for more applications. This trend can be clearly sensed from the number of publications between 1995 and 2006 (Figure 1). The number of papers only limits to the recorded by "web of science" which may not be accurate but reflect the increasing interest yearly.

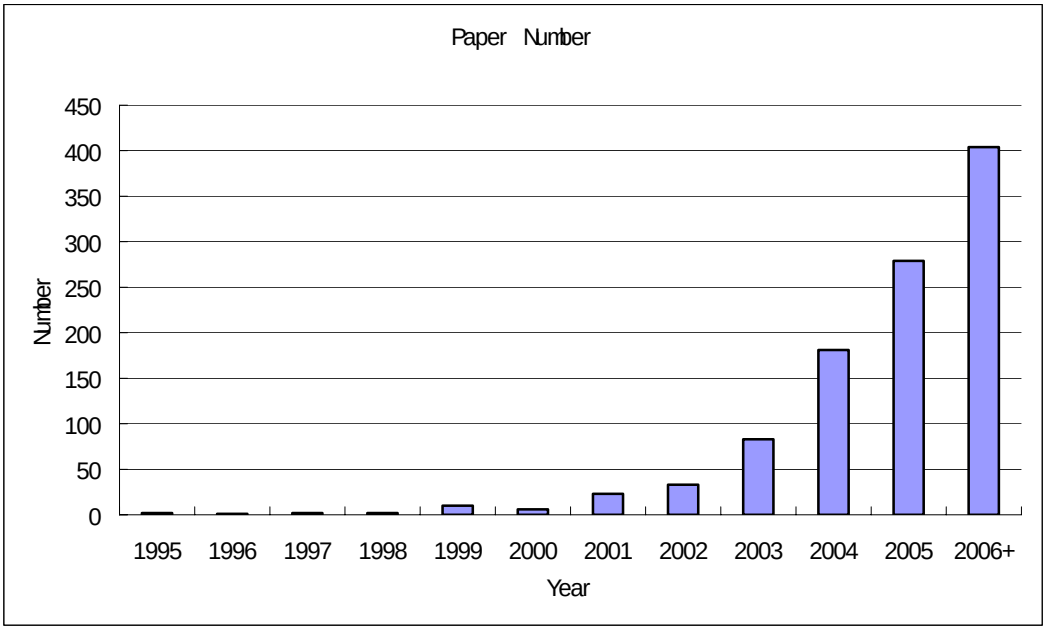

Figure 1 Number of publications on electrospinning and the year

Most of current studies deal with organic polymers or biopolymers. On the other hand, due to some special requirements in applications such as high temperature or strong mechanical strength, inorganic filaments have also been attracting huge focus. Some of them are quite interesting, for example, carbon nanotubes on carbon fibers

[20] and Vanadium Oxide whiskers on Titanium oxide fibers [21]. Polymeric fibers containing strengthening agents such as carbon nanotubes [22-24], silica nanoclays [25-27] and graphite [28] et al. are also hot topics in the field of electrospinning. Coaxial electrospinning is another branch of electrospinning which can produce fibers with multiple layers [29-31] or hollow fibers [32]. And current researches on electrospinning can be categorized into four categories: electrospinning of different materials; functionalization of as-spun fibers; various applications of electrospun fibers; structural studies of electrospun fibers; Simulation of the electrospinning process.

1.2 Electrospinning Process

Figure 2 shows a basic solution electrospinning setup. A syringe pump controls the flow rate through a nozzle. The electrical field is maintained by a high voltage supply which usually can provide voltages up to 30kV. A grounded or opposite-charged collector is used to collect the as-spun fibers. In the electrospinning, the traveling liquid jet stream is subject to a variety of forces with opposing effects [19]. Electrostatic repulsion of the charges in the jet tends to increase its surface area and stretch the jet. Therefore, the effect of electrostatic repulsion is similar to that of stretching by mechanical drawing in conventional fiber spinning. In the stretching stage, if the liquid is a solution, solvent evaporates causing the jet to be more viscous and instability region follows. If the liquid is a melt, due to thermal loss, jet becomes more viscous similarly. On the other hand, as in any liquid, the surface tension tends to reduce the total surface of the jet thus reduce the free energy of the liquid. If the viscosity is not enough to keep the jet as a continuous shape, what usually occurs is an instability that causes the jet to break up into droplets. This effect is known as Rayleigh instability. Which of these two opposing effects prevails depends on the

nature of the fluid, especially its viscosity and surface tension. If the viscosity is sufficiently high with good cohesiveness, the charged jet undergoes a straight jet stage and whipping instability takes place, the amplitude of which depends on the material and solvent involved and as a result dry thin fibers are collected.

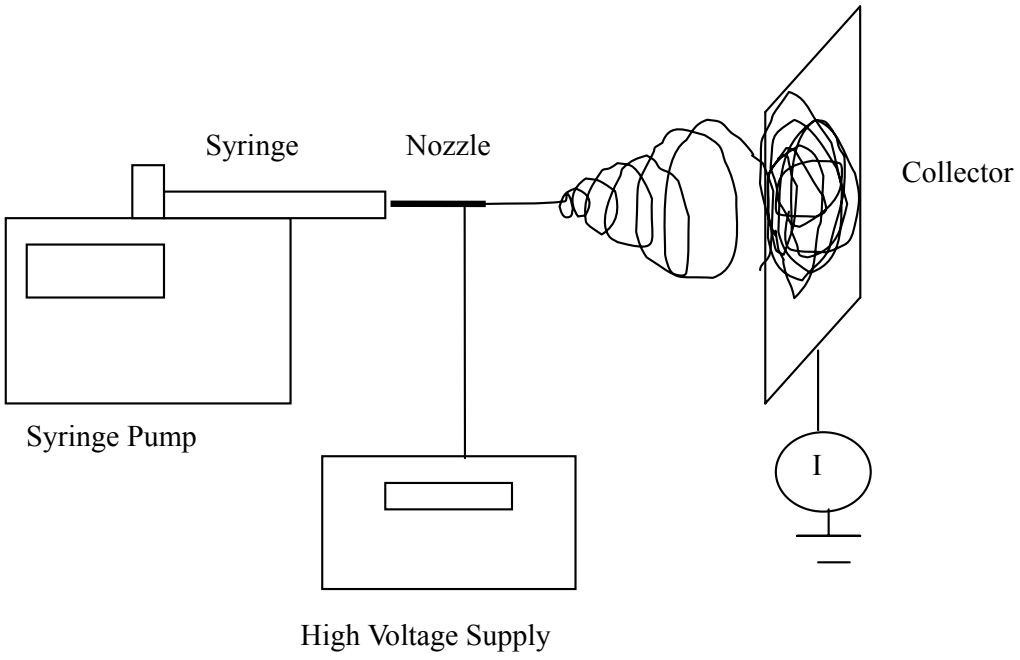

Figure 2 Typical electrospinning setup

Although the setup is relatively straightforward, the inherent mechanism and process control of electrospinning is quite complicated. Studies by Taylor on the initial jet formation shed light on the electrospinning process and laid the foundation of understanding the whole process. He derived the condition for the critical electric potential where surface tension is in equilibrium with the electrical force:

$$V_c^2 = 4\frac{H^2}{L^2}(\ln\frac{2L}{R} - \frac{3}{2})(0.117\pi\gamma R)$$

where Vc is the critical voltage, H is the distance between the capillary exit and the ground, L is length of the capillary with radius R, and γ is the surface tension of the liquid. Although Taylor cone has been observed in many studies, the exact shape and the angle of the cone are not fixed and only applicable to slight conductive, monomeric fluids.

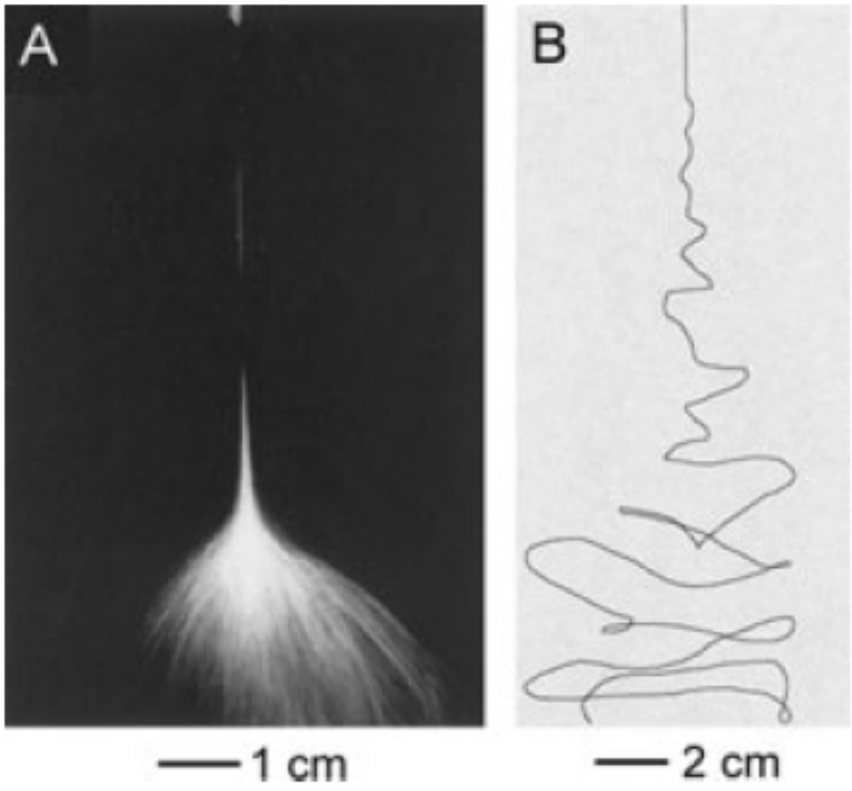

Figure 3 Jet image of a 2 wt% PEO (2,000,000) in water solution during electrospinning a) 1 ms exposure b) close-up of the onset of instability with 18 ns exposure

Colman et al. [33] studied the initial jet formation through computer simulation and compared with the experimental results. They found that the thinning of the jet in the initial stage is influenced by many factors. Viscoelasticity is found to be the key factor in the initial jet thinning behavior. Fluid with higher viscoelasticity thins quicker at the very beginning and toward the end of the initial stage, however it is thicker. Formation of ultra-thin fibers was considered as a result of splitting of the jet into multiple thin jets. Studies on the whipping motion revealed that in the envelope of the cone it only contains a single jet [34-37]. Figure 3 displays the pictures captured by high speed camera during electrospinning of PEO in water solution [34]. The jet undergoes a fast whipping motion and the whipping is so fast that conventional camera cannot distinguish the splitting (splaying) with whipping.

One of the recent developments in electrospinning worth mentioning is the process of co-axial electrospinning. In co-axial electrospinning, two spinnerets are adopted with concentric setup. Fibers with two components are obtained with one component as core and the other as shell layer. This processing method enables us to achieve fibers with more functionality or direct hollow fibers.

From above, we have known that electropsinning can produce nanofibers with different structures and functionalities. However the key part of electrospinning is how to control the process. Thus understanding the influence of variable parameters is very important. These parameters include fluid viscosity, elasticity, conductivity, solvent volatility, spinning voltage and distance as well as ambient parameters such as humidity, temperature.

Solution concentration is one of the most important parameters to control fiber diameter and fiber morphology such as beaded fibers. Viscosity of solutions is closely associated with the concentration. For a number of solutions, if the concentration is too small, there is no fiber formed except beads due to the inadequate viscosity and

concentration cannot be too high either since the jet solidifies too fast. During the spinnable range for the certain solution, usually lower concentrated solutions produce beaded fibers and as the concentration increases, the number of beads decreases [18]. The beaded structure is not only related to the concentration of the solutions, but it is also related to the surface tension of the solutions. Fong et al. [18] changed the surface tension by changing the content of ethanol in aqueous PEO solution system. Increasing the ethanol concentration gradually eliminates the existence of beads by increasing the viscoelasticity and decreasing the surface tension.

Solvent selection for polymers is another issue worth mentioning. Different solvents carry different properties in the aspect of conductivity, viscosity, volatility and surface tension. In some cases, solvent with two components are favored because of the balanced viscosity and volatility. Wannatong and co-workers [38] compared the polystyrene (PS) fibers obtained from four different solutions: 27 % (w/v) of PS in m-cresol, 23 % (w/v) of PS in toluene, (f) THF, and DMF. It was found that diameter of resulting fibers decreased with increasing solvent density and boiling point. Bead and string morphology was found in the solution where a larger difference in dielectric constant and solubility parameter between PS and solvent. These results are confirmed by Jarusuwannapoom and co-workers in their study of the effect of solvent on fiber morphologies. Additionally, they found higher conductivity of solvent favored the process of electrospinning. Similar effects were also reported by other authors [39].

Voltage and flow rate compared to the parameters mentioned above are less significant in controlling the fiber diameter [40]. In general, increasing voltage results in smaller fibers. If voltage is so high that corona discharge takes place, the resulting neutralizing ions can play an important role in forming bead-string morphology [18].

Additional controlling of the electrospinning process was recently achieved by modifying the electrical field and collectors.

Confining ring or ring set with positive polar connections was put between the nozzle and the collector. Electrostatic ring set was employed by Deitzel et al. [41] to act as a condenser for the electrospun jet and they found that by using these rings bending instability could be controlled or eliminated. Single ring was also reported by others to play a role in controlling the fiber deposition on the collector.

Fibers collected in electrospinning are usually presented as non-woven mats since the whipping motion itself is directionally non-preferable and homogenous in every direction considering no other perturbation is involved. But recently, researchers have designed several methods to guide the fibers into an organized way. Among all the approaches, Xia and Li [42] utilized a gapped collector to collect well-aligned fibers in the gap. Figure 4 shows the gapped collector and a SEM micrograph for aligned Nylon-6 fibers using this approach that we collected. In this approach, a charged jet lying in the gap is aligned across the gap due to the net transverse force.

Other collectors that have been designed so far include rotating drum [43], rotating disc [44, 45], parallel-placed rings [46] and even liquid collectors [47, 48]. High-speed rotating drum or discs can generate highly aligned fibers. The rotational speed was found to affect the crystallinity of PET fibers by Kim and co-workers [49]. Ring collector placed in a parallel way works in the same way as gap collector but can produce fibers as long as 10cm. By rotating one the rings, twisted yarns can be fabricated. Liquid collector is demanded mostly because of coagulation required for some polymer fibers. But Smit et al [47] found the liquid collector could be more useful than just coagulation. He demonstrated an easy method of collecting continuous yarn composed of electrospun fibers by first depositing them on a liquid medium then drawing the fibers from the liquid reservoir. A theoretical production rate of 180 m of yarn per hour for a single needle electrospinning setup was estimated and in this way lab-scale production of electrospun yarns was made possible.

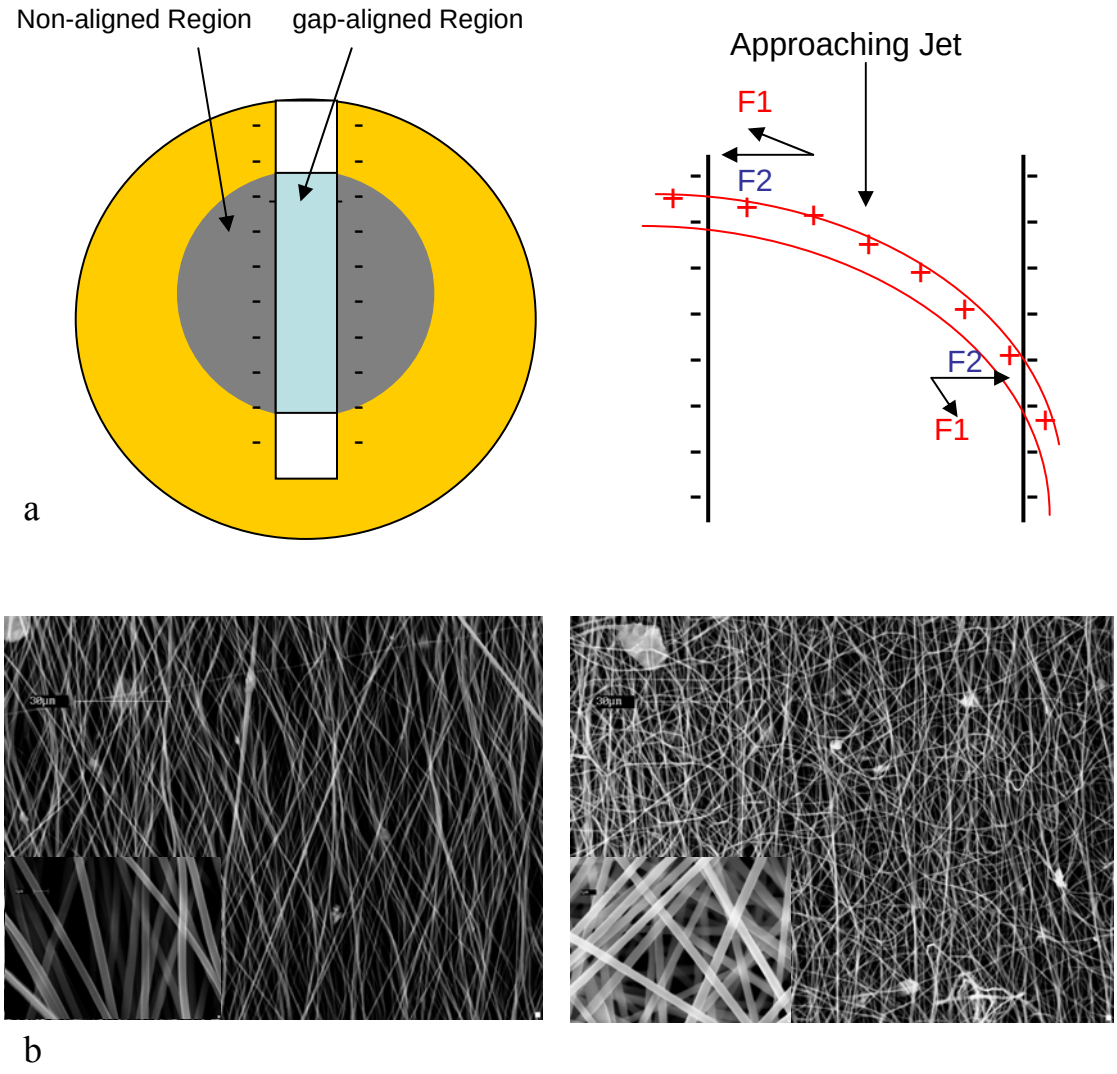

Figure 4 a) Gapped collector used in aligned fiber collection and a simple force analysis b) SEM micrograph of aligned Nylon-6 nanofibers

1.3 Electrospinning of Functional Materials and Hybrid Materials

Researchers have been striving to incorporate functional materials into the electrospun fibers in order to achieve certain functionality. One of the most focused types of materials is biodegradable polymer. Poly(caprolactone) [50], poly(L-lactic)

acid [51], poly(glycolide) [52] and block copolymers composed of these components have been successfully electrospun into fibers. Studies on biodegradability of fibers, cell growth on these fiber mats and efficiency of drug delivery have also been carried out by several groups. In addition to these synthetic organic polymers, natural biopolymers such as DNA [53], silk fibroin [54], human or bovine fibrinogens [55], dextran [56], collagens [57, 58], and even viruses [59] have also been successfully electrospun.

Electrospun fiber mat with nano-sized 1D filament can be a suitable template for post processing and functionalization. Functional group or its precursors can be directly blended into the solution to make nano-size fibers. After additional processing, precursors turn into functional components. Incorporating carbon nanotubes (CNT) into nanofibers have been an interesting topic in recent years since carbon nanotubes carry many advantages such as high mechanical strength and excellent thermal and electrical conductivity. By controlling the amount of nanotubes in the fibers, Sundaray and co-workers [60] could control the conductivity of PMMA single fibers and they found that increasing the content of CNT from 0.05wt% to 2wt%, the conductivity of PMMA with CNT increases by one order of magnitude from 4.5×10^{-3} to 5.3×10^{-2}. The conductivity of PAN fibers with CNT was also studied by several researchers [61] and the results of theirs studies agree with the above trend. Moreover, Ra and co-workers [62] also discovered that the conductivity of the PAN fibers is anisotropic. The conductivity along the fibers is three times of that across the fibers. Besides the enhancement of the electrical conductivity of fibers, CNT have been widely used to enhance the polymer strength [22, 58]. Frank Ko et al. [22] obtained PAN fibers with modulus of 140GPa with inclusion of 4wt% CNT.

Nano-composite materials can be adopted in the field of electrospinning. Organically modified silica nanoclays have strong interactions with polymer matrices

and provide additional mechanical strengthening than conventional nanoclays. Many studies have been carried out to investigate the effect of nanoclays on the structures and properties of the electrospun fibers. We compared the mechanical properties of nylon-6 nanofibers and nylon-6 nano-composite fibers (Figure 5) as well as their cast film. Mechanical test results showed that addition of 3 wt% of nanoclays increased the yield strength of cast film by 48% while the improvement is 125% for the fibers. The major mechanism was believed to the aligned nanoclays in the fibers played a synergic effect and strain hardening was also an important factor.

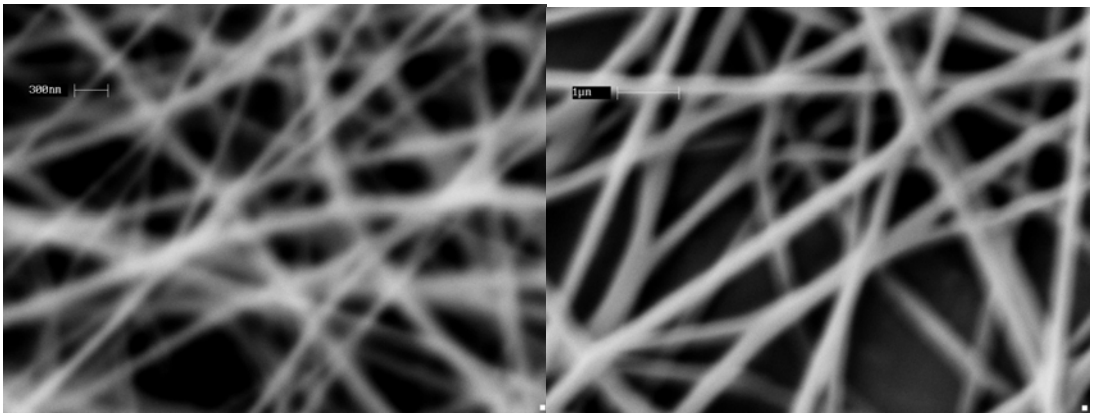

Figure 5 SEM images of Nylon-6 nanofibers and Nylon-6 nanofibers compounded with 3 wt% of nanoclays

Not only can inorganic material provide polymeric fibers with more functionality, but polymeric materials also can introduce new features or enhance the existing advantages of the electrospun polymer fibers. Polymer blending is well known to be a feasible and simple method to achieve a combination of advantages possessed by the components. Lee et al. [63] studied the effect of polyurethane (PU) on the mechanical properties of poly(vinyl chloride) (PVC) fibers and found that pure PVC fiber has low strength and flexibility and PVC fibers blended with PU displays significant

improvement in strength and elongational behavior. Kim et al. [64] demonstrated that the physical properties (mechanical properties, hydrophilicity) and biodegradability can be fine tuned by controlling the blending ratio of the components.

1.4 Post Processing and Functionalization

Post processing is another important method towards the functionality of fiber mat. Surface coating, calcinations, etching and hydrolysis et al. are widely implemented in achieving additional functionalities. Such post processing generally does not change the morphology of the fiber mat and nano-sized fibers are preserved. Calcination usually creates porous structures into fibers and produce high surface area materials. Etching is an effective way to produce hollow fibers from two component coaxial fibers and it is also an alternative to remove one component to create porous structures into fibers made of multi-component polymer blend. Hydrolysis as seen in literature is mostly used to introduce inorganic particles.

Surface coating is one of the most straightforward ways to introduce more functionality to the fibers. Drew and co-workers have shown that the surface of electrospun nanofibers can be modified by via liquid-phase deposition to titania nano-particles [65]. Gold [66] or silver films [67] have been deposited onto the electrospun fiber surface via chemical vapor deposition or sputtering coating. Calcination is a well established method for producing carbon fibers from PAN fiber precursor [68, 69]. Fibers composed of other inorganic materials such as silica [70], alumina-borate oxide [71] and titanium oxide [72-74] et al. have been successfully prepared by calcinations of their electrospun composite fiber precursors. For polymer blend fibers, selective removal of certain component can form highly structured morphologies such hollow fiber from co-axial electrospinning or porous fibers. Bognitzki et al. [75] removed

PVP domain using water as a removing solvent and found that nearly 100% PLA fibers with highly porous structures can be obtained.

1.5 Structures of Electrospun Fibers

Structures of electrospun fibers are affected by several factors: nature of electrospun materials, electrospinning conditions and post-processing. In electrospinning process, fluid jet is stretched by the electrical force and for a typical solution electrospinning. The reduction ratio of the jet cross-section before and after thinning can be well over 1000. Taking account of the solvent evaporation, the reduction ratio directly caused by the stretching is well over 100. As a result, well aligned structures can be created.

Although studies on micro-structural change caused by electrospinning have been carried out along with the development of this technique, studies on the process itself and spinning different materials prevailed over the structural studies. It was believed by many researchers that the strong deformation was able to strengthen the crystallization of the polymers as in conventional melt or solution spinning so that strong fibers could be produced. However in most of the studies, reduced crystallinity and weakened mechanical strength were reported possibly due to the fast solidification [26, 76] and prevalent defects [77, 78] in the fibers caused by the solvent evaporation et al. The fast solidification and 1D confinement are believed to the key factors to forming meta-stable structures in the electrospun fibers as described by many authors [79, 80].

XRD results (Figure 6) of our electrospun nylon-6 fibers from its HFIP solution showed that only meta-stable γ crystal structures were observed while after annealing it turned into stable α crystal structures. Subiah and Reneker [15] demonstrated the order in the electrospun aramid fibers by electron diffraction pattern. Gao and co-

workers [81] found that the crystallinity of electrospun PVDF fibers was decreasing from 42.3% to 39.2% with increasing average fiber diameter and highly oriented structures existed in the fibers according to the XRD study. Dersch et al. studied the internal structure of electrospun nylon-6 and PLA fibers [82]. Their electron diffraction results showed only inhomogeneous, weak elongation of nylon crystals resulted from electrospinning. As to PLA fibers, however, there is only a negligible amount of crystals formed during electrospinning, and thus no (even local) orientation of crystals was observed. DSC studies on electrospun PLA fibers demonstrated that aligned structures may form during the electrospinning which caused the enhancement of the cold crystallization peak at lower temperature [26, 83].

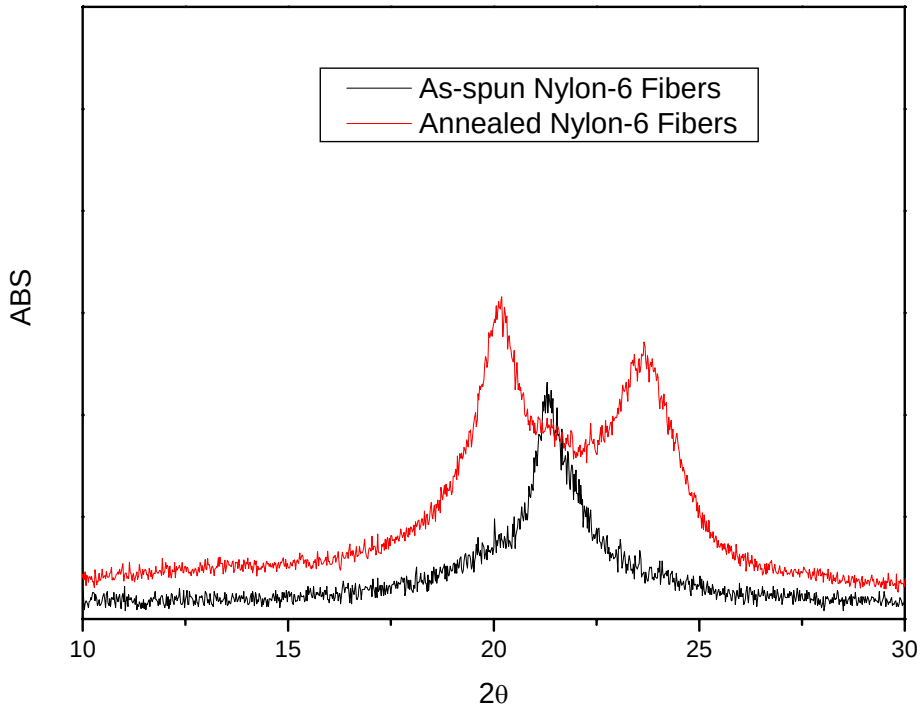

Figure 6 XRD patterns for electrospun nylon-6 fibers before and after annealing at 120°C

Recently studies of structural behaviors of electrospun self-assembly block copolymer fibers have been a new topic in the electrospinning field. Self-assembly block co-polymers, in the environment of the nano-size confinement, presents some unique morphologies such concentric rings, stacked discs et al [84]. The studies of the structural change in the electrospun fibers mostly benefit from the development of inorganic material electrospinning, coaxial electrospinning and synthesis of new di-block copolymers. Electrospun fibers provide a perfect template for such studies with tunable size, continuous length and functionality. However, the results by Ruotsalainen [85] showed that the self-assembled structures in electrospun PS-b-P4VP fibers were ill shaped and underdeveloped due to the fast solvent evaporation. Similar results were reported by Kalra et al. [86] on their study of electrospun PS-b-PI fibers. Annealing did make the structures more developed and locally patterned cylindrical and lamellar structures could be easily distinguished. However the annealing temperature was limited by the melting temperature of the block copolymer which was at 90^{o}C. Recently they employed co-axial electrospinning and prepared PS-b-PI fibers covered with silica shell which enabled them to increase the annealing temperature above 90^{o}C while maintaining the fiber morphology (Figure 7). Well developed stacked circular discs were observed at annealing temperature of 125^{o}C and this structure tended to transit into parallel layered structures as annealing time increased at the temperature of 175^{o}C.

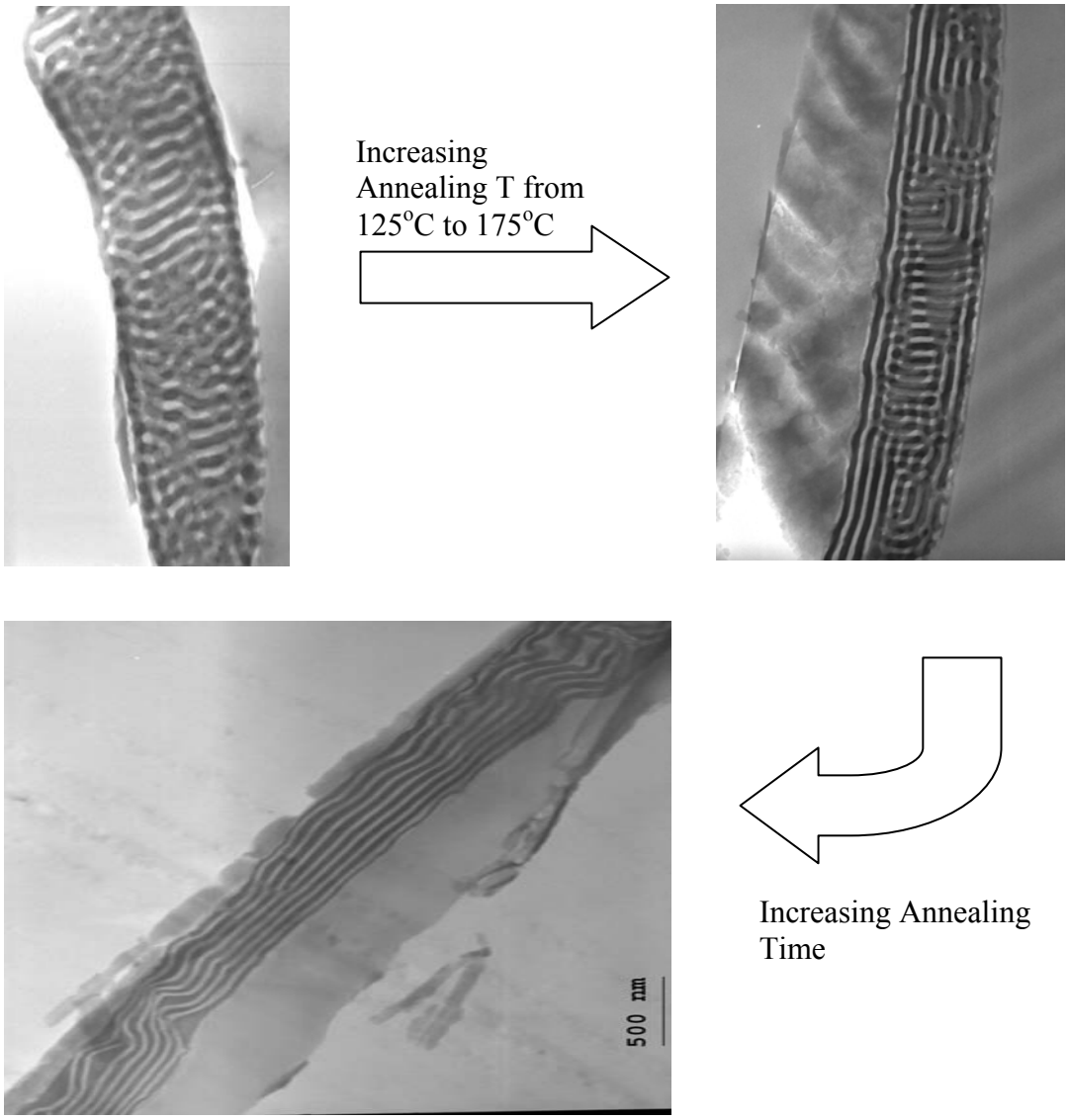

Figure 7 Self-assembled structures in confined space of silica shell

1.6 Applications

1.6.1 Nanofiber-Reinforced Composites

Although most of electrospun fibers are weaker compared to conventional spun fibers or even the cast films, electrospun poly(p-phenylene biphenyltetracarboximide) nanofibers produced by Huang et al. [87] exhibit a high mechanical strength of 630 MPa and high modulus of 15.3 GPa comparing to the strength of 600 MPa for its film.

And most of the electrospun fibers still possess relatively strong mechanical properties. Using these fibers as a reinforcement material is an optional application. Reneker and Kim [88] have demonstrated that a rubber film reinforced with electrospun poly(benzimidazole) nanofibers presents significantly improved mechanical strength. The Young's modulus for the composite film was measured to be one order of magnitude higher and tear strength was twice as large as the pristine rubber material. Fong Hao studied the electrospun-Nylon-6-nanofiber reinforced BIS-GMA/TEGDMA resin as dental material and found that addition of relative small amount of Nylon-6 nanofibers greatly improves the resin strength.

1.6.2 Filtration Application

Conventional filter media for air and water purification are not efficient in filtering small-sized particles such as in the range of 300-700 nm. Small fibers especially sub-micron sized fibers provide better filtration efficiency than larger fibers at the same pressure drop in the interception and inertial impaction regimes. For nanofibers, the effect of slip flow is non-negligible. According to the slip flow theory, when the fiber size goes below 500 nm, the Knudson number is over 0.1 calculated based on following equation assuming the free path of air molecules at 0.066 μm [89].

$$Kn = \frac{\lambda}{r_f}$$

Graham et al. presented their results on applying nylon nanofibers to filtration application and found that the filtration efficiency of cellulose filter media had improved from 68 % removal of sub-micron sized dust to 92 %. Shin and Chase [90] studied the nanofiber application on water-in-oil emulsion separation. They deposited

1 wt% of nanofibers with diameter of 150 nm on glass fibers and the measured results showed that separation efficiency was enhanced from 71% to 84%.

Zhou and co-worker [91] studied the application of sub-micron sized PLA from melt electrospinning on conventional air filtration and found that with only 0.1 g/sqft of coverage, the efficiency for filtering 300 nm dust particles increased from 20% to 46 % and pressure drop only rose slightly. In addition, upon the examination on SEM micrograph of the nanofibers (Figure 8) deposited filter media, good adhesion between PLA fibers and cellulose microfibers were observed.

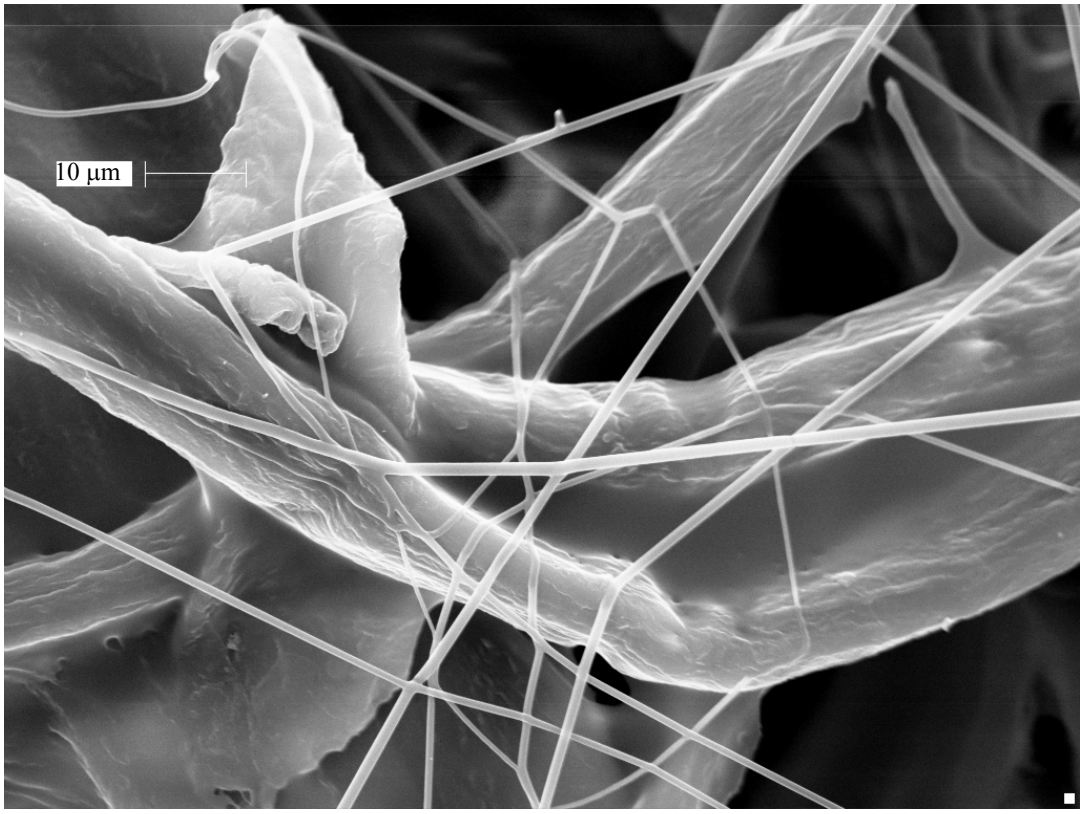

Figure 8 SEM images of melt electrospun PLA fibers collected on filter media

1.6.3 Scaffold for Tissue Engineering

Electrospinning of bio-degradable and bio-compatible polymeric fibers from both synthetic and natural materials has been widely researched. Electrospun fiber mat as scaffolds for tissue engineering is one of the most promising applications. It has high surface-area-to-volume ratio and can be customized to match native extra cellular matrix (ECM) with similar morphology, chemical composition and functional groups. Electrospun PLGA fiber mats have been shown to have porosity greater than 90% [92]. Anisotropic fiber textures can also be obtained from aligned electrospinning to mimic natural tissue texture.

Studies on how cells respond to the nano-structured polymeric scaffolds have been extensively carried out in recent years. Yoshimoto et al. [58] prepared tissue scaffold made of electrospun PCL fiber mat and Mesenchymal stem cells (MSCs) derived from the bone marrow of neonatal rats were seeded and cultured in the scaffolds matrix mineralization and collagen type I deposition throughout the construct were observed after 4 weeks. In *vivo* studies with the scaffolds showed a rigid bone-like construct formed after being implanted into the omenta of rat after 4 weeks. Cells and ECM were observed throughout the construct as well as mineralization and type I collagen.

Ji and co-workers [93] successfully electrospun a 3D HA-DTPH nanofibrous scaffolds and with fiber diameters ranging from 50 to 300 nm. NIH 3T3 fibroblasts were seeded on FN-adsorbed HA-DTPH scaffolds to study the cell morphology. The 3T3 fibroblasts were found to have penetrated the scaffold and grow 30 μm deep into the scaffold.

For the natural polymer scaffolds, polymers such as collagen, protein, silk, fibrinogen, and chitosan have been successfully electrospun into fibers. These

scaffolds carry the inherent bio-compatibility and bio-functionality while further possessing the great advantages of electrospun fibers.

1.6.4 Other Applications

Since electrospun fibers can be functionalized in many ways, either from the source materials or post processing and functionalization, these fiber mats can be suitable for many other applications such as scaffold for drug delivery, sensors, carriers for catalyst and conductive bridge in transistors.

Electrospun fiber carrying catalytic materials offer advantages of high coverage and good permeability. Jia et al. [94] prepared bioactive polystyrene (PS) nanofibers by chemical attachment of α-chymotrypsin on PS and observed a high catalytic activity with improved enzyme stability over other forms of immobilized enzymes. A novel sensor made of an electrospun membrane as a highly responsive fluorescence quenching-based optical sensor for detection of explosives was designed by Wang and co-workers [95, 96].

1.7 Comparison of Solution Electrospinning and Melt Electrospinning

Electrospinning from polymer melt is more challenging since it involves more complications considering the experimental setup and melt properties. Compared to electrospinning fibers from polymer solution, only few reports on it have been made till now [12-14, 97-101]. Some difficulties underlying melt electrospinning process are high temperature, high viscosity of polymer melts and poor conductivity.

In principle, solution electrospinning and melt electrospinning are similar. They both utilize strong electrical field to stretch the jet of fluid and after solidification fibers are collected onto collector. Some distinct differences are the solidification mechanism and the resulting fiber diameter. In solution electrospinning, fast solvent

evaporation is the major driving force for solidification while it is temperature gradient in melt electrospinning. Electrospinning of polymer solutions produces generally smaller fibers than from melts. So far the diameter of melt eletrospun fibers is at the micron scale. Zhou et al. [91] reported that for melt electrospinning of PLA, after a series of optimization of processing conditions, fibers with average diameter of 800 nm were produced.

Nonetheless, electrospinning from polymer melt is still promising which has several advantages over electrospinning from polymer solution. First of all, dissolution of polymers in organic solvents and their removal/ recycling are no longer required. In biomedical applications, the cytotoxic residue solvent could be an issue for viable cells and their growth. Recently Dalton et al. studied the possibility of using directly melt electrospun PCL-b-PEO fibers with PCL as tissue scaffolds [101] and have demonstrated that fibroblast could grow successfully on the electrospun fiber mat and formed a spindle-shaped morphology. Secondly, a higher throughput can be achieved due to no loss in mass by solvent evaporation. Thirdly, sub-micron scale fibers of polymers which do not have appropriate solvents at room temperature such as polyethylene and polypropylene can be obtained. Multi-component systems such as blends and composites are another example that favors melt electrospinning, because in many cases no common solvent for all of the components may be found. Besides the above advantages, this solvent-free approach also opens the door to theoretical routes to model electrospinning without the complications associated with solvent evaporation. The comparison is compiled into a table listed in Table 1.

To compromise some of the inherent defects, heated solution electrospinning is another choice for certain material and certain solvent. Polyolefin fibers collected in this study are usually above one micron. To obtain sub-micron scale polyolefin fiber, electrospinning fibers from its heated solutions is desirable since there is no proper

solvent at room temperature for polyolefin. In other cases, for example, PLA in DMF solution, solution heated to 70^{o}C was found to generate more homogenous and smaller fibers.

Table 1 Comparison of solution electrospinning and melt electrospinning

	Solution Electrospinning	Melt Electrospinning
Solidification Mechanism	Mass Transfer (Solvent Evaporation)	Heat Transfer (Cooling)
Solvent Free	No	Yes
High Throughput	No	Yes
Environmental Friendly	No	Yes
Easier to Model	No	Yes
Smaller Fibers	Yes	No
Viscosity Limitation	No	Yes

CHAPTER 2

EXPERIMENTAL SETUP, MATERIALS AND METHODS

2.1 Design and Features of the Melt Electrospinning Setup

As we introduced in the section 1.6, the basic principle of melt electrospinning resembles that of solution electrospinning. It is composed of several basic components: syringe pump, high voltage supply and collector. For the melt electrospinning setup, a heated chamber of the melt is a necessary part. Since the viscosity of melts is usually at least one order of magnitude higher than typical solutions but it is tunable in a limited range by adjusting the polymer molecular weight and processing temperature. In our design, a separate nozzle heater is also included. After the jet ejects out of the nozzle, the temperature gradient is critical in controlling the solidification thus elongational viscosity of the fluid jet. Therefore the temperature in the spinning region needs to be controlled too. Controllable temperature for the collector is another consideration in our design since it can not only make sure we can obtain solidified fibers but also determines the in-situ annealing temperature for the fibers.

Figure 9 shows our setup for the studies of melt electrospinning and heated solution electrospinning. The experimental setup includes basic components such as a micro-flow controller (PHD2000, Harvard Apparatus), a high voltage supplier (ES30P, Gamma High Voltage Research, Inc.) and a collector as well as some critical components for melt electrospinning such as a heating oven for polymer melt reservoir (T_1), a nozzle heater (T_2), a heated guiding chamber (T_3) and a temperature controllable collector (T_4). But difficulties underlying the engineering design of the

setup for melt electrospinning such as the interference between high electrical field and the heating elements throughout the setup require additional attention.

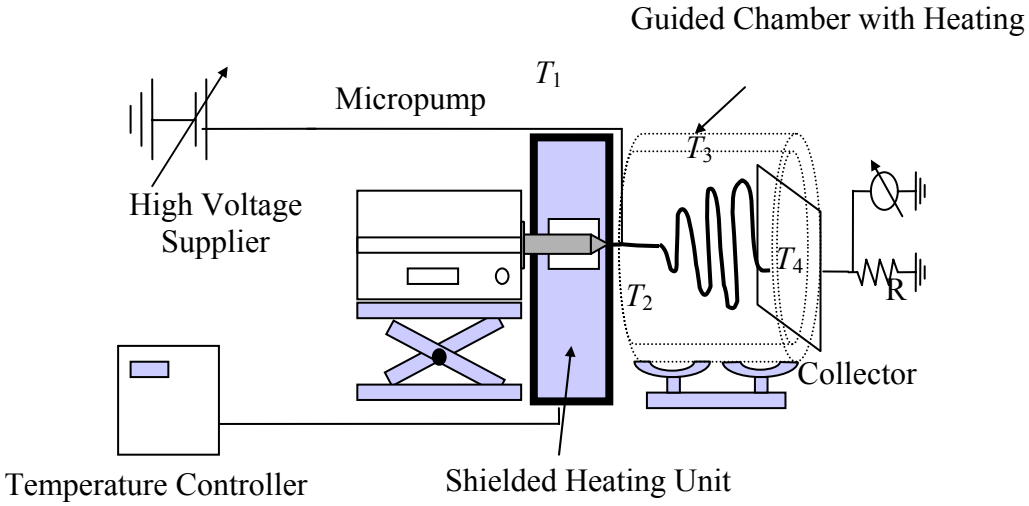

Figure 9 Schematic diagram of the melt electrospinning setup used in the current study

2.1.1 Design of the Shielded Heating Unit

The whole heating chamber is composed of a shielded heating unit, a temperature sensor and a temperature controller. The temperature controller and the type J sensor were purchased from Watlow, Inc. The housing for the shielded heating unit is made of ceramic material (Zircal-95) purchased from ZIRCAR REFRACTORY COMPOSITES, INC. This ceramic material has good mechanical strength, good electrical insulation, good humidity resistance and small thermal expansion. The heating element inside is a U-shaped tubular heater designed by Antech Sales, Inc. To prevent the induced voltage on the heating element and temperature sensor, a grounded shielding screen around the heating element is employed. We found that without the screen, the induced voltage always interfered with the temperature controller and sometimes caused the controller to break down. Temperature read by

the type J sensor corresponds to the value measured by other temperature readers. The sketch for the design is shown in Figure 10.

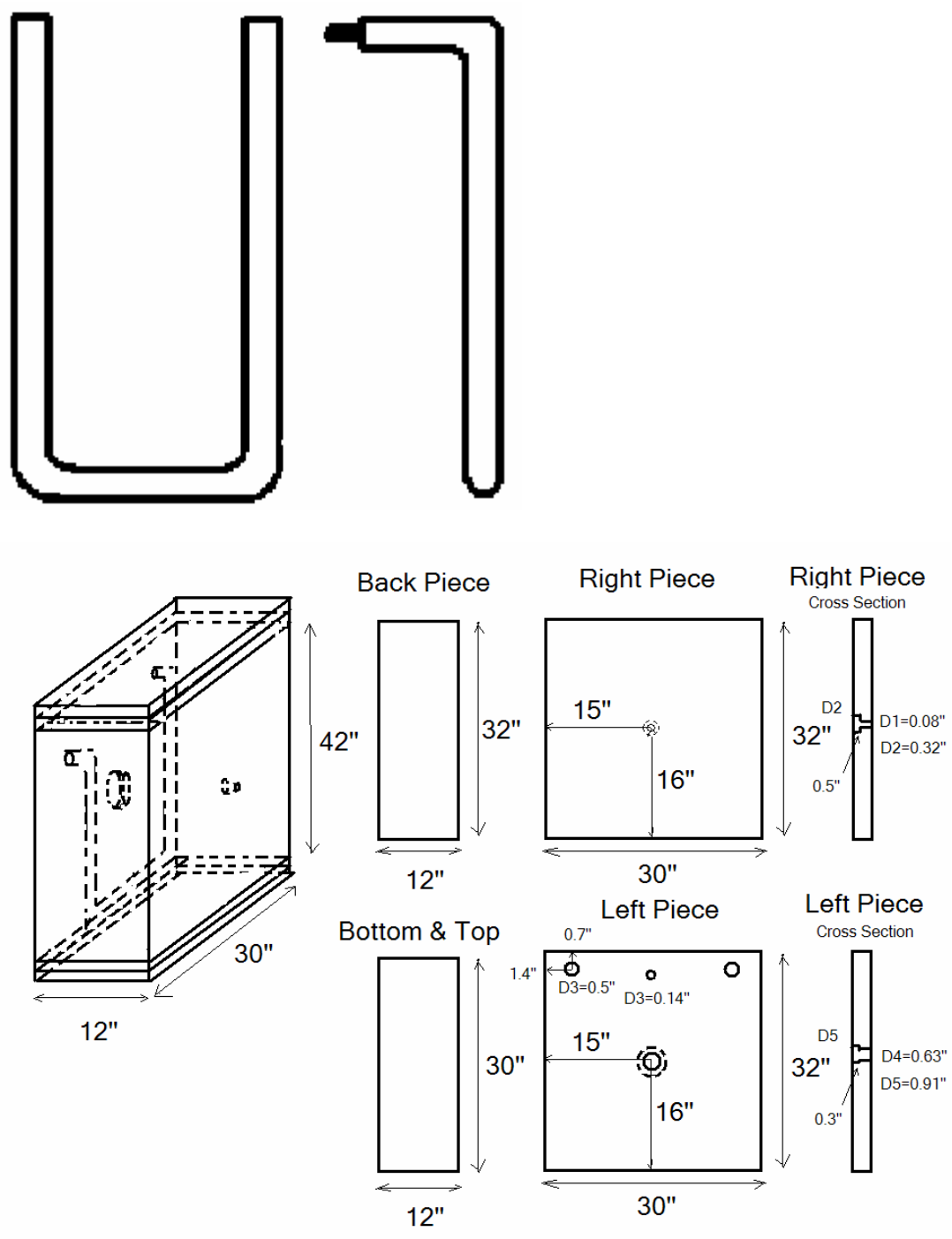

Figure 10 Sketch of U-shaped tubular heater and the heating chamber

2.1.2 Design of Nozzle Heater

The nozzle temperature plays an important role in controlling melt viscosity thus is a critical parameter for resulting fiber diameters. In most cases, high voltage is directly applied to the nozzle. How to avoid the mutual influence between the nozzle heater and high voltage puzzled for a while. And we determined air heating is more appropriate for in the melt electrospinning. Air blower with digitally controllable air temperature was provided by US Air Specialist, Inc. The design for the heating tube is shown in Figure 11.

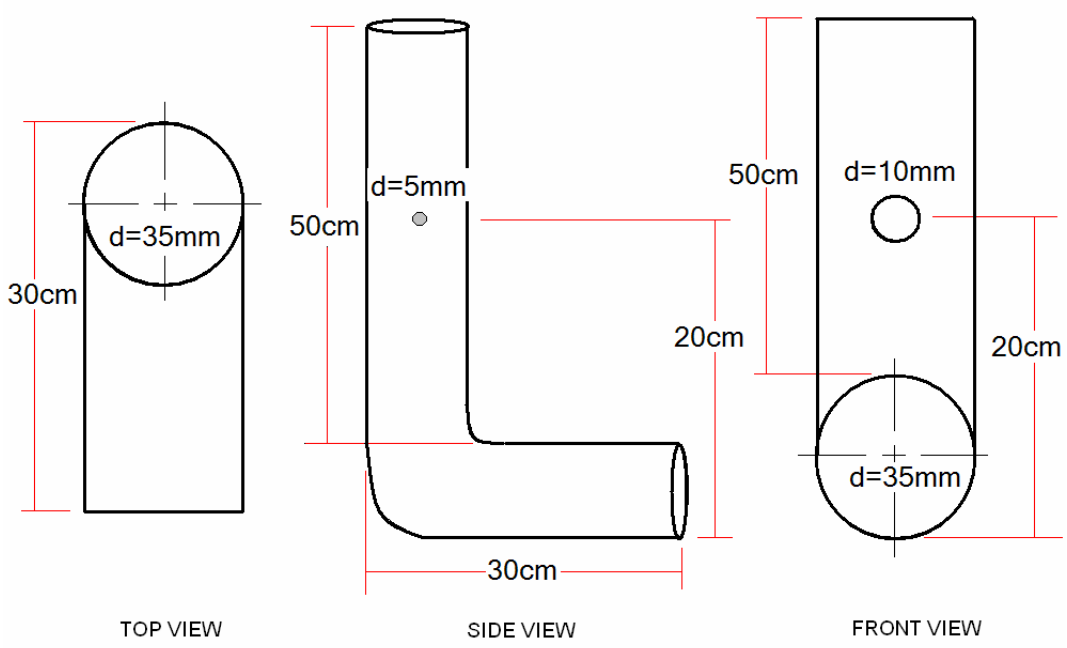

Figure 11 Sketch for the design of nozzle heater

2.1.3 Design of Guided Heating Chamber

The objective is to design a stable heated environment for the fluid jet. In other word, there should have no perturbation done to the fluid jet while in heating. This

requirement together with the precise temperature control of nozzle is critical in acquiring data for simulations since the initial jet formation and jet motion in the spinning region is quite sensitive to these parameters. Again we employed the idea of air heating while trying infrared heater for this application. The basic idea is to pass hot air through a gap channel between two concentric cylindrical glass tubes (Figure 12). The temperature inside the tube can be adjusted and measured before each experiment.

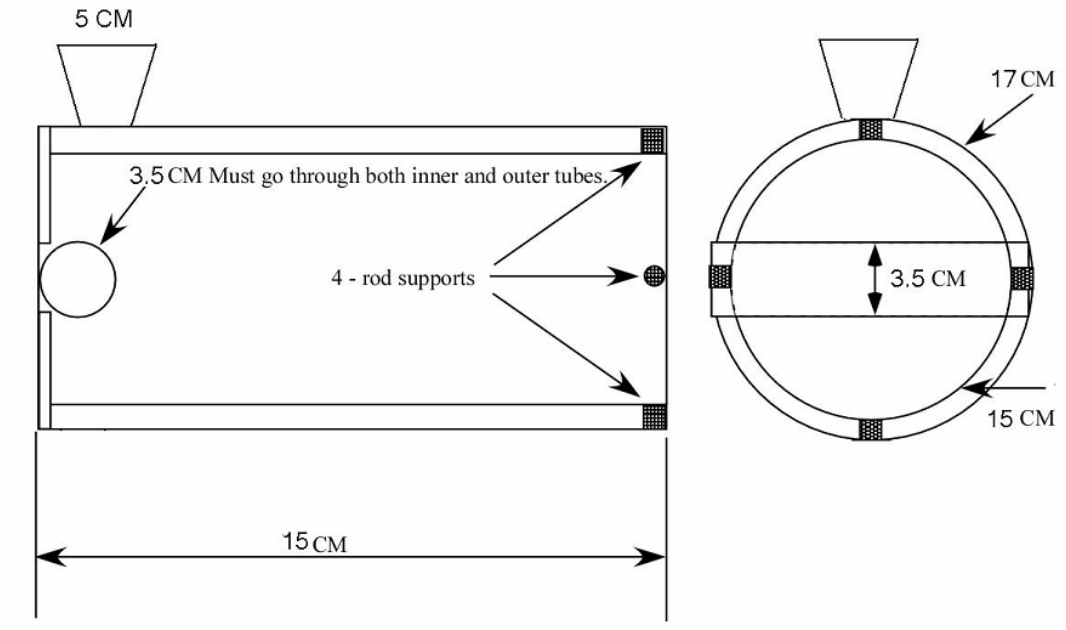

Figure 12 Guided heating chamber as a stable environment for fluid jet

2.1.4 Collector with Cooling and Rotational Collector

For melt electrospun polymer fibers, the melt jet can remain as in melt state after collected onto the collector. And to study the morphology and structures of as-spun fibers, quenching is an effective way as reported in the doctorate dissertation by Jason Lyons. In his study, the oriented polypropylene structures could only be observed by

a collector cooled by liquid nitrogen. In our PLA melt electrospinning process, the glass transition temperature of PLA is rather high at around 55 ^{o}C. So a chilled water cooled collector is desirable and effective. Copper is a good thermal conductive material and suitable as the cooling material for the collector.

Rotational collector in our study is mostly used for preparation of filter media samples. These filter media is usually 12'' x 12''. And since we did not employ any multi-jet system, a rotational collector is an alternative to prepare filter media covered with sub-micron scale fibers homogenously. Figure 13 shows the real image of these two collectors.

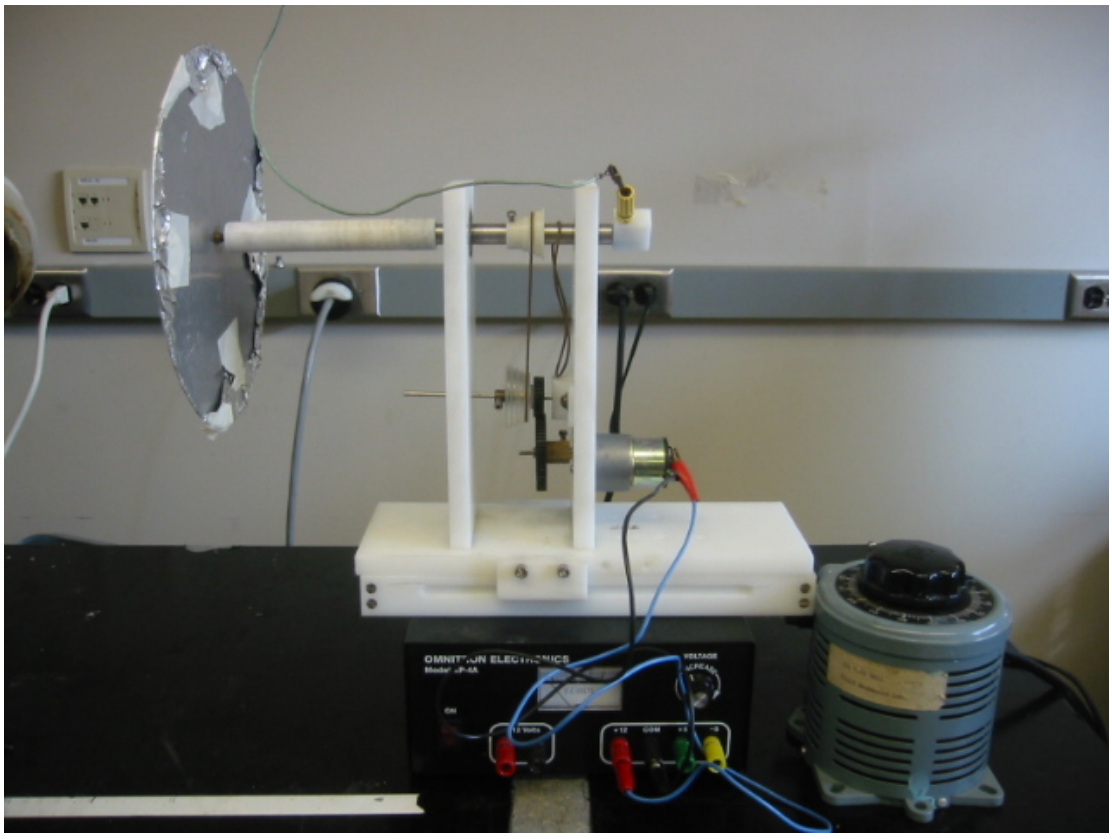

Figure 13 Spinning collector with speed controller

After assembling all the components, the setup for our studies of melt electrospinning has been completed. The picture of this setup is displayed in Figure 14. To summarize our design, the setup meets our demand in this study. It has relatively precise temperature control without interfering with the strong electrical field. Parameters that may affect the process have been considered accordingly in our design.

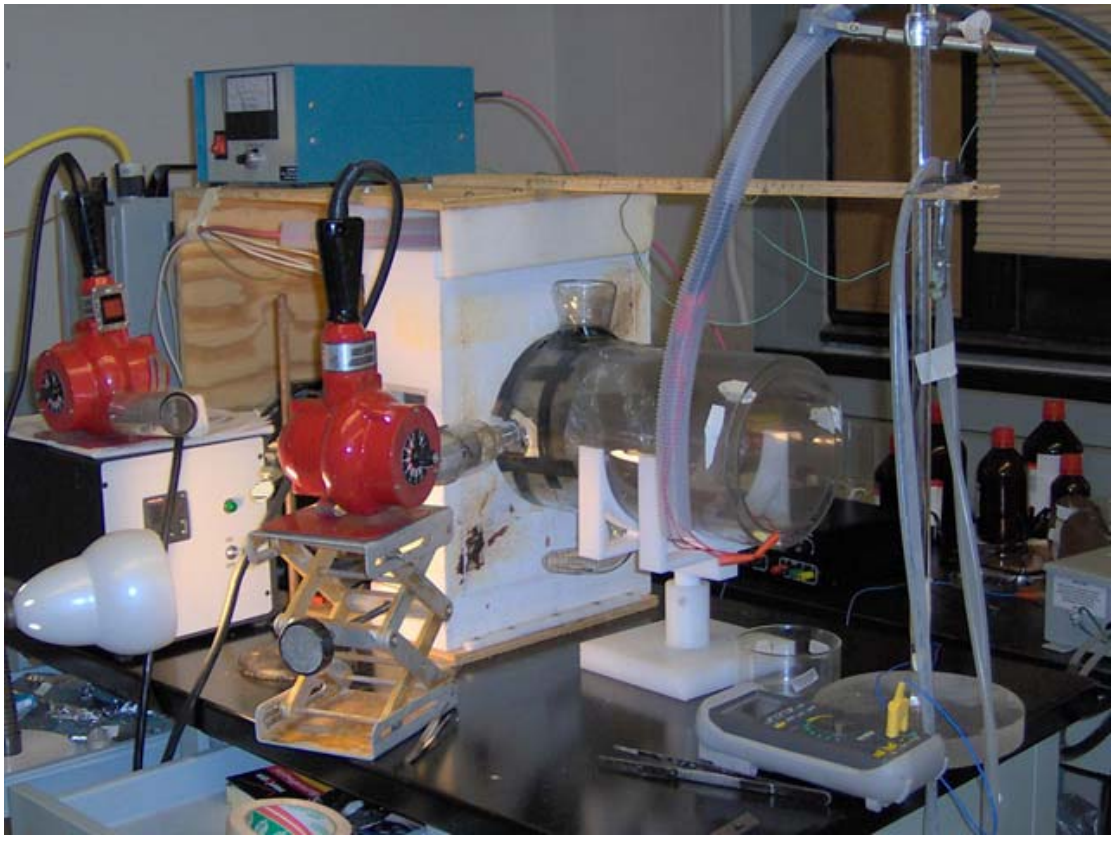

Figure 14 Melt Electrospinning setup

2.2 Materials

Poly(L-lactic) acid (PLLA) and its nano-composites, PLLA/PEO polymer blend, polyethylene and polypropylene were the four major types of materials studied in completion of this work. Poly(lactic) acid (PLA) which is derived from renewable

resources such as corn has received much attention as a biodegradable and biocompatible replacement for various polymers in packaging and biomedical applications. The PLA used in this study has a molecular weight around 186,000 and polydispersity of 1.76 and consists of major L configuration (>98%). Since the PLA resins used in this study are all made of PLLA, the notation "PLA" from now on only refers to "PLLA" unless otherwise indicated separately. The glass transition temperature (*Tg*) of the PLA is approximately 55°C and melting temperature (*Tm*) is about 165°C. The synthesis is shown in Figure 15.

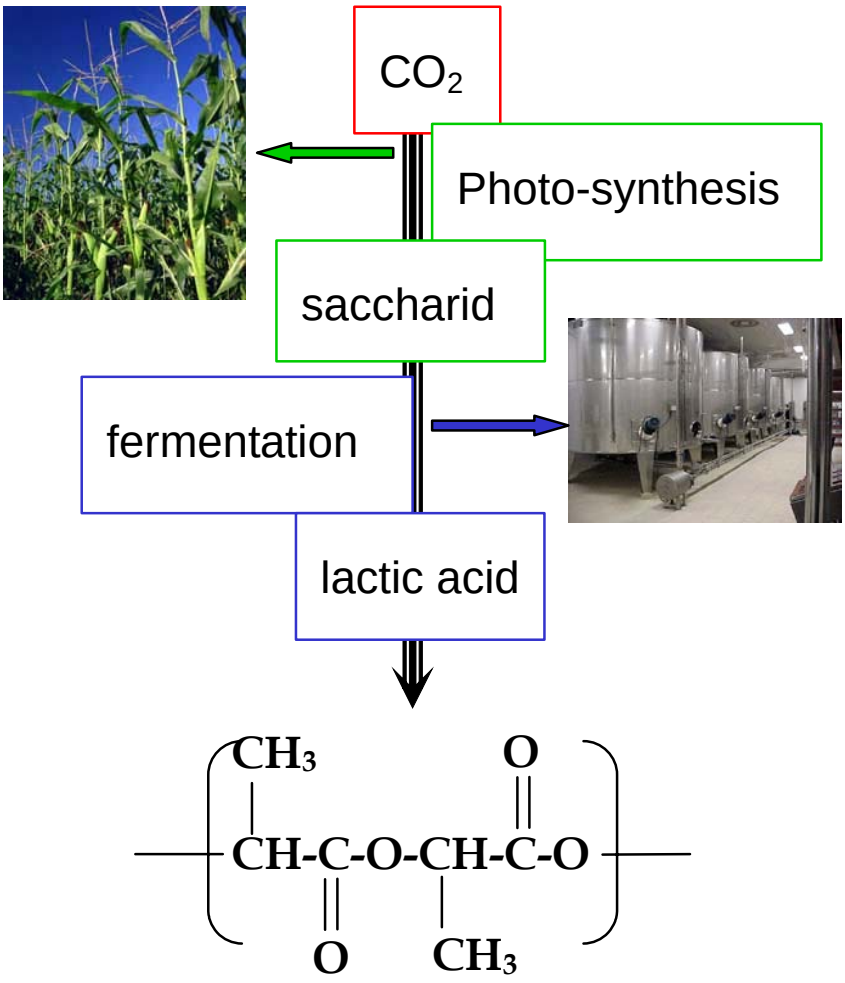

Figure 15 Poly(L-lactic) acid synthesized from renewable resources

PLA/Nanoclay nano-composites were prepared through melt extrusion. To prepare PLA nano-composites, PLA pellets were first ground into fine powders with an average size of 0.5 mm using a Retsch ZM 100 ultra-mill (Glen Mills, Inc.). A polymer/nanoclay premix was prepared by combining appropriate amounts of organically modified montmonrillonite (Closite 30B, Southern Clay Products, Inc.) and polymer powders in a DAC 150FV speed-mixer (Flacktek, Inc.). These premixed powders were then dried in vacuum oven at 80^{o}C for 12 hours followed by melt-extrusion at 220^{o}C in a nitrogen atmosphere, with a screw speed of 100 r.p.m. and a residence time of 3 minutes using a bench-top microextruder. Various compositions of nano-composites were then prepared in the similar procedure.

PLA/PEO blends with various compositions were also prepared using the same procedure described above for making PLA nano-composites. The PEO was obtained from Sigma-Aldrich with a molecular weight of 100,000.

Polypropylene and polyethylene are two widely-used thermoplastic polymers. And structures and physical properties of polypropylene are not only determined by the molecular weight but also by the tacticity [102-104]. Polypropylene can have three different tacticities: isotactic, syndiotactic and atactic. Films and fibers of these materials are typically melt-processed industrially. Polyolefin non-woven fibers are to our great interest due to some of their advantageous properties such as hydrophobic feature, good mechanical strength, good chemical resistance, and so on. Gel spun UHMWPE fiber is the strongest fiber among all synthetic fibers. It is approximately fifteen times stronger than steel of the same weight while Kevlar fiber is only five times stronger. Polypropylene fiber is the lightest synthetic fiber and comprises the majority of non-woven polyolefin fibers. In recent years, sub-micron polyolefin fibers

are sought to meet the demands in the field of filtration, battery separators and protective coating because of the high surface area to volume ratio.

Two polypropylenes were employed in this study. One of the polypropylene used in this study was isotactic with a molecular weight of 129,000 and polydispersity of 2.8 obtained from Clarcor. It has a high melt flow index of 1100 good for melt blowing. The other polypropylene was also isotactic with a molecular weight of 178,000 and polydispersity of 2.0 acquired from Dow Chemical Co. HDPE (GHR 8110) and UHMWPE (GUR 4120) were provided by Ticona, Inc. with a molecular weight of around 800,000 and 2 million respectively.

2.3 Sample Characterizations

Detailed experimental description on electrospinning process will be addressed separately in later chapters since melt electrospinning and heated solution electrospinning do not share the same parameters. However, to characterize the fibers, we used the same methodology. Before electrospinning, we typically did pristine material characterization: molecular weight measurement, thermal property characterization, structural characterization and rheological study. After electrospinning, the electrospun fibers were subject to a series of characterizations physically and chemically: SEM for morphology; DSC for thermal properties; XRD for structural information; FT-IR for chemical composition; POM for crystal composition; TEM for internal structures; AFM for morphology; Instron for mechanical properties; contact angle measurement for hydrophobicity and filtration efficiency test of electrospun fiber mat. The whole process can be described as following flow chart (Figure 16):

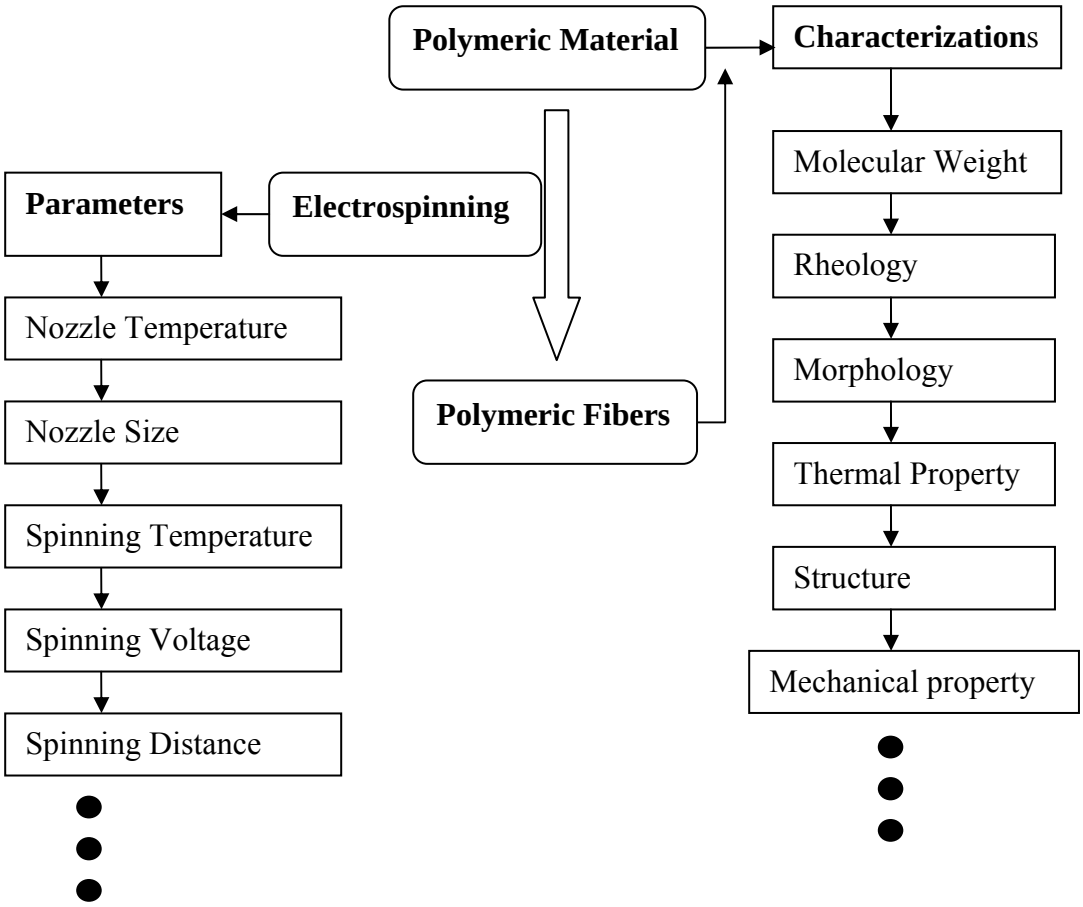

Figure 16 Flow chart for the studies of melt electrospinning and heated solution electrospinning

2.3.1 High Temperature GPC and Molecular Weight

Polymer molecular weight can be characterized in many ways depending on the definition and measuring method. High temperature gel permeation chromatography (GPC) is particularly useful for characterizing the molecular weight and obtaining the molecular weight distribution (MWD) of polyolefin. The instrument operates at 160^{o}C and dilute polyolefin solutions in trichlorobenzene are required to perform the test. The instrument we used is Waters Alliance GPCV 2000 GPC equipped with a Waters

DRI detector and Capillary Differential Viscometer (VIS). The column set (four Waters HT 6E and one Waters HT 2) was eluted with 1,2,4-trichlorobenzene containing 0.01 wt. % di-tert-butylhydroxytoluene (BHT) at 1.0 mL/min at 140 °C. Data were calibrated using mono-modal polyethylene standards (from Polymer Standards Service).

2.3.2 Intrinsic Viscosity Measurement and Molecular Weight

Intrinsic viscosity measurement is a procedure involving measuring the time for pure solvent and a series of dilute solution passing through a capillary tube. Then reduced or inherent viscosities are calculated based on equation:

$$\eta_{re} = \frac{\eta - \eta_0}{\eta_0 c}$$

where η_{re} is the reduced viscosity, η and η_0 is the viscosity of polymer solution and solvent respectively. Intrinsic viscosity is then extrapolated at c=0 which can be described by:

$$\eta_{in} = \lim_{c->0} \eta_{re}$$

Then the viscosity average molecular weight of the polymer can be computed according to Mark-Houwink equations:

$$\eta_{in} = KM_v^a$$

where η_{in} is the intrinsic viscosity, K and a are constants the values of which depend on the nature of the polymer and solvent as well as on temperature. In our experiment, Ubbelohde viscometer modeled as DCP-UBB-1B by DC Scientific Glass, Inc was used.

2.3.3 Rheological Characterization

Studies on rheological properties of materials are performed through Rheometrics Dynamic Analyzer (RDA II). For melts, circular sample disk were prepared by melt compressing polymers in a customized a mold and in this case, plate-and-plate fixture with 10mm diameter was employed. For solutions, Couette fixture was used instead. Dynamic frequency sweep was performed to acquire information on zero shear viscosity and shear thinning. For PLA and other melts studied, this dynamic frequency sweep test was done at various temperatures ranging from 180^{o}C to 240^{o}C to determine the temperature dependence of melt viscosity.

2.3.4 Scanning Electron Microscopy (SEM) and Fiber Morphology

To measure the fiber diameter and characterize the general morphology of fiber membrane, SEM is an indispensable tool. In our experiments, all the samples were pre-coated with Au-Pd and then loaded into the vacuum chamber of the SEM (Leica 440). Then using the free software ImageJ available online, we analyzed the fiber diameters and their distribution.

2.3.5 Transmission Electron Microscopy (TEM) and Internal Structures

SEM is mostly useful in determining the characteristic features on the fiber surface and it can not provide the information of element information at the first place unless back scattering electrons are analyzed. To probe into the internal structures of the fibers, TEM is more helpful in providing higher resolution images and distinct chemical compositions.

To obtain good-quality images, polymer samples were usually embedded into epoxy matrix and after curing for a certain amount of time microtomed into 90nm thin sections. All experiments were done on JEOL 1200EX with conventional film.

2.3.6 Differential Scanning Calorimetry and Thermal Properties

Differential scanning calorimetry (DSC) is a thermal-analytic technique that measures the difference of heat required to increase the temperatures of reference pan and sample pan. The principle underlying this technique is that different physical transitions and sometimes chemical transitions will give off or absorb heat. These physical transitions usually include crystallization, melting and phase transition. Figure 17 shows a typical DSC curve under heating.

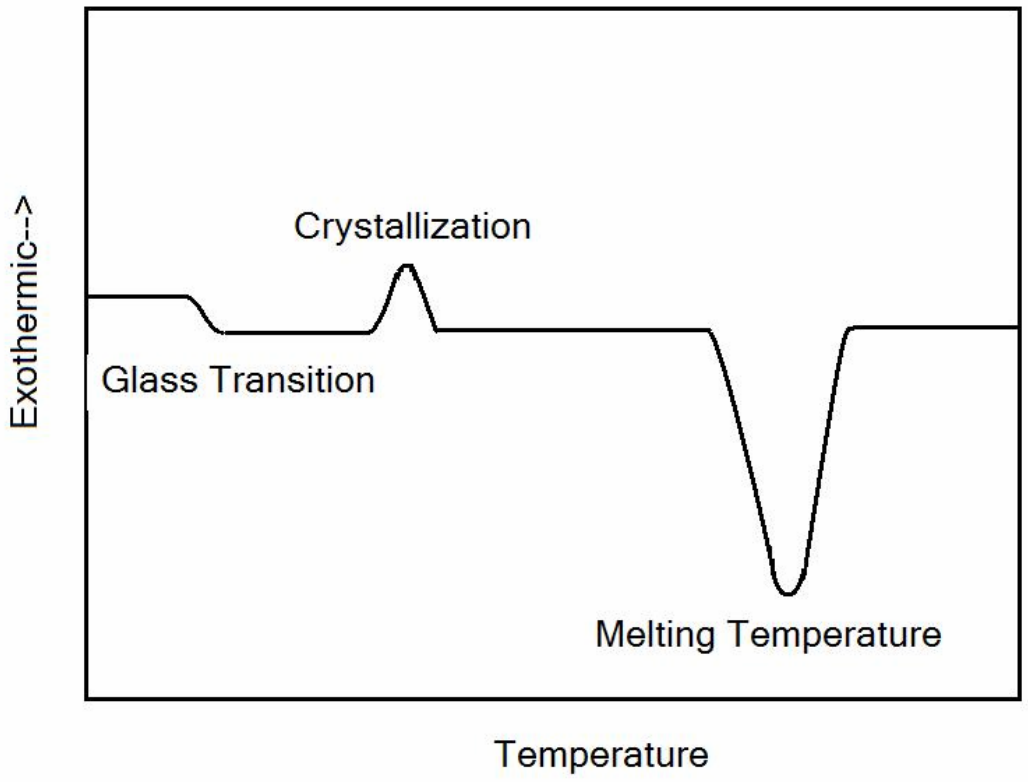

Figure 17 Typical DSC curve of heating

Analysis of DSC curve can provide us great information on transition glass temperature, melting temperature and crystallinity et al. These data are often influenced by the thermal history of the samples. For instance, two samples with same

chemical composition can have different crystallinities if one was produced using quenching method and the other using natural cooling. Glass transition temperature and melting temperature are determined by the energy state of the samples which is often affected by different processing history such as thermal history or mechanical history. Programming the heating and cooling stage in a manipulated way is able to generate other useful information on the behavior of nucleation and crystallization.

In most of the cases of our study, 1-3 mg of fiber samples were loaded into DSC pan and characterized in a DSC instrument (Seiko, DSC 220C). Heating rate of 10^{o}C/min was picked typically. Temperature range was from 10^{o}C to 200^{o}C.

2.3.7 X-ray Diffraction and Crystal Structures

All the XRD studies were performed on Scintag, Inc. Theta-Theta Diffractometer. XRD data were collected usually in the 2θ range of 1-40^{o} sometimes 5-35^{o} depending on the material and objective, in steps of 0.02^{o} and a scanning rate of 3^{o}/min. XRD is one the most important implementations to characterization the crystal structures of materials. Through the well-established database and open literature, defining the crystal structure of a polymer is simple and handy. One of the greatest features coming with Scintag is the temperature evolution scan. This feature enables us to quickly find out the crystallization behavior using XRD.

This technique works based on the Bragg's Law which can be described as:

$$2d\sin\theta = n\lambda$$

where n is an integer, λ is the wavelength of the exerting waves such as x-rays, electron beams and so on, d is the spacing between the planes in the atomic lattice, and θ is the angle between the incident ray and the scattering planes.

2.3.8 FTIR Spectroscopy and Chemical Structures

Fourier transform infrared spectroscopy measures the intensity of infrared beams after passing through the sample or being reflected by the sample. This technique works because the change of molecular dipoles when they move in a certain way: symmetrical and asymmetrical stretching, scissoring, rocking, wagging and twisting. The resonant frequencies are affected not only by the motion the molecule undergoes but also by the other conditions such as the strength of molecular bond and the surrounding influence by other molecular groups. Typically for the same bond, stretching corresponds to higher frequency compared to other motions and for the same motion, stronger bonds have higher frequency (triple bond > double bond> single bond).

In this study, solid fiber mat was directly mounted on a sample holder with a transmission window. Sample holder with the sample then was loaded into Mattson Model 5020 FTIR Spectrometer. This instrument has a resolution of $0.4cm^{-1}$ and covers the range from $400cm^{-1}$ to $6000cm^{-1}$.

2.3.9 Polarizing Optical Microscope and Crystallization

Conventional optical microscope (POM) with plain light is useful in taking images of surface morphologies insensible by human eyes while polarizing optical microscope offers more advantages such as in-situ study of nucleation and crystallization et al. POM is used to detect birefringence in the materials. Birefringence results from the different interaction in different direction between the incident light and the atoms in the materials. These birefringence materials possess multiple refractive indices depending on the orientation of incident light with the crystallographic axes.

Crystal structures in a material are highly aligned structures which have consistent interactions with the incident light at one propagation direction. By analyzing the outcoming light using an analyzer, images resulting from the different refractive indices can be obtained. Thus, crystal structures can be distinguished as well as the crystal morphologies such as spherulite and lamellar structure.

To acquire images, samples were loaded into an Olympus BX2-51 Microscope. Using the attached the digital camera, pictures were easily captured.

2.3.10 Instron and Mechanical Properties

Mechanical properties of materials can be characterized by many means: elongation test, compression test, hardness test and bending test et al. For our fiber mat samples, elongation test was implemented to obtain the stress-strain curve. Young's modulus, yield strength and breaking strain can be extracted from this curve.

However, these data clearly do not represent the real modulus or strength of the electrospun fibers. They are affected by a combination of many factors: fiber strength, friction between fibers, porosity of fiber mat or density of the fiber mat [105]. To precisely characterizing the mechanical strength and modulus, single fiber test is preferred. Nevertheless, fibers generated from electrospinning are so small that handling the fiber and the sensitivity to test it are challenging. AFM has been reported to be able to test the fiber modulus quite precisely [106-108] but measurement of strength is still long way to go.

In the tensile test, a fiber mat was cut into a rectangle with the measurable length of 2 inch and width of 10 mm. These rectangular strips were then mounted on the clamp-style sample holder coming with the INSTRON instrument (Model 1125). Strain rate was set as 1 inch/min until the sample broke.

2.3.11 Contact Angle Analyzer and Hydrophobicity

Water contact angle was measured through Contact Angle Analyzer manufactured by Electric Time Co. Inc. Fiber mats were cut into a rectangular strip of 1 inch long and 10mm wide and the strip was then mounted onto a bar sample holder with the help of double-side tape. After the bar was inserted into the instrument, the surface of the projected sample was adjusted to overlap the baseline of a protractor. Two displacements: x and y (Figure 18) were then measured. The contact angle was the calculated based on following equation:

$$\theta = \cos^{-1}\left(\frac{x^2 - y^2}{x^2 + y^2}\right)$$

where θ is the contact angle and x, y is the distance from the origin.

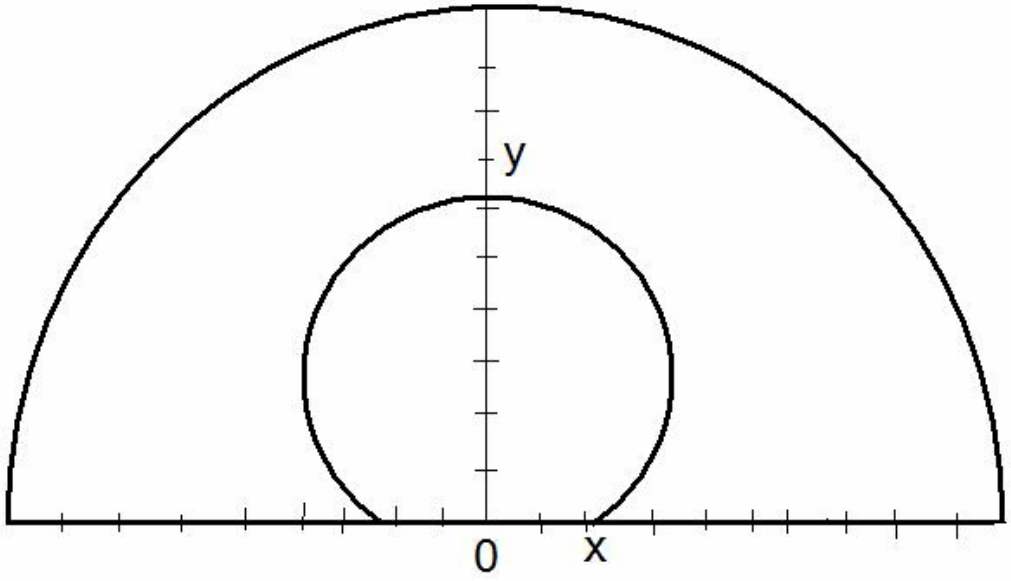

Figure 18 Measurement of contact angle

2.3.12 Air Filtration Efficiency Test

The collection efficiency of dust particles in air was measured using a custom-built filtration efficiency tester. Dust particles were counted before and after passing air through the filter media. Air was fed at a rate of 6.9 cfm through each flat-sheet filter and the collection efficiency of dust particles in the size range of 0.03 to 5 □m was measured. At the same time, pressure drop before and after the filter media was monitored.

To prepare the sample for the air filtration efficiency test, measured amount of fibers were directly electrospun onto a cellulose filter media mounted on the rotational collector with rotation speed of around 10 rpm.

CHAPTER 3

ELECTROSPINNING OF PLA AND ITS COMPOSITE FIBERS FROM SOLUTION: EFFECT OF NANOCLAYS*

The promising applications of PLA in packaging and biomedical field are only part of the reason of our interest. The other important point is that PLA is a slow crystallizable polymer [109-112] which can minimize the complicity of including crystallization in the process. It is critical for a straightforward computer simulation. And the high glass transition temperature is well suitable for our studying the impact of electrospinning process on fiber structures.

Despite its promises, the widespread use of PLA is limited by its thermo-mechanical properties. To improve the mechanical properties, barrier properties and thermal stability of PLA, researchers have been developing its composites with nanoclays. Blends of PLA with organically modified layered silicate (OMLS) were first prepared by Ogata et al. using a solution casting method [113]. Their results demonstrated that only tactoids which consists of stacked silicate monolayers were observed in the composites. Even with this level of poor dispersion, however, mechanical properties are shown to be slightly improved. Due to the advances in nano-composite technology, OMLS nanoclays with a few nanometer of layer thickness and very high aspect ratio (e.g., 10-1000) can be homogeneously dispersed in a polymer matrix by various processing schemes including solution casting [113], melt extrusion [114] and in-situ polymerization [115]. It has been reported that mechanical properties, barrier properties and even biodegradability of PLA can remarkably be improved by the inclusion of nanoclays [116-118]. Such improvements

* Zhou HJ, Kim KW, Giannelis E, et al. ACS SYMPOSIUM SERIES 918: 217-230 2006

in material properties are evidently caused by the enhanced interfacial interactions between clays and polymer molecules in nano-composites via either intercalated structures or exfoliated morphologies. The diagram shown in Figure 19 illustrates the forming process of nano-composite with intercalated or exfoliated morphologies.

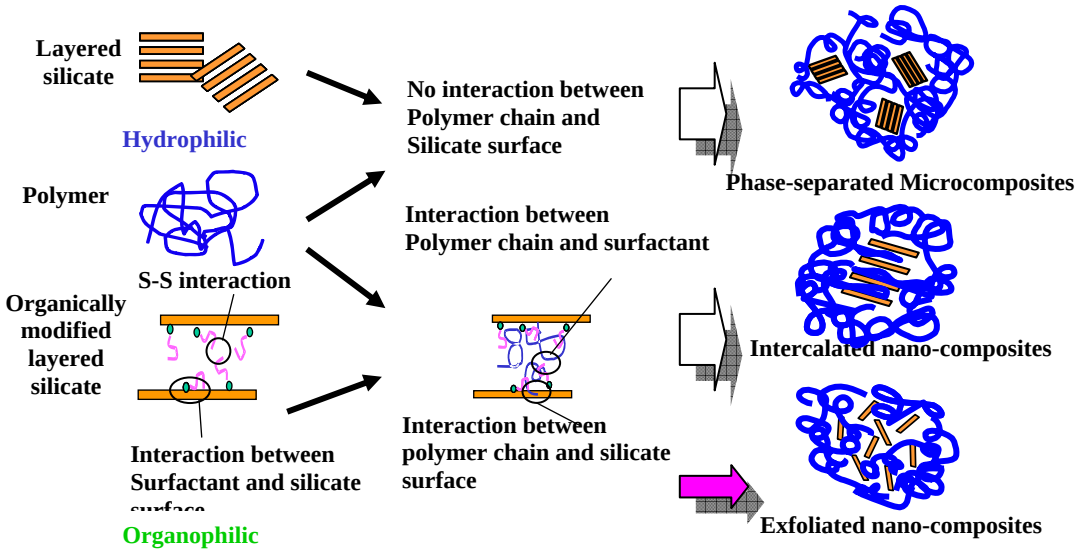

Figure 19 Formation of nano-composite with intercalated and exfoliated morphology

Studies of electrospinning have not been sufficient to investigate the crystalline structures of nano-composite fibers. The effects of nanoclays on the degree of crystallinity in electrospun fibers were investigated by a few researchers and they agreed on one point that nanclays greatly inhibited the growth of crystals in the fibers [124, 125]. Fong et al. studied in detail the alignment of the exfoliated clays along the nylon-6/montmorillonite nanocomposite fibers [126]. α crystal structure dominates nylon-6 casting film from solution and γ crystal structure is adopted into the electrospun fibers with crystal layer normal parallel to the fiber axis. However, no studies on the structural study of PLA nano-composites nanofibers have been done till

now. The structural study of electrospun PLA nano-composite fibers is particularly important because PLA exhibit two types of crystal structures: α structure with a lamellar folded-chain morphology and β structure with a fibrillar morphology [127]. The pseudo-orthorhombic α structure is found at relatively low drawing temperatures and/or low hot-draw ratios. A second so-called β structure appears only at higher hot-draw ratios, and thus probing β crystal structures can provide useful information associated with elongational deformation during the electrospinning process.

In this chapter, we will demonstrate the electrospinning process of PLA and its nano-composites. And we will also portray how the inclusion of nanoclays influences the molecular structures of the electrospun fibers from both its solutions.

3.1 Experiments

Solutions of PLA/nanoclay composites were prepared in two different ways. The first scheme was to dissolve 10 to 25 wt% of these compounded PLA/nanoclay nano-composites in chloroform (Sigma-Aldrich). The second method was a simple blending scheme in which nanoclay particles are simply stirred and blended with chloroform until nanoclay particles are dispersed homogeneously in chloroform, and then pre-dried PLA powders are directly added to nanoclay/chloroform suspension. Hence, compounding PLA and nanoclay in a twin screw extruder is by-passed in the second scheme. Solutions made by these two schemes are named as follows; for example, in PLA-NC3, NC denotes the first scheme with twin-screw extrusion compounding and 3 denotes the content of nanoclay in PLA composites. PLA-BL5 represents PLA composites with 5 wt% clay prepared by the second blending scheme. The abbreviations are listed in table 2.

Table 2 Meaning of abbreviations

PL	Pure PLA dissolved in the solvent
BL	Direct mixture of PLA and C30B in the solvent
NC	Pre-mix PLA and C30B using twin extruder and then dissolved in the solvent

Electrospinning experiments were conducted in a horizontally placed electrospinning setup. A high voltage source (ES30P, Gamma High Voltage Research, Inc.) was used to apply 10 to 30 kV to a 24 gauged needle on a syringe through copper wiring. A precisely-controlled syringe pump (PHD2000, Harvard Apparatus) was used to continually renew the droplet at the syringe tip. The volumetric flow rate ranged from 0.005 to 0.025 ml/min. Grounded aluminum foil on a metal sheet was placed 6 to 12 inches away from the syringe tip acting as a collector. As the applied voltage is increased, a droplet at the needle tip deforms into a conical shape and then an electrically charged jet is formed. The jet solidifies due to the evaporation of solvent, as it goes through a vigorous whipping motion. As a result, non-woven fiber mats are formed on the surface of the collector.

These fiber fabrics were then characterized by various methods described in Chapter 2. Thermal analysis was conducted by DSC (Seiko, DSC 220C). Morphology of electrospun fibers was examined by SEM (Leica 440). Structural study was performed through XRD (Scintag, Inc. Theta-Theta Diffractometer) and TEM (JEOL 1200EX). Tensile test was carried out on Instron 1125 test system. For comparison purposes, casting films were also prepared. First, powders of PLA or nanocomposite were dissolved in chloroform. After removing solvent in air at room temperature, PLA

cast films were put into a vacuum oven for 24 hours. These films were then characterized under the same conditions as electrospun fibers.

Biodegradability studies in a buffer solution of KCl/NaCl/Na_2HPO_4/ KH_2PO_4 at pH = 7.38 and 37°C. For PLA fibers, six samples with the same weight were loaded into bottles containing the buffer solution. These bottles were then put in a water bath maintaining a temperature of 37°C. And after one week, one piece of sample was removed for weight measurement and crystallinity characterizations. The biodegradability studies of other samples including PLA, PLA-BL5, PLA-NC5 fibers and their corresponding cast films were carried out following the same procedure.

3.2 Fiber Morphologies

Single electrospun fiber is typically circular shaped. But other shaped fibers were also reported [128, 129] such as ribbon-like which is caused by collapse after the evaporation of solvent, round fibers with pores and string-bead morphologies. The electrospun PLA fibers are homogeneous circular-shaped. With close examination of the surface, pores can be clearly spotted (Figure 20a). These pores are also caused by the evaporation of the solvent. The formation of pores is associated with not only the nature of solvent but also humidity [130] according to Casper et al. They found for electrospun polystyrene, higher humidity produced more pores and larger pore size.

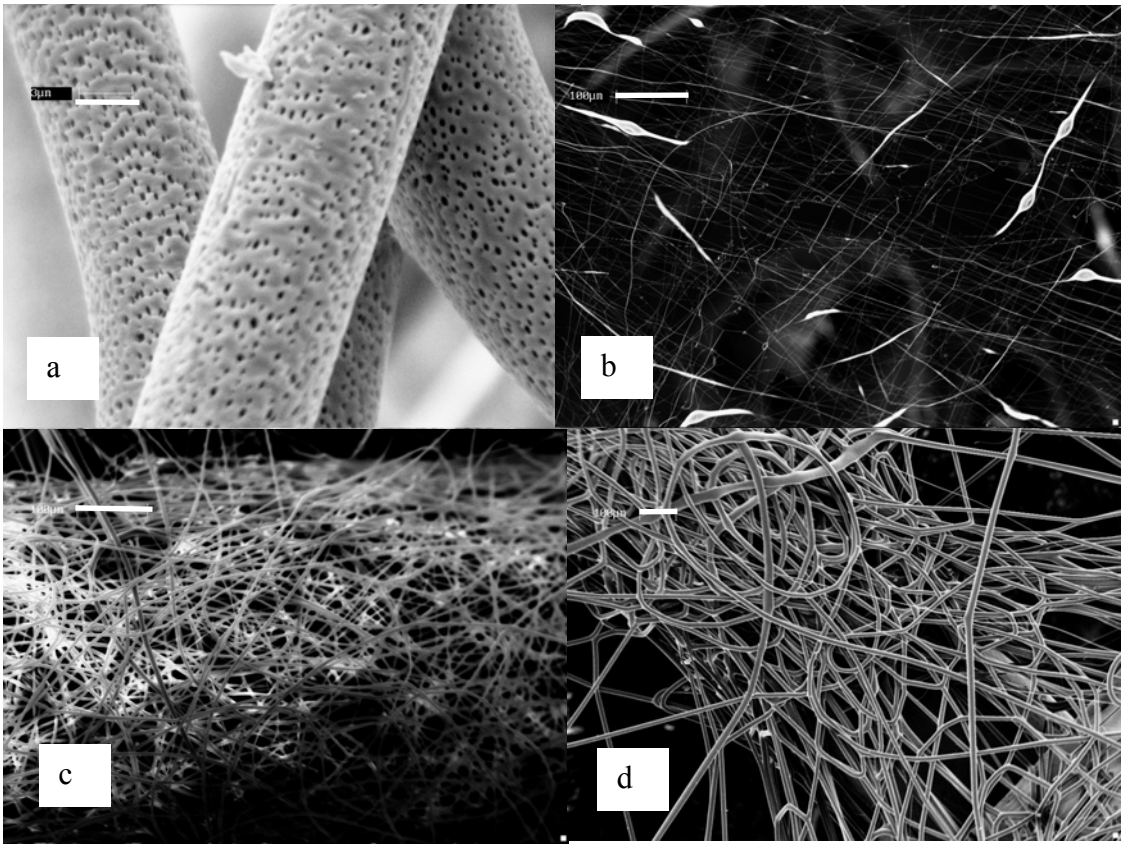

Figure 20 SEM micrographs of a) PLA fibers with pores PLA fibers from b) 10 wt% solution c) 15 wt% solution d) 25 wt% solution; scale bar: 3 micron for a) and 100 micron for all others

3.2.1 Effect of Solution Concentration

The effect of concentration on fiber diameter has been widely studied and basically same trend is observed in our study. Diameter of fibers produced from 10 wt% solution ranges from 100 nm to 500 nm. As concentration increases, average fiber diameter increases. At 25 wt%, double mode distribution of the diameter is observed with average fiber diameter of 15 microns. Thus we achieved a way to control the fiber diameter in a wide range from 100 nm to 20 microns depending on the applications we are targeting at. The diameter-concentration relation is plotted as

Figure 21. Also the average fiber diameter is increased with increasing solution concentration. However, to our surprise, the variation of the fiber diameter is relatively fixed to around 45 % of the average value.

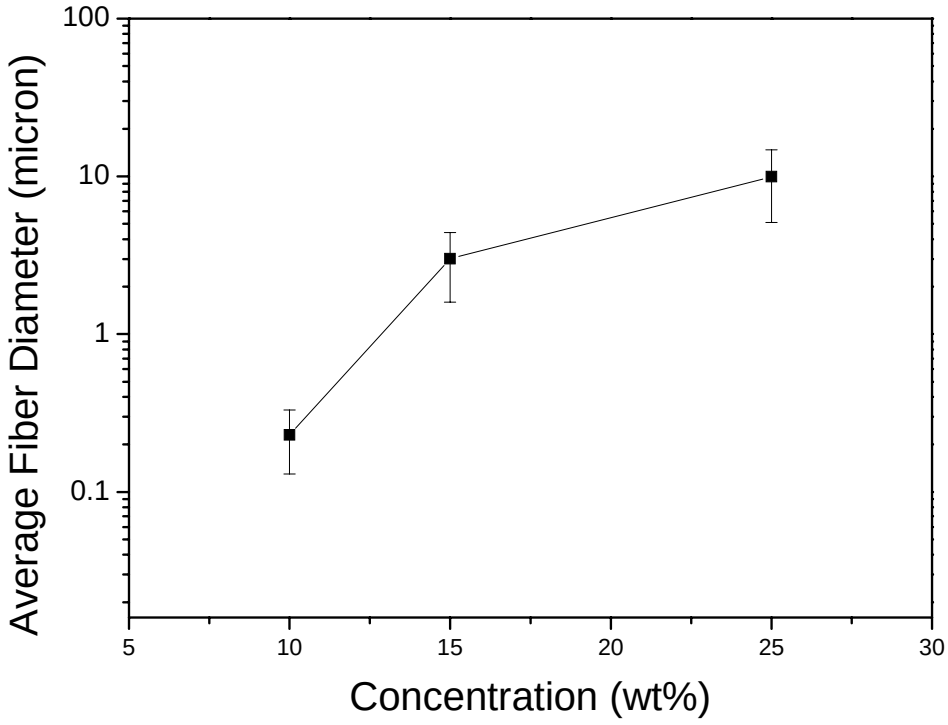

Figure 21 Effect of solution concentration on average fiber diameter and variation of diameter

3.2.2 Effect of Nanoclay Inclusion

Figure 22 demonstrates the effect of inclusion of 3 wt% of nanoclay. Both composite materials result in 30% smaller fibers and nano-composite PLA/nanoclay fibers are slightly smaller than micro-composite fibers. The inclusion of nanoclay has two influences on the fiber formation: increasing the conductivity of solutions; molecular alignment induced by the aligned nanoclays. Nanoclays in the nano-composite have better interaction with the polymer chain and thus more orientation

can be introduced by the alignment of nanoclays than those in micro-composite. Other than these changes, there is no significant change in morphological properties. It is barely observable of the existence of the nanoclays.

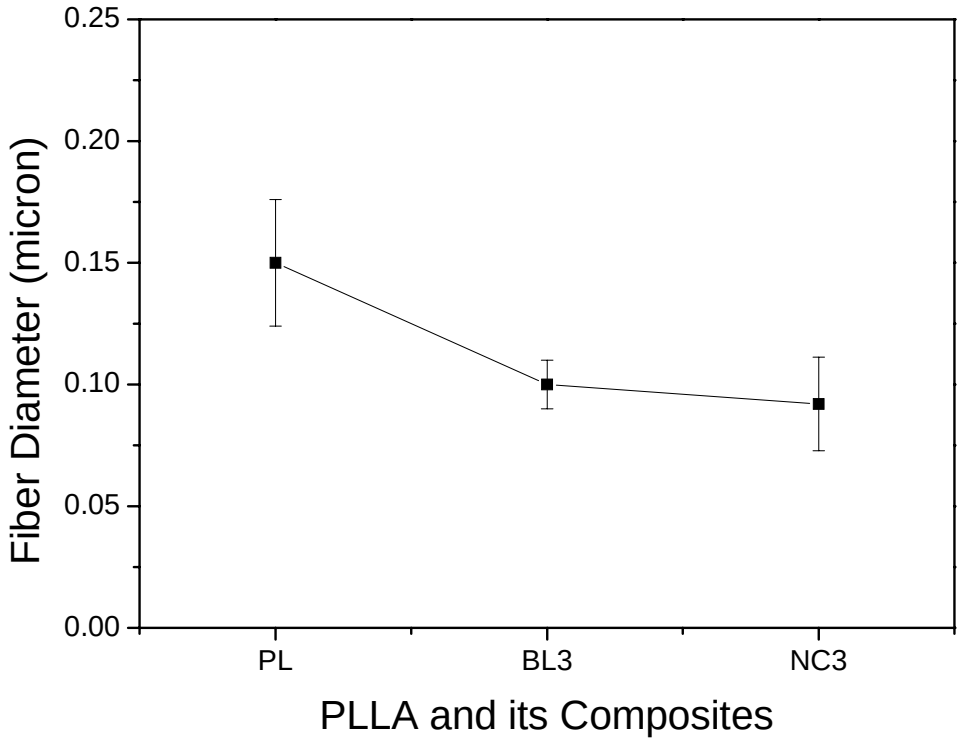

Figure 22 Effect of nanoclay inclusion on fiber diameters produced from 10 wt% in chloroform solutions

The dispersion of the clay layers in electrospun fibers is examined using TEM studies. TEM micrographs taken from a cast film and an electrospun nanofiber of a PLA nano-composite are compared in Figure 23. The micrograph of the cast film, Figure 23a, shows that the organoclays are well dispersed in the PLA matrix, although some parts of agglomerated layers still exist. As expected, no significant orientation effect could be observed for this bulk sample. In contrast, the TEM images of the

electrospun fiber microtomed along and perpendicular to its axis (Figure 23b and 23c) show the clay layers aligned along the fiber axis suggesting strong processing-structure correlation. Highly aligned montmorillonite layers have also been reported in electrospun fibers of nylon nano-composite [126]. The TEM study also reveals that intercalation is preserved during electrospinning.

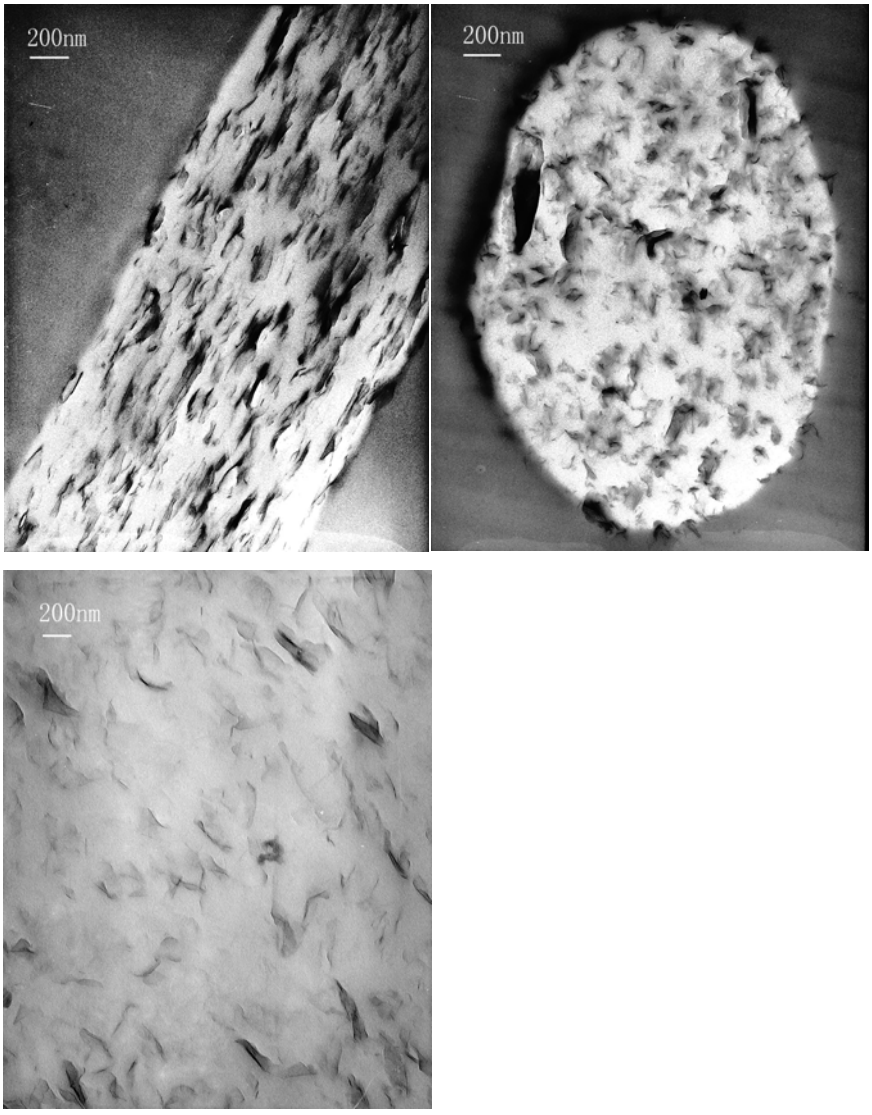

Figure 23 TEM micrographs of a) PLA-NC5 cast film, b) PLA-NC3 fiber microtomed along its axis and c) cross section of PLA-NC3 fiber

3.3 Nanoclay Effects on Fiber Molecular Structures

An electrically charged jet of polymer solution can significantly be elongated during electrospinning. The micro-structural state results from interaction between the dynamics of the polymer molecules and the deformation during electrospinning process is not well understood. In particular, we are interested in the effect of nanoclays on such micro-structural development. Figure 24 shows the first run of the DSC for various electrospun PLA and its nano-composite fibers. It should be noted here that the residual solvent was removed by drying in all the samples before testing. Compared to cast film, all electrospun fibers have two distinct melting peaks which can be deconvoluted by Gaussian fitting (dotted lines). The melting peak at lower temperature is for fibrillar β crystal, created by elongational deformation [131, 132], whereas the other peak at higher temperature is for that of α crystal. The presence of the melting peak for β crystal becomes more prominent in nano-composite fibers (PLA-NC3).

We also note that due to highly aligned molecular structures, the cold crystallization occurs between 100^{o}C and 130^{o}C, and the degree of cold crystallization becomes more prominent in nano-composite fibers. The cold crystallization peak for nano-composite fibers (PLA-NC3) is much sharper and stronger than those of neat PLA fibers and simply blended composite fibers (PLA-BL3). The cold crystallization temperature is also shifted to lower temperature, around 110^{o}C. These results may suggest that the alignment of intercalated (partially exfoliated) nanoclays caused by elongational deformation during electrospinning enhance the formation of oriented PLA molecules which transform into crystals upon heating.

The characteristics of these curves are summarized in Table 3 including glass transition temperature Tg (^{o}C), cold crystallization temperature T_{cold*} (^{o}C), β crystal melting temperature $T_{m\beta}$ (^{o}C), α crystal melting temperature $T_{m\alpha}$ (^{o}C) and the degree of

crystallinity χ (%). The fraction of β crystal is also calculated by the ratio of β crystal peak area to the total peak area. Crystallinity is determined using the following equation:

$$\chi = \frac{\Delta H_f - \Delta H_c}{\Delta H_f^0} \times 100\%$$

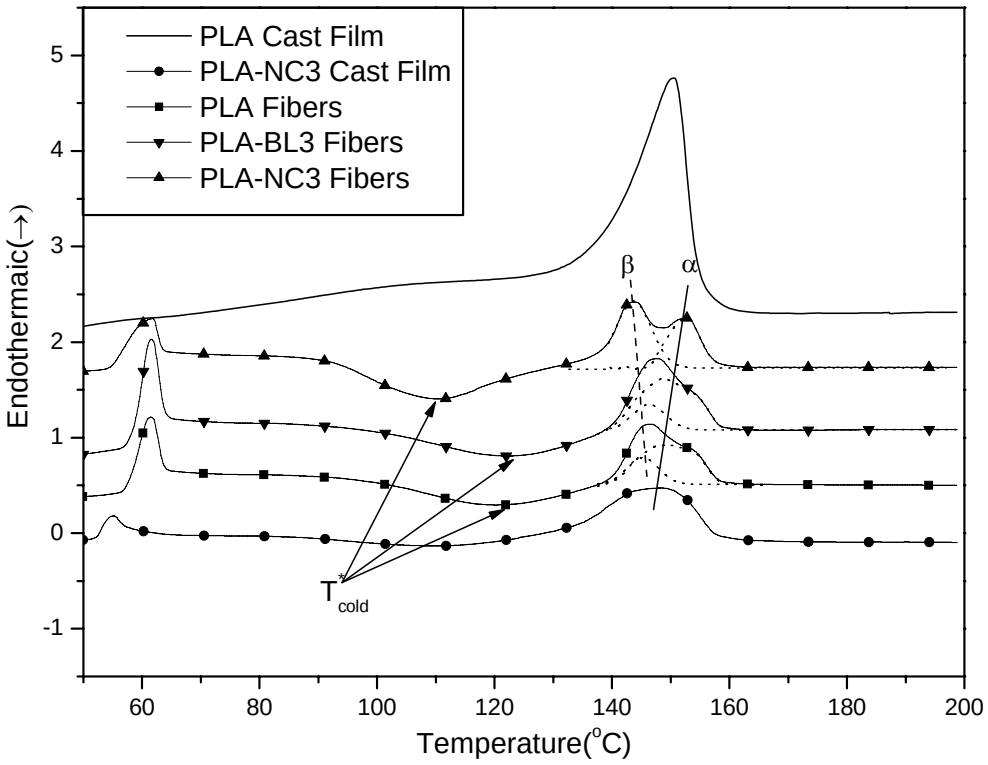

Figure 24 DSC thermograms of various electrospun PLA fibers; cast films of PLA and PLA/3 wt% nanoclay are included for comparison

where ΔH_f is the heat of fusion, ΔHc is the heat of cold crystallization and $\Delta H_f{}^0$ is the heat of fusion for 100% crystalline PLA, 93 J/g [133]. It is observed that crystallinity of PLA-NC3 cast film is significantly smaller than that of neat PLA cast film. Despite

the fact that nanoclays can act as nucleates [134], recent studies [135] demonstrated that nanoclays may impede the mobility of polymer molecules thus slow crystallization kinetics [136]. We note that the degree of crystallinity for electrospun fibers is remarkably smaller than that of cast films. This decrease in crystallinity may be associated with the rapid solidification during the solvent removal process. Contrary to casting films, the inclusion of nanoclays of 3 wt% in electrospun fibers greatly enhances crystallization, indicating that the presence of nanoclays under the deformation may induce crystallization. Crystallization, however, appears to be suppressed at higher nanoclay contents (5 wt%). It should also be noted that electrospun PLA fibers exhibits significant β fractions, which indicates that substantial deformation during electrospinning. The fraction of β crystal is greatly increased in electrospun PLA nano-composite fibers.

Table 3 Summary of DSC curves for different PLA films/fibers*

Film/Fiber	T_g	T_c^*	T_m^β	T_m^α	$\chi(\%)$	$F(\beta)$
Neat PLA Cast Film	N/A	N/A	N/A	150.6	32.4	0
PLA-NC3 Cast Film	52.3	N/A	N/A	148.6	15.7	0
Neat PLA Fibers	57.8	119.2	145.3	149.3	2.2	0.27
PLA-BL3 Fibers	58.6	121.4	146.3	148.7	1.8	0.23
PLA-NC3 Fibers	55.1	109.9	143.8	152.9	4.4	0.59
PLA-BL5 Fibers	60.5	113.5	143.4	148.9	0.8	0.20
PLA-NC5 Fibers	59.9	108.9	144.2	153.2	1.4	0.59

* Data for PLA-BL5 and PLA-NC5 are also obtained from DSC which are not shown in Figure 24

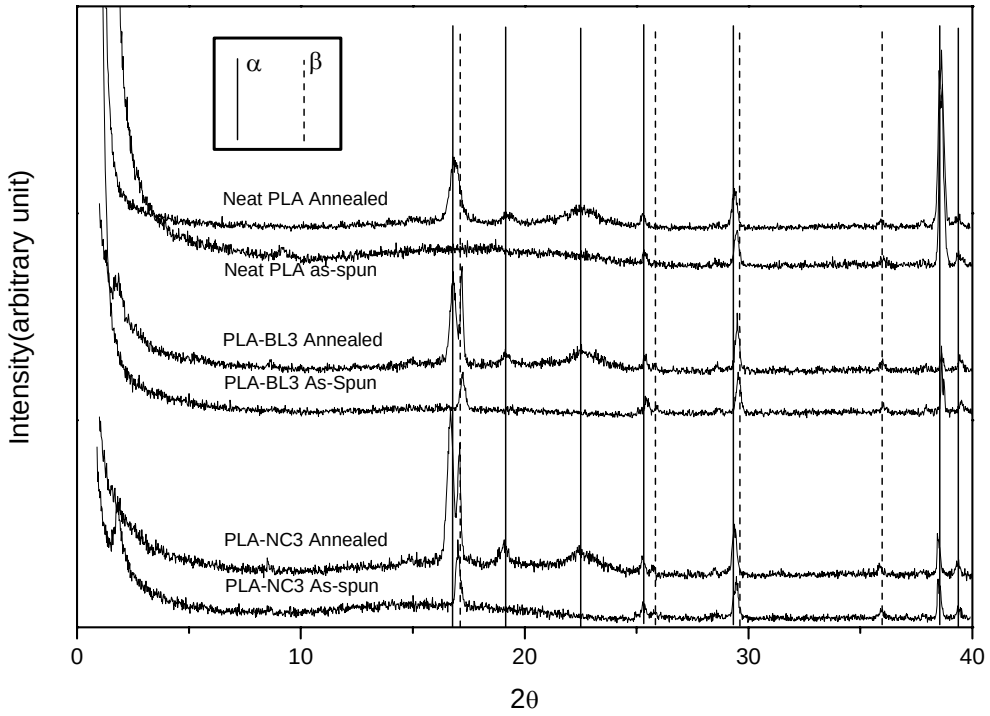

Figure 25 XRD patterns of various electrospun PLA fibers before and after annealing at 120 ^{o}C for 3hours

The existence of β structures can also be verified by the XRD study. The electrospun PLA and PLA nano-composite fibers are annealed at 120°C for 3 hours and the XRD patterns of samples before and after the annealing are shown in Figure 25. Peaks marked by dotted lines belong to the β crystal structure [127]. It is observed that electrospun fibers exhibit a peak associated with the β structure at 2θ = 29.5° (orthorhombic (330) or (003) reflection) and nano-composite fibers exhibit significant β peak at 2θ = 17.2^{o} (orthorhombic (200) reflection). Meanwhile, the XRD patterns of annealed fibers show a significant increase in both α and β crystals. The intensity of the α peak at 2θ = 16.8° (pseudo-orthorhombic (200) or (110) reflection) and that of the β crystal peak at 2θ = 17.2° are increased significantly after annealing. Finally, we note that after annealing the β peak at 2θ = 29.5° shifts to 2θ =29^{o} which can be for the

α structure (pseudo-orthorhombic (216) reflection). This may indicate the chain relaxation of the β crystal and its transformation into the α crystal since the α form is the more stable phase. Similar transformation has been observed the nylon fibers [137]. The transformation of crystal structures will be discussed using temperature-dependent XRD studies in the melt electrospinning section.

The DSC thermograms and XRD patterns of PLA and PLA/nanoclay nanofibers suggest that the β structure of PLA is formed during the electrospinning process and that the presence of highly aligned nanoclays enhances the formation of the β structure.

3.4 Nanoclay Effect on Fiber Mechanical Properties

Nanoclay with the high strength and high modulus enhances the general mechanical properties of polymer materials. The intercalation and exfoliation of nanoclays makes the composite material even stronger. In our electrospun PLA nano-composite fibers, the morphology of intercalation and partially exfoliation is preserved throughout the electrospinning process. The enhancement is demonstrated in Figure 26. The detailed mechanical data are organized into Table 4.

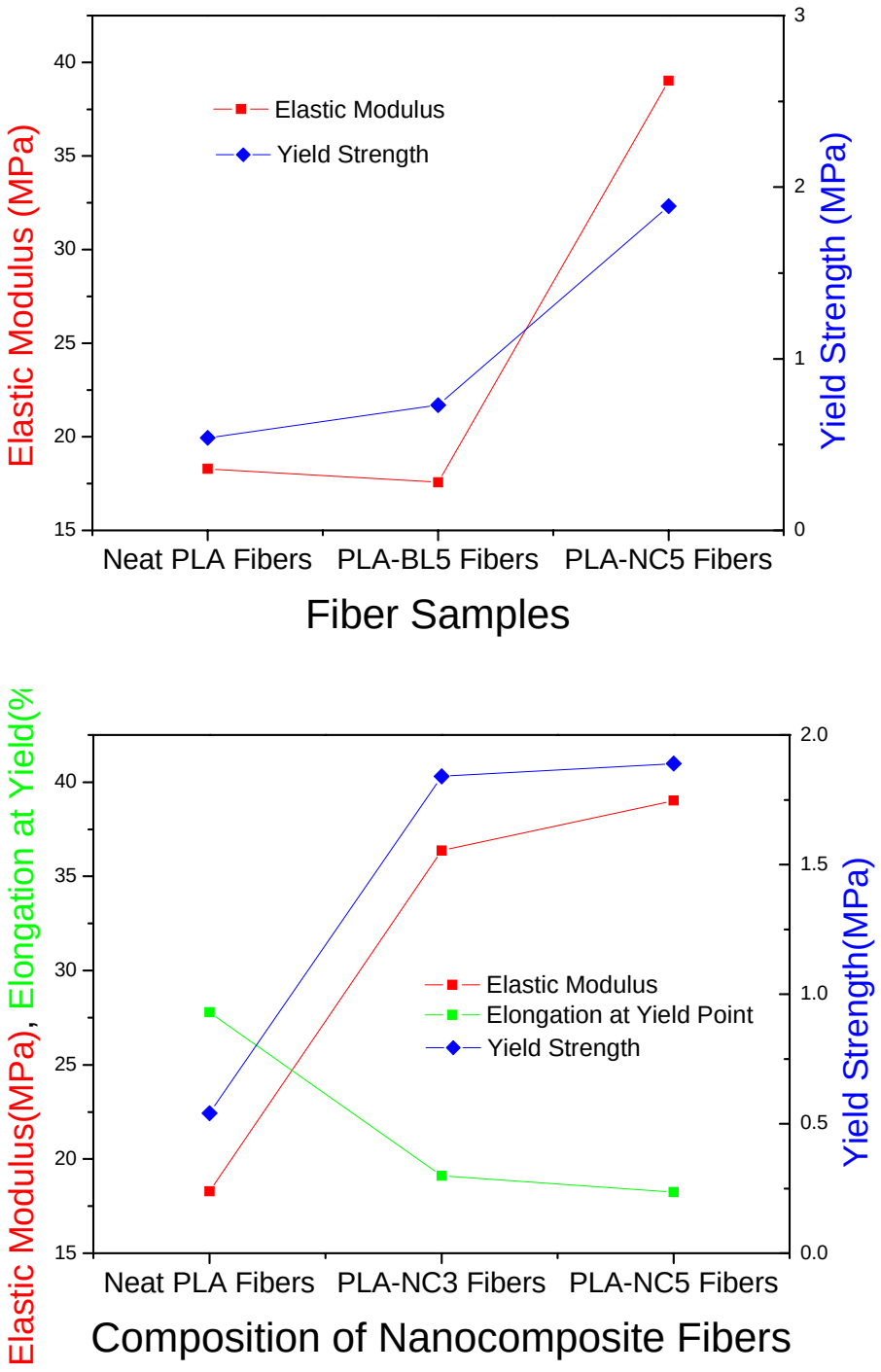

Figure 26 Mechanical properties of electrospun PLA fibers compared to its micro-composite and nano-composite fibers with different nanoclay concentrations

Table 4 Fiber mechanical properties (Dr. Kim's data)

	Modulus(MPa)	*Yield Strain(%)*	*Yield Stress(MPa)*
Neat PLA Fibers	18.29	27.79	0.54
PLA-BL5 Fibers	17.56	24.11	0.73
PLA-NC3 Fibers	36.36	19.11	1.84
PLA-NC5 Fibers	39.03	18.25	1.89

For the same amount (5 wt%) of nanoclays in PLA fibers, micro-composite fibers show slightly higher yield stress and no significant affect on the modulus. At the same time, flexibility is decreasing according to the elongation at the break. Due to the intercalated structures, nano-composite shows an over 100% increase in elastic modulus and around 250% increase in yield modulus at the compensation of 30% loss in flexibility. For the nano-composite fibers with different amount of nanoclays, the general trend is that the elastic modulus and yield strength increases with increasing nanoclay while flexibility decreases accordingly. As nanoclay content exceeds over 3 wt%, the increase is gradually saturated.

3.5 Nanoclay Effect on Fiber Biodegradability

Figure 27 shows the hydrolytic degradation behavior of PLA and its nanocomposites. Electrospun non-woven fiber mats show lower weight losses than cast films at first four weeks but faster degradation after four weeks. The high surface area to volume ratio of the fiber mats and their low degree of crystallinity may contribute to this improvement. The reason for the slow degradation at the initial stage could be caused by the highly tensioned surface of the fibers due to the strong shear. When this tensioned layer hydrolyzed, degradation of electrospun fibers with relative

low crystallinity sped up. The drastic increase in hydrolysis rate is caused by the large surface area of the fiber samples. However, the inclusion of nanoclays appears to slow down the degradation partly due to the increase in crystallinity (Figure 28). And we also notice that as time passes amorphous domain is hydrolyzed gradually and crystallinity of the sample increases drastically which leads to an equilibrium state of the degradation. And nano-composite shows relatively higher crystallinity and has the lowest weight loss among all the fiber samples. Also comparing the change of crystallinity among cast films, the differences among them are not as significant as the fiber samples which accounts for the similar degradation behavior of the cast film.

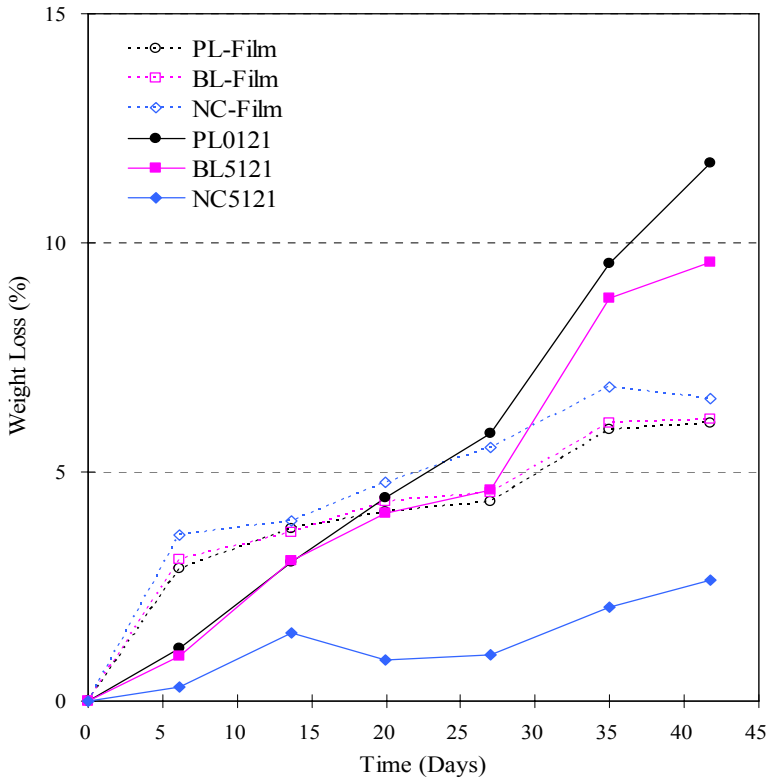

Figure 27 Hydrolytic degradation of PLA and its nanocomposites cast films and electrospun non-woven fiber mats

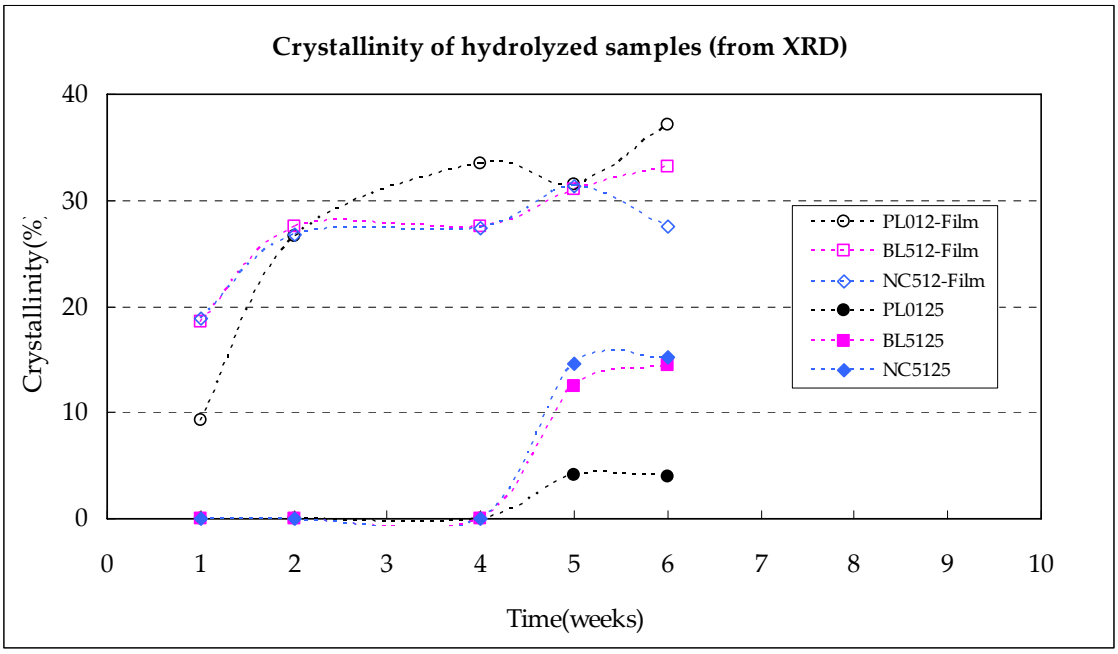

Figure 28 Degree of crystallinity of hydrolyzed films and non-woven fiber mats of PLA and its nano-composites

CHAPTER 4

ELECTROSPINNING OF PLA FIBERS FROM MELT*

As we discussed earlier in the comparison between melt electrospinning and solution electrospinning. Some underlying difficulties in melt electrospinning include a high temperature setup, high viscosity and low conductivity of polymer melts. In addition, a major drawback of melt electrospinning is that resulting fibers tend to be relatively thicker than those from solution electrospinning. Except these drawbacks, melt electrospinning offers great advantages over solution electrospinning such as no involvement of solvent which can be toxic et al. The residue solvent in the as-spun fibers was measured to be 3 wt% of the fiber mass for all PLA fibers. The exclusion of any cytotoxic solvent is critical for biomedical applications.

However the studies on melt electrospinning so far are so limited that only a few issues have been addressed regarding this technique. In the 1980's Larrondo and Manley devised the first melt electrospinning setup [12-14], but the instabilities to cause thinning of the jet via the whipping motion had not been explored. Lyons and co-workers [97, 98] studied the effect of processing parameters on the fiber size of polypropylene and found that the molecular weight is crucial to the final fiber diameter. Dalton et al. [101] studied melt electrospun PEO-block-PCL with PCL fibers as a tissue scaffold. But only effect of flow rate was reported. Key processing parameters such as nozzle size, nozzle temperature and spinning temperature have not been explored.

In Chapter 3, we have done structural studies on electrospun fibers of PLA from solutions, we found that molecular structures of electrospun nanofibers are

* Zhou HJ, Green TB, Joo YL. Polymer 2006; 47 (21): 7497-7505

significantly influenced by electrospinning conditions, inclusion of nanoclays and post-spinning processes, mostly annealing. Highly oriented structures of PLA, which give rise to the formation of a fibrillar β crystal, were observed in solution electrospun fibers. In this chapter, we will present the effects of processing parameters such as temperature at the nozzle and in the spinning region on melt electrospinning and demonstrate that sub-micron fibers of PLA can also be produced directly from melt. Thermal properties and structural changes of fibers upon annealing are carefully investigated. The effects of nanoclay on the processing and structures of fibers are briefly discussed. In the end, PLA nanofibers are directly electrospun on to filter media, and a drastic enhancement in collection efficiency of sub-micron sized dust particles is demonstrated.

4.1 Experiments

Experimental setup and materials used has been described in details in Chapter 2. It contains four temperature zones: polymer melt reservoir (T_1), a nozzle heater (T_2), a heated guiding chamber (T_3) and a temperature controllable collector (T_4).

In the melt electrospinning experiments, PLA resins were put in a 5 mL syringe and heated for half an hour in the shielded heating unit at 200^{o}C. The micro-flow controller then fed the PLA melt through a nozzle. The temperature of the nozzle ranged from 175^{o}C to 255^{o}C. The charged melt jet was spun either with or without the heated guiding chamber before being collected on an air-cooled copper collector. Collected non-woven PLA fiber mats were then subjected to characterizations.

Rheological tests were done on a Rheometrics Dynamic Analyzer (RDA II). Processing parameters, such as nozzle temperature, nozzle size, spinning temperature, electrical field and flow rate, were then studied in separate electrospinning experiments. First nozzle temperature (T_2) was varied and other processing parameters

were kept as T_1 = 200°C, $T_3 = T_4$ = 25°C, Q = 0.01 mL/min, V = 20 kV, d = 10 cm and Dnozzle = 0.16 mm. Second the effects of nozzle size were studied using four different inner diameters: 0.84 mm, 0.31 mm, 0.16 mm and 0.13 mm. Other parameters remained the same throughout this study: T_1 = 200°C, T_2 = 220°C, Q = 0.01 mL/min, V = 11 kV, d = 10 cm and $T_3 = T_4$ = 25°C. Experiments on the effects of spinning temperature were designed by varying T_3 at four different temperatures: 25°C, 50°C, 60°C and 80°C, keeping constant T_1 = 200°C, T_2 = 255°C, T_4 = 25°C, Q = 0.005 mL/min, V = 30 kV, d = 10 cm and Dnozzle = 0.16 mm. Finally spinning distance and flow rate was adjusted to study the effect of electrical field and flow rate separately keeping constant $T_3 = T_4$ = 25°C.

To probe the motion of the PLA melt jet during electrospinning, a high speed camera (MotionPro HS-3, Redlake) was utilized. A close-up high speed (1000 to 5000 frames per second) movie of the PLA melt jet near the collector was taken at various spinning temperatures, and selected digitized images are taken to demonstrate the effect of spinning temperature on the whipping motion of the melt electrospun jet.

To study the degradation of PLA molecules during electrospinning, the molecular weight of PLA before and after spinning was measured from the intrinsic viscosity with dilute PLA in chloroform solutions at 25°C. Morphologies of electrospun fibers were examined by scanning electron microscopy (Leica 440). The thermal properties of melt electrospun fibers were analyzed by differential scanning calorimetry (Seiko, DSC 220C). Structural study was performed through a polarized light microscope (BX51, Olympus Japan) and XRD (Scintag, Inc. Theta-Theta Diffractometer). The collection efficiency of dust particles in air was also measured.

4.2 Rheological Properties of PLA and its Nanocomposite Melts

The melt electrospinning process is strongly influenced by the viscosity of the polymer melt which is typically higher than that of solutions. Therefore, it is important to investigate the rheological behavior of the polymer melt at various temperatures in order to select an appropriate processing temperature. The results of our rheological studies show that the average viscosity of PLA melt is 1-2 orders of magnitude higher than that of typical PLA/chloroform solution, and PLA does not exhibit a strong shear thinning over a wide range of shear rates (Figure 29) [138, 139]. The temperature dependence of the shear viscosity for the PLA melt is determined by plotting the logarithm of the zero shear viscosity versus $1/T$ (inset in Figure 29). The zero shear viscosity is sensitive to temperatures [140] and follows the Arrhenius equation in which activation energy is 83.8 kJ. At the temperature around 240^{o}C, the zero shear viscosity of the PLA melt is 120 Pa•s which is closer to that of some spinnable polymer solutions (117 Pa s for 7.77wt% poly(p-phenylene biphenyl tetracarboxamide acid) in dimethyl acetamide [87]). A wide range of melt temperature (180 ~ 255^{o}C) below the thermal decomposition temperature (330^{o}C) was applied to investigate its effect on electrospinning. It should be noted that only the nozzle temperature was kept at higher temperature up to 255^{o}C, while the melt reservoir temperature was always kept at 200^{o}C since PLA is prone to degradation at a temperature 10^{o}C above its melting temperature without stabilizers [141-143]. Through this approach, we can minimize the possibility of chemical decomposition during melt electrospinning, while achieving low viscosity at the nozzle. The resident time of the melt in the nozzle is estimated to be less than 0.1 sec for a nozzle with ID of 0.16 mm at the typical flow rate of 0.005 mL/min.

Compared to neat PLA melt, the zero shear viscosity of PLA-NC3 at each temperature is higher due to the inclusion of nanoclays. One noticeable issue for the

nanocomposite is that at small shear rate viscosity tends to rise up, which could mean that the initiation of the melt jet could be difficult due to the high viscosity. And this phenomenon was actually observed during our experiments. For electrospinning, characterization of shear viscosity only accounts partially for the processability of the polymer. To make a continuous jet, elongational viscosity needs to be high enough.

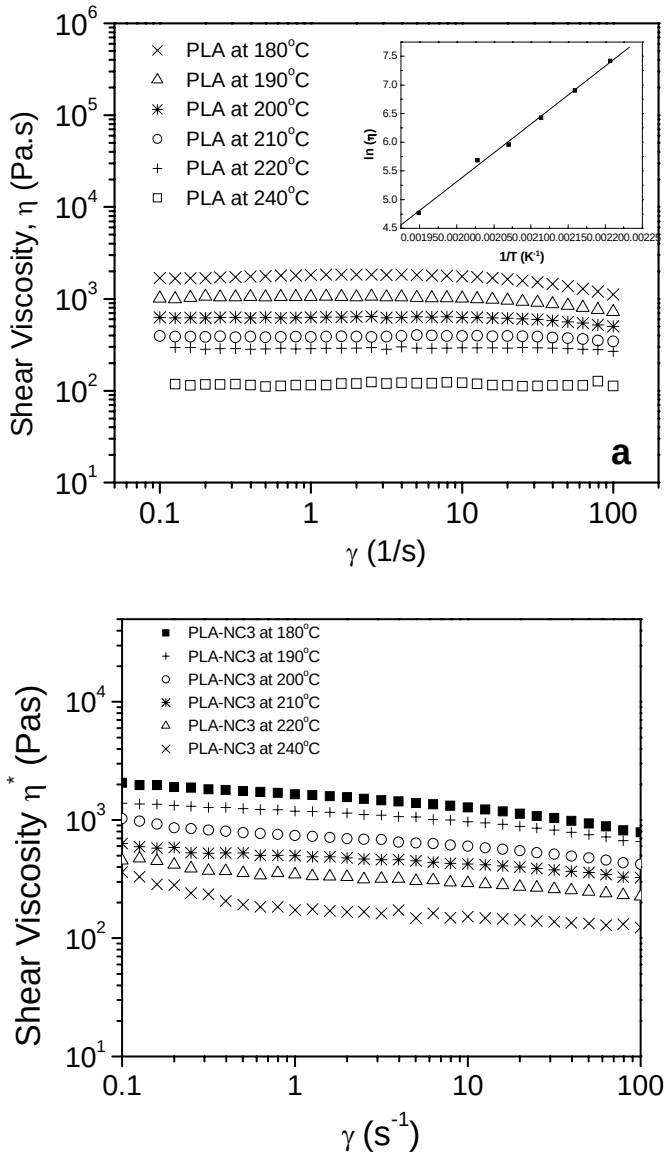

Figure 29 Shear viscosity and its temperature dependence of a) neat PLA and b) PLA-NC3 melts

4.3 Micron-sized PLA Fibers from Melt Electrospinning

Without the optimization of the processing of melt electrospinning, fiber size is typically above one micron size. Most of studies on melt electrospinning of polymers with relatively high molecular weight produced 10 micron scale fibers. The same thing happened to our study.

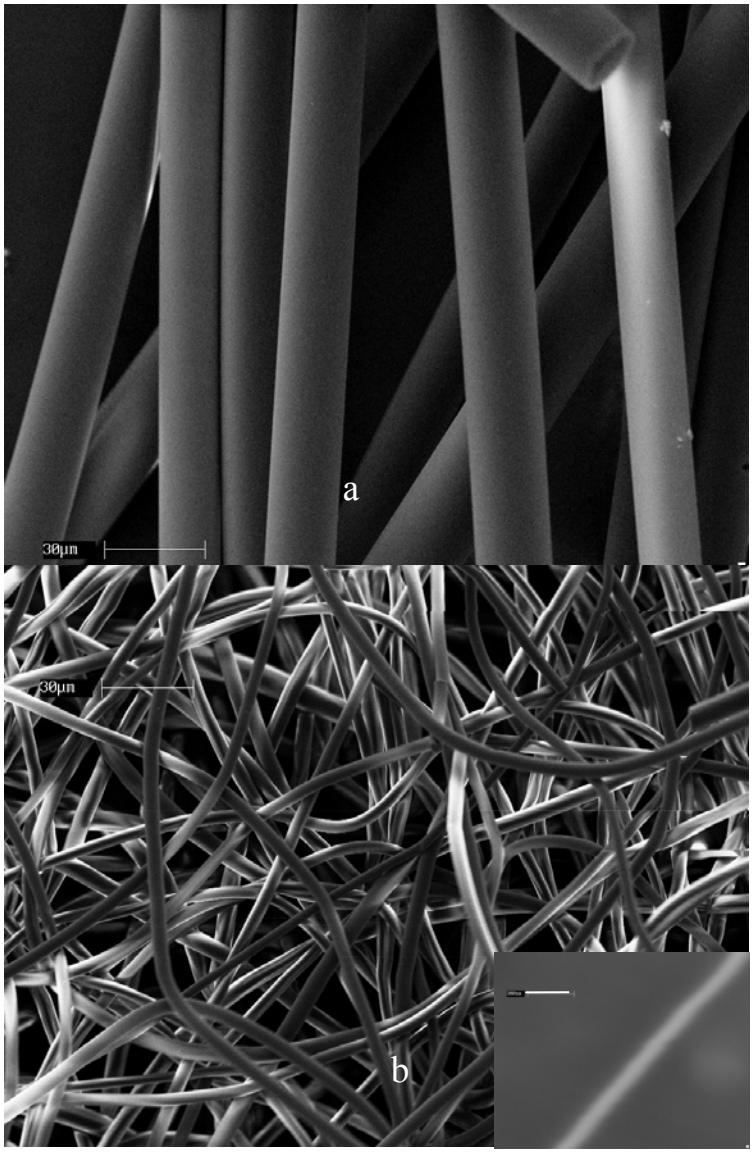

Figure 30 SEM micrographs for neat PLA fibers produced a) without heating the guiding chamber T_3=25°C and b) with guiding chamber at T_3=100°C

Figure 30 shows the PLA fibers collected using a 18 gauge needle, flow rate at 0.005 ml/min, voltage at 20 kV, collecting distance at 6 cm and T_1 = 200°C, T_2 = 220°C, T_4 = 25°C. If the temperature in the spinning region T3 is kept at room temperature and thus the ejected polymer melt jet is nearly quenched, thicker fibers are formed (Figure 30a). The average diameter of fibers spun at room temperature is 15 μm which is about three times as thick as that of fibers with T3 at 100°C under the same processing condition. For the case of T3=100°C, water cooling was employed to keep the collector temperature at 25°C. It is also observed that the fiber diameter steadily increases with increasing flow rate in the range investigated in the current study. It should be noted that compared to previous studies on melt electrospinning [97-98], the size distribution of melt electrospun fibers in the current study is relatively uniform possibly due to the precise temperature control in various regions in the process. However when T3 is raised to 100°C, variation of fiber diameter starts to increase.

The internal structure of melt electrospun PLA nanocomposite fibers obtained using above conditions is quite different from that of solution electrospun fibers. More exfoliated structures are observed in the TEM micrograph of melt electrospun nanocomposite fibers (Figure 31a). The picture also shows skin-core morphology of the fibers, in which nanoclays are aligned along the fiber axis but the extent of their alignment varies along the radial direction. The skin area exhibits a higher degree of alignment than the core region. In addition, the dispersion of the nanoclays is quite non-uniform in the transverse direction. The absence of solvent and large radial thermal gradient in melt electrospinning can induce such inhomogeneity. This skin-core differentiation can also be manifested by the SEM micrograph of partially peeled fibers (Figure 31b).

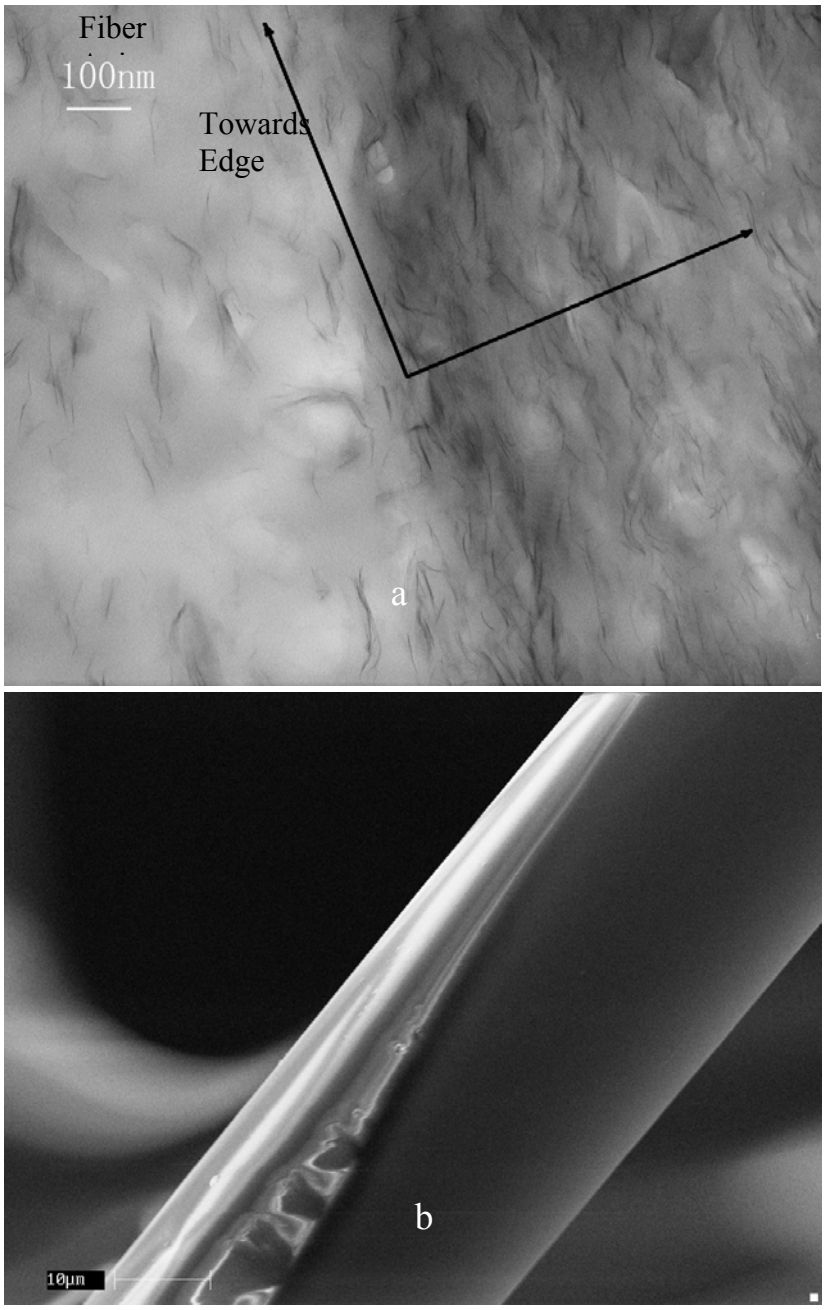

Figure 31 a) TEM micrograph of PLA-NC5 fibers microtomed along its axis and b) SEM micrograph of partially peeled PLA-NC5 fibers

4.4 Processing Conditions and Fiber Morphologies

It has been demonstrated that many parameters such as flow rate, voltage, collecting distance, solution viscosity and surface tension have effects on the fiber morphology in solution electrospinning [144, 145]. Lyons and coworkers [97] found that in melt electrospinning of polypropylene, the molecular weight and thus the shear and extensional viscosity of the melt plays a significant role in obtaining smaller sized fibers. In the present study, we focus on the non-isothermal effects on the fiber morphology by changing the temperature at the nozzle and in the spinning region.

4.4.1 Whipping Motion of the Melt Jet

Numerous studies and models [146-149] have confirmed that the whipping motion of the jet in solution electrospinning causes drastic stretching and consequently thins the fiber. However, the presence and characteristics of the whipping motion in melt electrospinning have not been explored. In this section, we report the effect of the spinning temperature on the jet motion and provide an insightful view of the motion of the polymer melt jet during electrospinning. To this end, a high speed camera was utilized to closely probe the motion of the PLA melt jet in the spinning region. A series of snapshots was taken and (a) the emergence of a limited jet vibration at low spinning temperature (T_3 = 25^{o}C), as we increase the spinning voltage, and (b) the vigorous whipping motion at high spinning temperature (T_3 = 80^{o}C) are shown in Figure 32. Other experimental conditions including T_1 = 200^{o}C, T_2 = 255^{o}C, Q = 0.05 mL/min, d = 10 cm, T_4 = 25^{o}C, D_{nozzle} = 0.84 mm are kept constant for both cases.

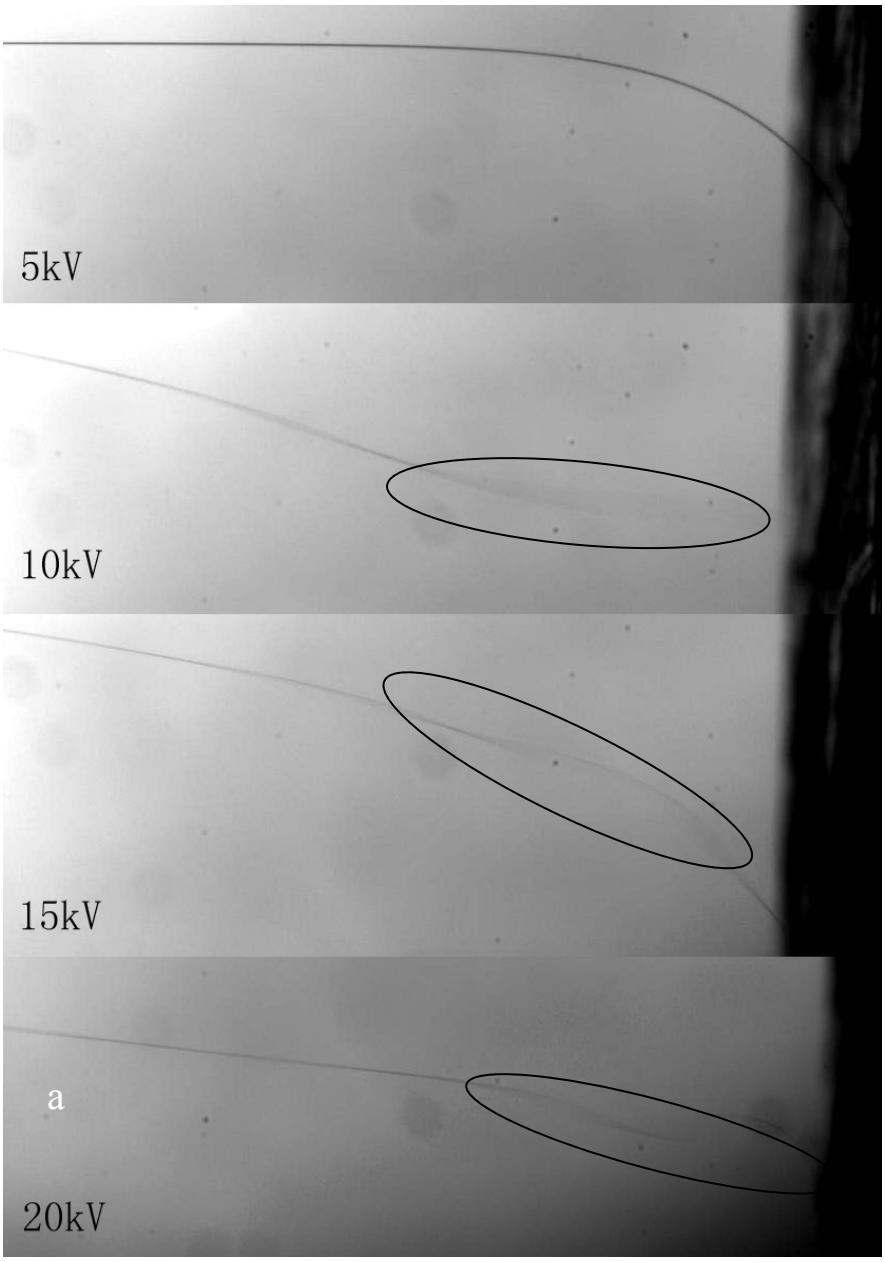

Figure 32 Effect of voltage on (a) the jet motion at T_3 = 25°C and Q = 0.05 mL/min (the limited whipping is pointed out in the oval), and (b) the whipping motion at T_3 = 80°C. The last image at high spinning temperature is for a small flow rate (Q = 0.02 mL/min)

Figure 32 (Continued)

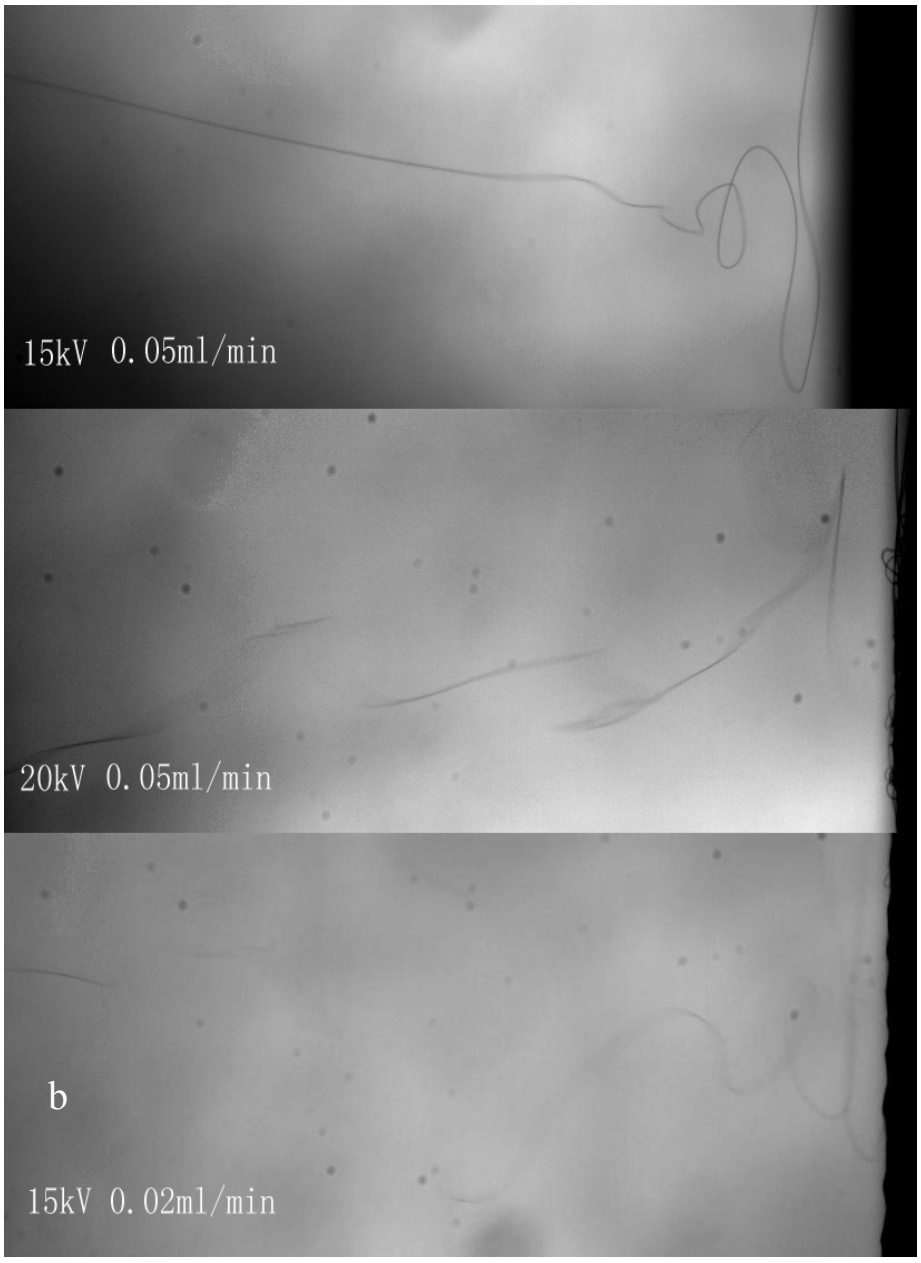

It should be noted that in Figure 32a, the image for V = 5 kV was taken at a frame rate of 100 fps, while all others were taken at the frame rate of 1000 fps since the melt jet at V = 5 kV moves relatively slow compared to other cases. All pictures in Figure 32 (b) were taken at the frame rate of 2000 fps due to the strong and fast whipping motion. The dark area on the right in each image is the collector. The PLA melt jet at V = 5 kV has a smooth contour and when the critical voltage 10 kV is reached, the jet starts to vibrate locally near the collector. As a higher voltage is applied, the vibration strengthens and at 20kV it evolves into a fast spiral movement (whipping). However the whipping is much weaker and localized compared to that in solution electrospinning [148]. In the case of low spinning temperature, fast solidification of the jet is believed to suppress the whipping motion. When spinning temperature (T_3) is raised to 80^{o}C, a much stronger whipping motion appears (Figure 32b), which may result in the reduction in fiber diameter, as discussed in the following section. A high spinning temperature above the glass transition temperature can prevent the melt jet from solidifying before reaching the collector. In addition, the strong whipping motion extends the residence time of the jet in the spinning region, enabling the melt jet to go through thinning for a longer period of time. A higher voltage results in even stronger but a more irregular whipping motion as in solution electrospinning. It is also observed that at a low flow rate the whipping motion becomes more vigorous.

4.4.2 Effect of Nozzle Temperature on Fiber Diameter

One of the most imperative issues in melt electrospinning is how to obtain sub-micron scale fibers. Hence, we have investigated the effects of various processing parameters on the average fiber diameter. Figure 33 shows the effects of nozzle temperature on the fiber diameter of melt electrospun PLA fibers. As nozzle temperature increases, both average fiber diameter and standard deviation decrease,

and the curve eventually levels out at higher nozzle temperature. According to a recent study on electrically driven viscoelastic fluid flow by Carroll and Joo [33], increasing the fluid viscoelasticity causes a more rapid initial jet thinning. However farther away from the spinneret, viscoelastic jets are thicker than their Newtonian counterparts due to the higher elongational viscosity. On the other hand, the viscosity of the polymeric liquid mainly influences the initial jet thinning. When spinning and collector temperatures were kept low (T3 = T4 = 25^{o}C) such that the whipping motion was substantially suppressed, their results in the stable jet region during electrospinning can be utilized to explain the decrease in fiber diameter with increasing nozzle temperature observed in the current study: The increase in melt temperature decreases the viscoelasticity and thus the final jet gets thinner with increasing nozzle temperature. Nozzle temperatures above 255^{o}C are not applicable because the melt strength is not enough to maintain a continuous jet, and as a result droplets of the polymer melt were obtained. A comprehensive modeling of the electrically driven polymer melt jet which incorporates the non-isothermal aspects in melt electrospinning is currently studied by Zhmayev in Joo research group.

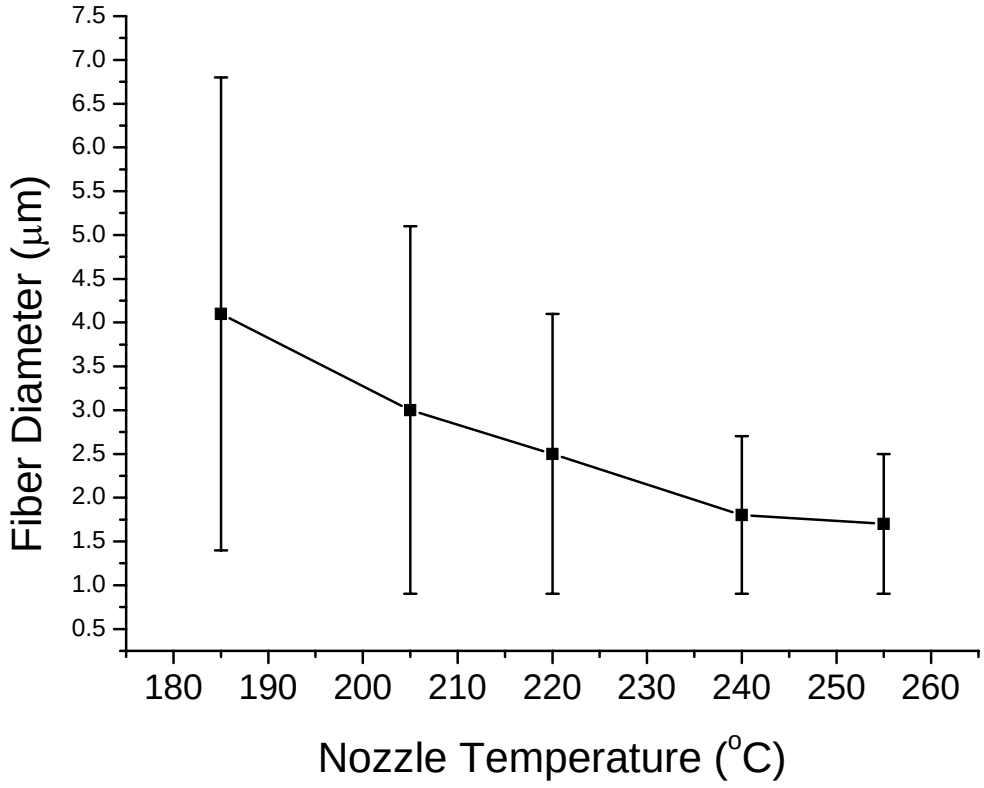

Figure 33 Effect of nozzle temperature on average fiber diameter (T3 and T4 were kept at 25°C)

4.4.3 Effect of Nozzle Diameter on Fiber Size

Studies on the effect of nozzle size are extremely limited since in solution electrospinning nozzle size is not a critical issue in obtaining sub-micron sized fibers. Sutasinpromprae and co-worker studied the effect of nozzle diameter on the PAN fibers and found that average fiber diameter increased from 310nm to 400nm using nozzle with ID of 0.47mm instead of 0.84 mm.

In melt electrospinning, nozzle size plays a very important role in achieving sub-micron size fibers. Figure 34 shows the effect of nozzle diameter on fiber size. In

general, smaller nozzle diameter gives rise to a smaller average fiber diameter which is mostly achieved by the decrease in the jet cross section. The additional result of the decreasing nozzle diameter is that melt in the nozzle is heated more homogeneously. So it is surprising that both average fiber diameter and standard deviation linearly decrease as the nozzle size decreases. When the nozzle size becomes smaller than 0.16 mm, the micro-flow controller cannot precisely control the flow rate due to a steep increase in pressure drop.

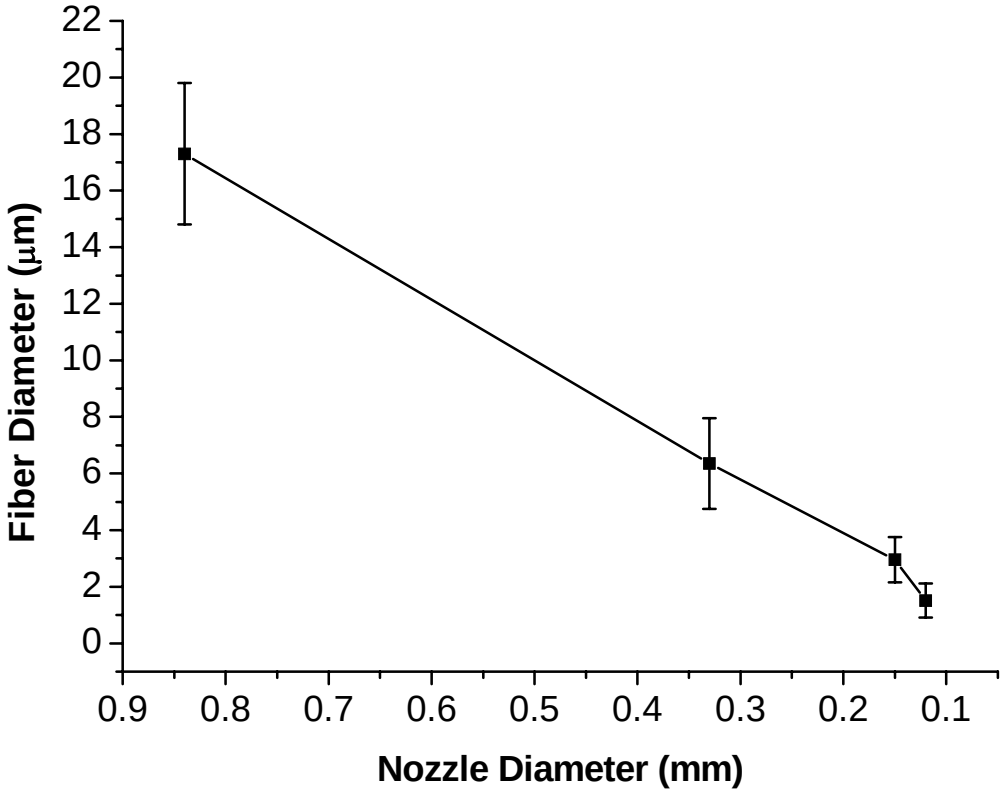

Figure 34 Effect of nozzle size on average fiber diameter

4.4.4 Effect of Spinning Temperature (T3) on Fiber Morphology

It is intuitive that increasing spinning temperature will reduce the jet viscosity and extend the stretching process thus produce smaller fibers. The diameter of resulting fibers spun at different spinning temperatures is shown in Figure 35. When spinning temperature is above the glass transition temperature of PLA ($T_3 \geq 55$), the average fiber size continues to decrease as T_3 increases. It suggests that more deformation is undertaken by the melt jet at higher spinning temperature, which is clearly caused by the strong whipping motion, as shown in high speed images. On the other hand, the stronger but more irregular whipping motion at higher temperature presumably results in the greater standard deviation of fiber size distribution.

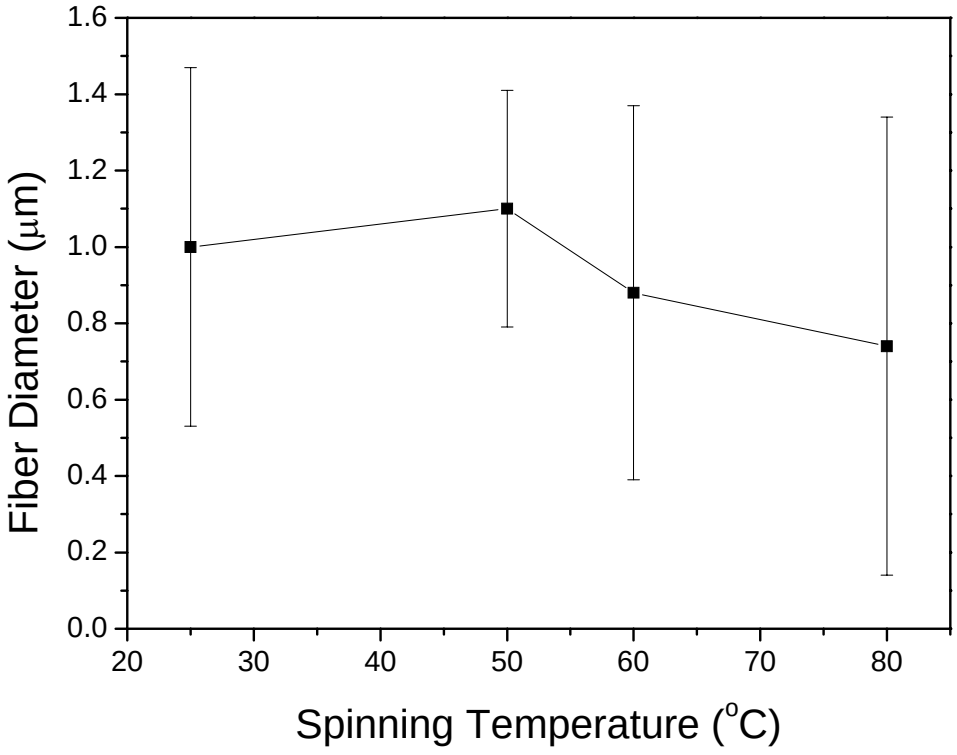

Figure 35 Effect of spinning temperature (T3) on fiber diameter

4.4.5 Effect of Voltage

The effect of voltage on solution electrospinning has been studied by many authors [150-153]. Deitzel et al. [152] studied the effect of voltage on the solution electrospinning process in a comprehensive way and found that there was no mode change for the electrospinning process with increasing voltage. Studying the jet initiation showed that at low voltages jet initiated from Taylor cone and as voltage increased, the Taylor cone receded and finally disappeared. How the voltage affects the fiber diameter can be addressed in two counteracting aspects: higher electrical field causing stronger electrical force on the jet and higher voltage causing higher flow rate due to the Taylor recession. Therefore it has been reported that the effect of voltage does not change fiber diameter significantly but there is an optimal voltage to produce the thinnest fibers.

Regarding the effect of voltage on melt electrospun fibers, it is positive according to Lyons and co-workers [97]. The diameter of PP fibers was decreased by more than 50% when electrical field was increased from 1kV/cm to 2.5kV/cm while keeping the distance at 10 cm. For melt electrospinning of PLA, the jet initiation voltage is around 5kV at 3 inches. Figure 36 shows the change of conical profile of the jet. It clearly speaks for the observation by Deitzel et al. It is worth noting that the nozzle size is 0.84 mm for the observation purpose. Results for melt electrospun PLA fibers show that as electrical field strength increases, the average fiber diameter decreases steadily (Figure 37). The average diameter of fibers collected at E = 10 kV/inch is around 800 nm with a considerable deviation and this deviation is associated with voltage.

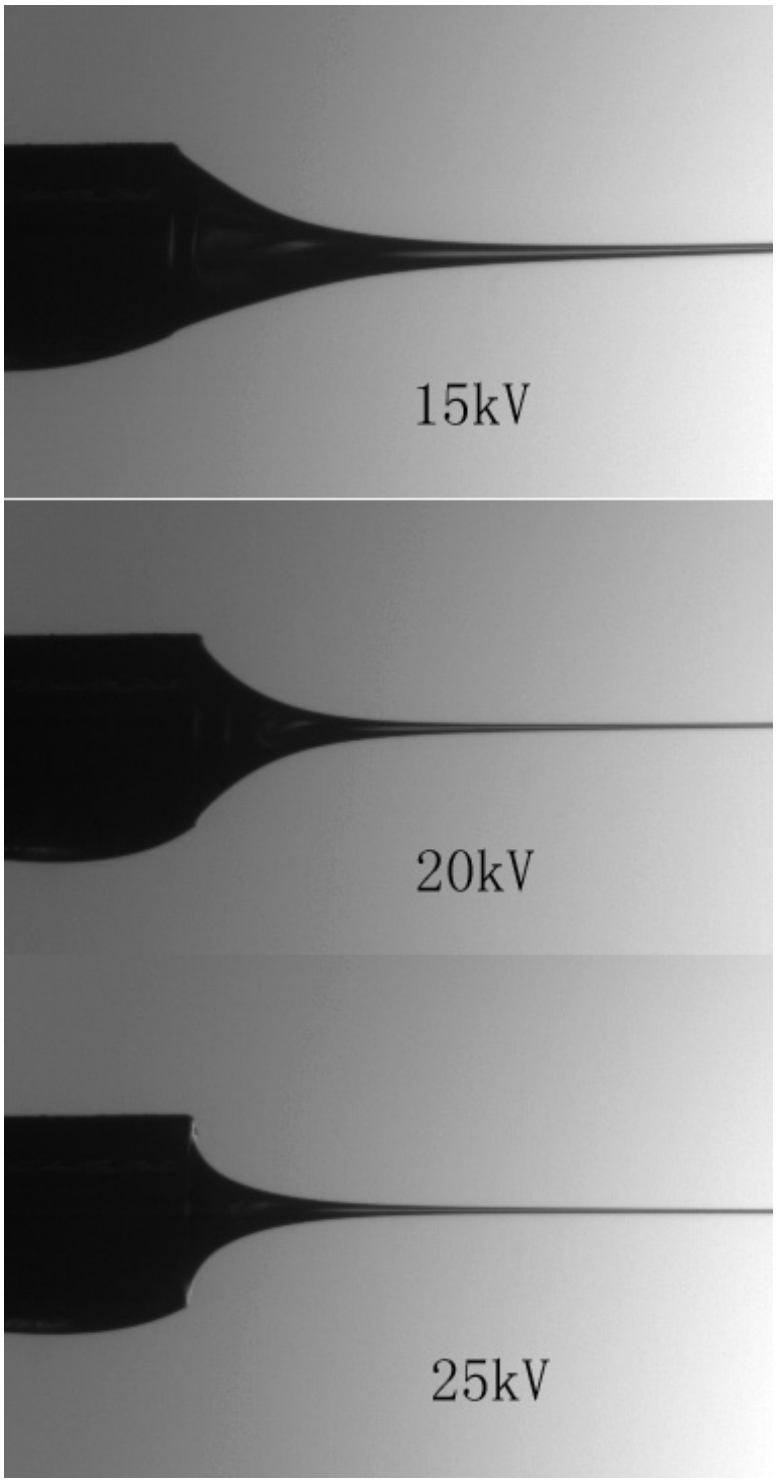

Figure 36 Effect of voltage on initial jet formation

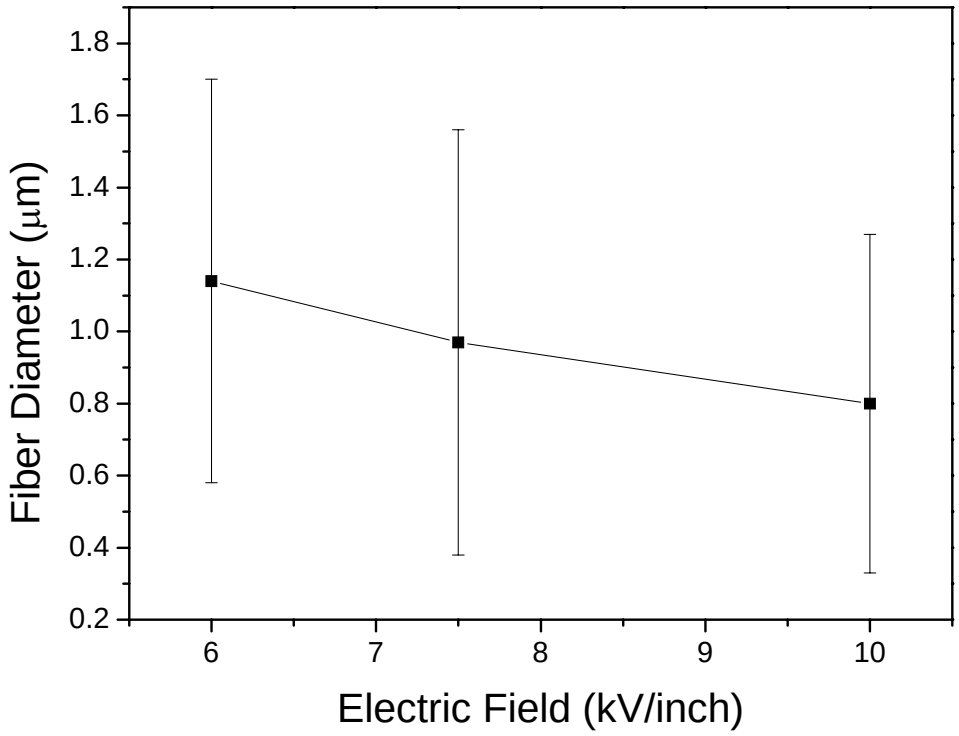

Figure 37 Effect of electrical field on average diameter of melt electrospun fibers

4.4.6 Effect of Flow Rate

To obtain small scale fibers, flow rate for melt electrospinning is almost one order of magnitude lower than for solution electrospinning. Although the flow rate in melt electrospinning is significant smaller than in solution electrospinning, attributing to the no loss in solvent mass, the yield rate at Q=0.005 mL/min is still about 50% higher than that of Q=0.02 mL/min in electrospinning of 12.5% PLA/chloroform solution.

As for the effect of flow rate, smaller fibers were achieved with decreasing flow rate. The average fiber diameter is 1.7 μm at Q = 0.01 mL/min but only 1.2 μm at Q = 0.005 mL/min. In a theoretical manner, the smallest flow rate could create the smallest

fiber. However, the effect of viscoelasticity and continuity issue limits the lower boundary of the flow rate.

The electrospinning parameters that were altered and the results of these experiments are summarized in Table 5.

After combining all the factors considered, sub-micron PLA melt electrospun fibers have successfully been obtained (Figure 38) under the following conditions: T1 = 200^{o}C, T2 = 255^{o}C, T3 = 80^{o}C, T4 = 25^{o}C, Q = 0.01 mL/min, V = 20 kV, d = 10 cm and Dnozzle = 0.16 mm.

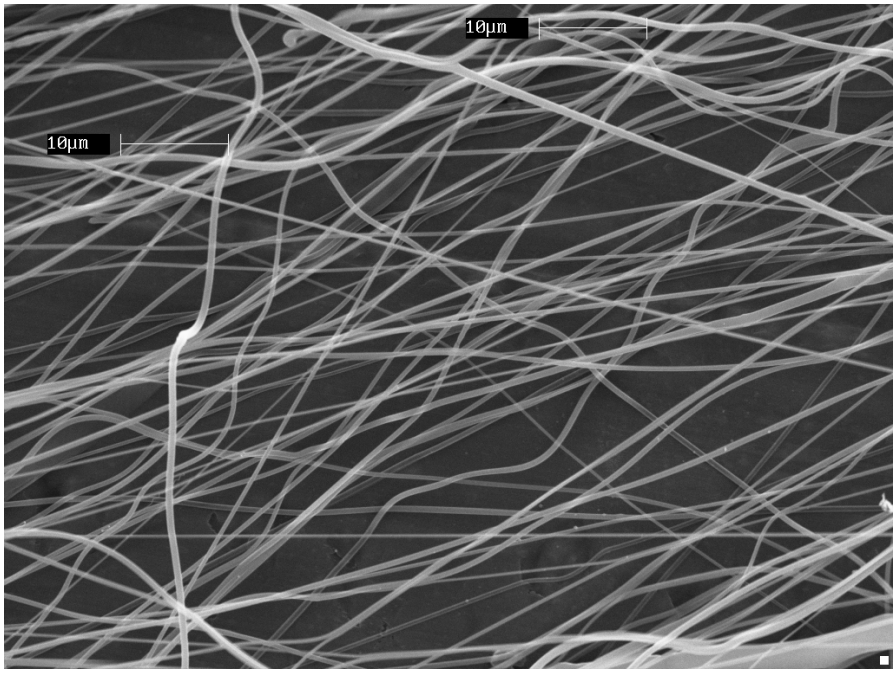

Figure 38 SEM image of sub-micron sized PLA fibers directly from its melt (fiber diameter around 800 nm)

Table 5 Summary of electrospinning parameters that were altered and the results of these experiments

Parameter varied	Parameters kept constant	Key observations
Nozzle temperature 185°C → 255°C	T1=200°C, T3=T4=25°C, Q=0.01mL/min, E=2.0kV/cm, Dnozzle=0.16mm	Decrease in fiber diameter
Nozzle diameter 0.84mm → 0.13mm	T1=200°C, T2=220°C, Q=0.01mL/min, E=1.1kV/cm, and T3= T4=25°C	Decrease in fiber diameter
Spinning temp 25°C → 80°C	T1=200°C, T2=255°C, T4=25°C, Q= 0.005 mL/min, E = 30kV/10cm, Dnozzle=0.16mm	Decrease in fiber diameter
Electric field strength 2.4kV/cm → 4.0kV/cm	T1=200°C, T2=220°C, T3=T4=25°C, Q=0.01mL/min, Dnozzle=0.16mm	Decrease in fiber diameter
Flow rate 0.02mL/min→0.005mL/min	T1=200°C, T2=220°C, T3=80°C, T4=25°C, E = 2.0kV/cm, Dnozzle=0.16mm	Decrease in fiber diameter

4.5 Degradation in Melt Electrospinning

Although the thermal decomposition temperature of PLA is around 330°C, extended exposure of PLA melt to the relatively high temperature in the melt reservoir may still cause thermal degradation. To quantify the degree of degradation before and

after melt electrospinning, the intrinsic viscosity [□] was measured, and the molecular weight, Mv is calculated by using the following equation [154]:

$$[\eta] = 5.45 \times 10^{-4} \times M_v^{0.73}$$

It is found that the molecular weight of PLA has changed from the original 186,000 to around 40,000 in the first hour of collecting, and after one hour the rate of degradation slows down for the fibers (Figure 39). Compared to bulk PLA resins at 200^{o}C, fibers undergo additional degradation during the spinning process. Two mechanisms of degradation are considered in this process: thermal degradation and mechanical scission. Thermal degradation happens in the melt reservoir and throughout the nozzle. Intramolecular trans-esterification reaction during heating is the major cause of thermal degradation for PLA below 250^{o}C [141]. Mechanical scission may take place when the melt is forced through the thin nozzle, and this effect is more prominent when a nozzle with smaller inner diameter (0.16mm) is used. We also used a nozzle with ID of 0.84 mm to collect fibers and find that fibers collected in the first hour have a molecular weight around 58,000 compared to 40,000 using the 0.16 mm nozzle. The difference is primarily caused by the different extent of mechanical scission. For comparison, the possible degradation during solution electrospinning was also investigated and it was found that no significant degradation occurred.

Although thermal degradation can be minimized by adding a thermal stabilizer [138, 142], it can be a useful means to obtain thinner fibers. However, the molecular weight has a close connection with the thermal, structural and mechanical properties. Therefore the discussion that follows is based on the fibers collected during the first 30 minutes of collecting thus with a similar molecular weight.

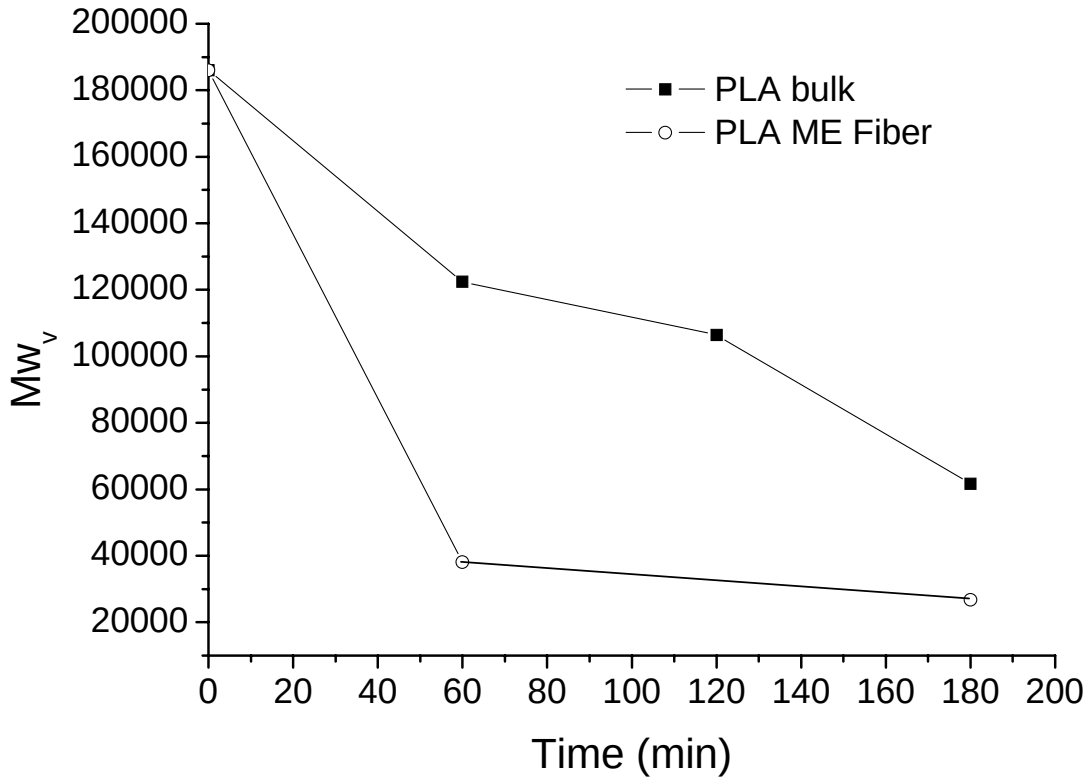

Figure 39 Thermal degradation of PLA bulk resins and melt-electrospun fibers

4.6 Thermal Properties of Melt Electrospun Fibers

The jet deformation with fast solidification during electrospinning often results in a meta-stable phase. Since PLA is a slowly crystallizing polymer and its glass transition temperature is above room temperature, fibers were collected at room temperature to study the effect of processing. This is an issue for polypropylene [97, 98] since melt electrospun polypropylene fibers cannot maintain the oriented structures at room temperature, and thus a collector cooled below its glass transition temperature by liquid nitrogen was used to keep the aligned structures.

As many articles have mentioned [26, 79, 80], PLA-related fibers electrospun from solutions usually exhibit a cold crystallization peak through DSC analysis as well as a separation of two peaks near the melting point which gives rise to different crystal structures: α structure with lamellar folded-chain morphology and meta-stable β structure with fibrillar morphology [127]. The presence of cold crystallization in solution electrospun PLA fibers has also been confirmed by the temperature dependent XRD studies in our previous work [26]. Figure 40 shows the DSC thermograms for two melt electrospun PLA fibers with different average diameters, and they are compared with PLA resin and solution electrospun PLA fibers. Melt electrospun PLA fibers with an average fiber size below one micron are produced through the 0.16mm nozzle, whereas 10 micron-sized fibers are produced through the 0.84 mm nozzle. For all the electrospun fibers from both solutions and melts, a cold crystallization peak at around 95^{o}C is observed (Figure 40). Other noticeable characteristics for electrospun fibers are a small melting peak at around 150^{o}C and a major melting peak at around 165^{o}C (α crystal). The degree of crystallinity before and after cold crystallization, χ_{bc}(%), χ_{ac}(%) and temperatures of major peaks from DSC thermograms of various PLA fibers are summarized in Table 6. Crystallinity was calculated based on the following equation

$$\chi = \frac{\Delta H_f - \Delta H_c}{\Delta H_f^0} \times 100\%$$

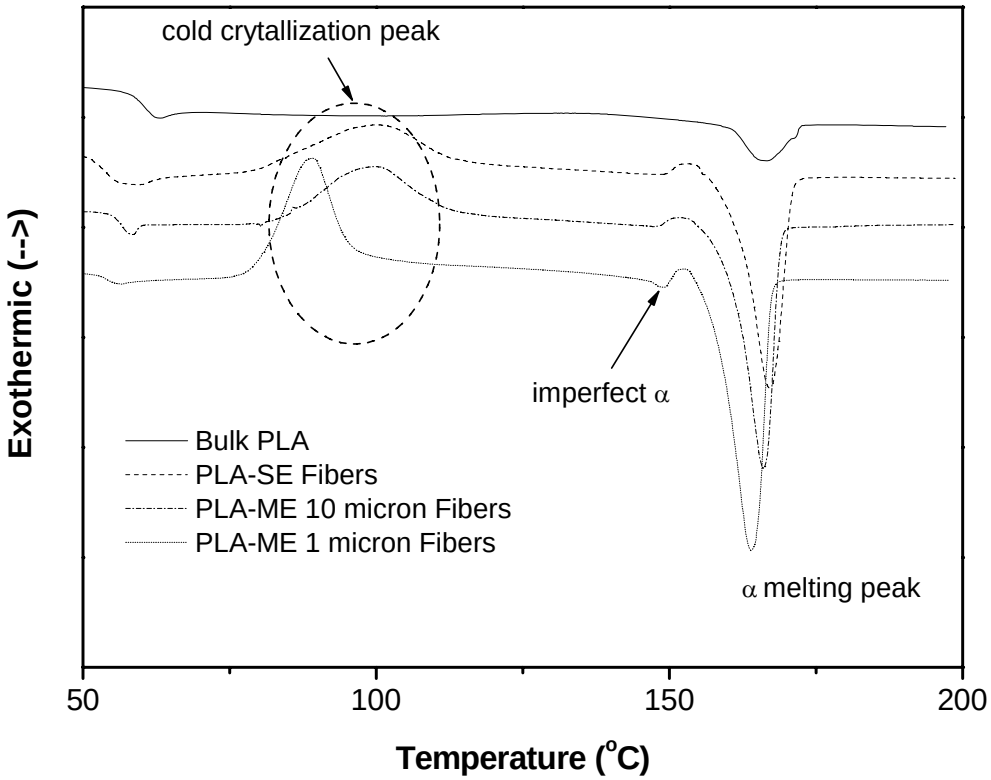

Figure 40 DSC thermograms for PLA resin and its electrospun fibers

Table 6 Summary of DSC curves for different PLA fibers

Resin/Fibers	T_c^* (°C)	T_m^α (°C)	χ_{bc}(%)	χ_{ac}(%)
Bulk PLA	N/A	167.5	46.2	46.2
PLA-SE Neat PLA Fibers	100.0	167.1	4.8	39.6
PLA-ME-1micron Fibers	88.9	163.9	5.1	49.4
PLA-ME-10micron Fibers	99.8	166.1	0.0	52.6
PLA-ME-1micron Annealed	87.9	163.4	42.6	47.0

where ΔH_f is the heat of fusion, ΔHc is the heat of cold crystallization and $\Delta H_f{}^0$ is the heat of fusion for 100% crystalline PLA, 93 J/g [133]. According to Table 6, as-spun

sub-micron sized PLA fibers exhibit a small degree of crystallinity which will be verified by XRD studies in the next section, and fibers with different average diameters exhibit different thermal properties. Thick PLA fibers (10 μm) are mostly amorphous, while sub-micron sized PLA fibers exhibit 5.1% crystallinity. After cold crystallization, the total crystallinity of both fibers rises to that of the resin. The lowering of melting temperature of thin fibers is caused possibly by additional mechanical degradation. As we have learned from the degradation study, sub-micron fibers were produced through a smaller 0.16mm nozzle which can lead to more severe chain scission and thus a lower molecular weight.

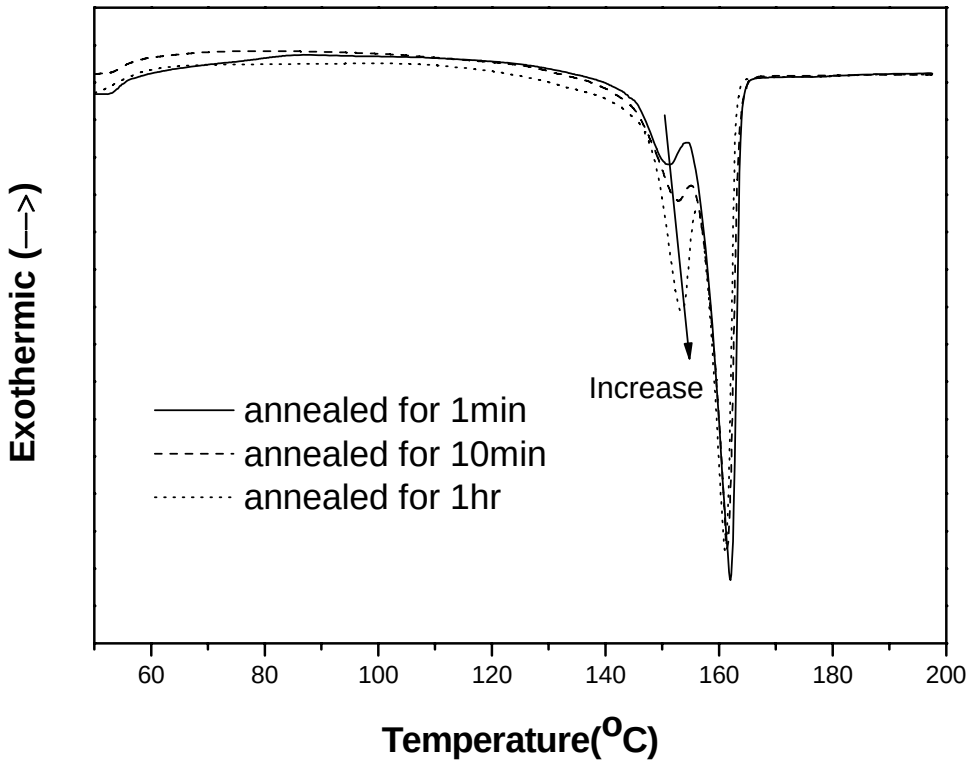

Figure 41 DSC curves of PLA-ME-1micron fibers after annealing at 100°C for various durations

To identify the unidentified peak at 150^{o}C, DSC studies of sub-micron PLA fibers annealed for various durations were carried out (Figure 41). It is observed that the peak strength around 150^{o}C gradually increases as the degree of annealing increases, while there is no indication in XRD studies that any β crystals form except for α crystals. However, the melting temperature is lower than that of normal α crystals and it usually identified as imperfect α crystal peak [155]. Besides the increase in the peak size, we note that the peak shifts towards higher temperature because imperfect α crystals start to convert into perfect α crystals as annealing time increases. Comparing as-spun PLA-ME-1micron fibers and the annealed ones, we also find that upon annealing, the cold crystallization peak almost disappears. In other words, upon annealing, most of the aligned structures have been converted into α crystal structures during the annealing process. Fibers now exhibit a higher degree of crystallinity compared to its low value before annealing. The XRD study of annealed fibers will also confirm the conversion of aligned structures into the α crystal structure in the next section.

As we mentioned in the past paragraph, cold crystallization is an important indicator to the alignment of molecular chains in fibers. Polarized light microscope is a great measure to directly observe this phenomenon. Figure 42 shows a bundle of PLA-ME-1micron fibers heated at a rate of 10^{o}C/min under the polarized light microscope. The first snapshot suggests that as-spun PLA-ME-1 micron fibers have a small degree of crystals. Upon heating, PLA fibers first undergo inverse glass transition --- relaxation at around 90^{o}C, we can clearly observe the new formation of crystals due to the cold crystallization by discerning those bright spots marked with arrows. With continued heating, more and more amorphous structures transform into crystals as temperature increases. This result of cold crystallization is in good

agreement with the temperature dependent X-ray diffraction study of solution spun PLA fibers by Zhou et al. [26].

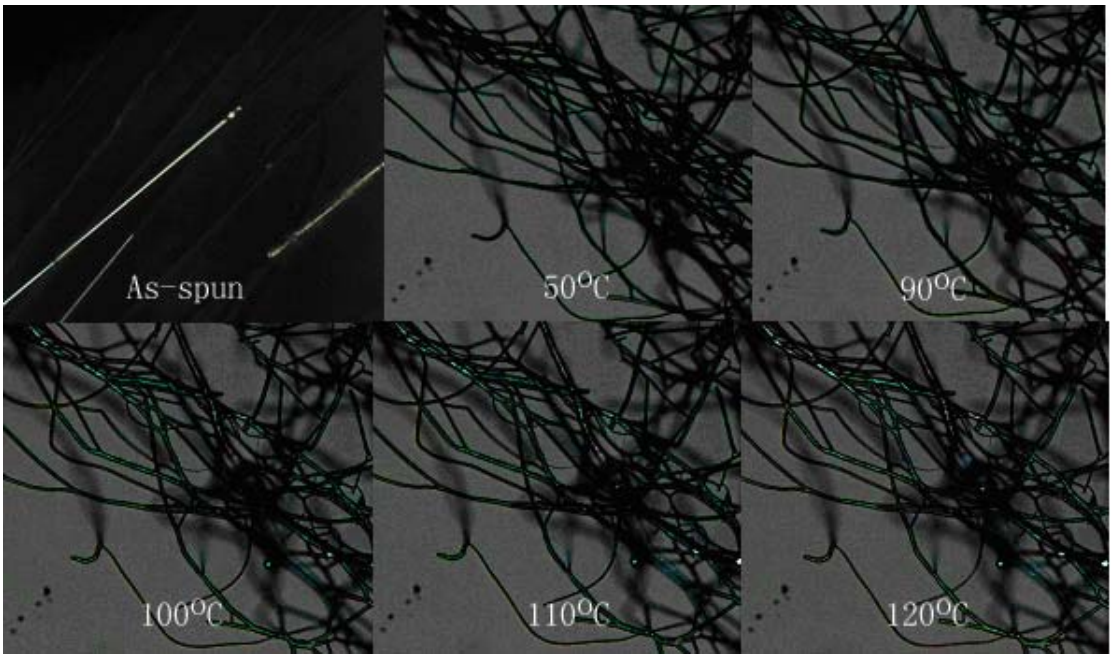

Figure 42 Microscopic views of a bundle of PLA-ME-1 micron fibers at different temperatures under polarized light microscope with a hot stage

4.7 XRD Studies and Crystal Structures

To determine the crystal structures in as-melt spun PLA fibers, X-ray diffraction studies were carried out and the diffraction patterns are shown in Figure 43. It is observed that melt electrospun PLA fibers of 10 micron scale show a strong amorphous halo, and no distinct crystal peaks are found in the diffraction patterns, on the other hand, sub-micron scale, melt electrospun PLA fibers clearly exhibit two small reflection peaks (near 26^{o} and 31^{o}) ascribed to the β crystals [154]. The formation of β crystals is caused by the different extent of deformation of the polymer

molecular chains during the melt electrospinning process [26, 127]. The critical factor for the formation of the β crystals is a high degree of deformation (a.k.a. draw ratio in literature [156]). We note that the β crystal peaks of micron sized fibers from PLA melt shift toward higher 2θ values compared with fibers from solution electrospinning probably due to different degree of stretching and deformation of crystal cell constants. The peak intensity is slightly weaker than sub-micron sized PLA fibers from solution possibly due to rapid quenching considering the high degree of cold crystallinity. Besides these two peaks, we also note that there is a broad shoulder bulging out near 22.8^{o} which can be assigned to the α crystal structure.

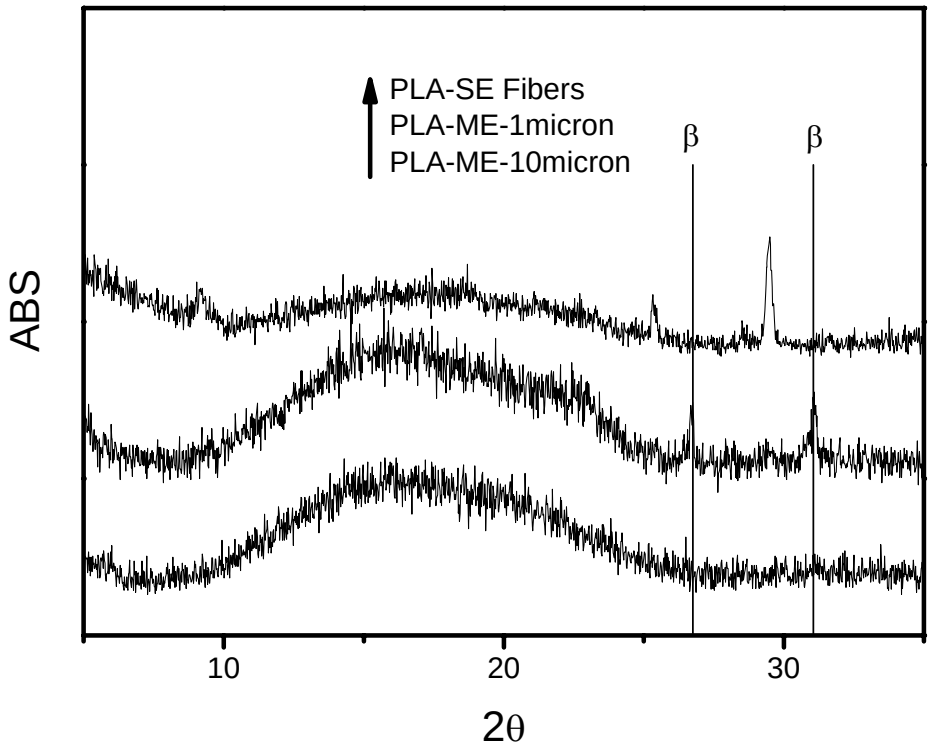

Figure 43 X-Ray diffraction patterns for PLA ME fibers

It has been reported that the β crystal structure can convert into the α crystal structure upon annealing. Two annealing tests were carried out: one at 50°C for 48 hrs and the other at 100°C for various annealing durations (Figure 44). After annealing at 50°C for 48 hrs, sub-micron PLA fibers exhibit strong α crystal peaks at 16.7° and 19°, while the β crystal peaks at 26° and 31° are almost diminished. When fibers are annealed at 100°C even for one minute, the β crystal structure completely disappears, and strong α crystal peaks form. As the annealing time increases, the strength of all α crystal peaks increases. Hence, we conclude that the small amount of β crystals converts into α crystals upon annealing and after cold crystallization, only α crystals are observed possibly due to this conversion.

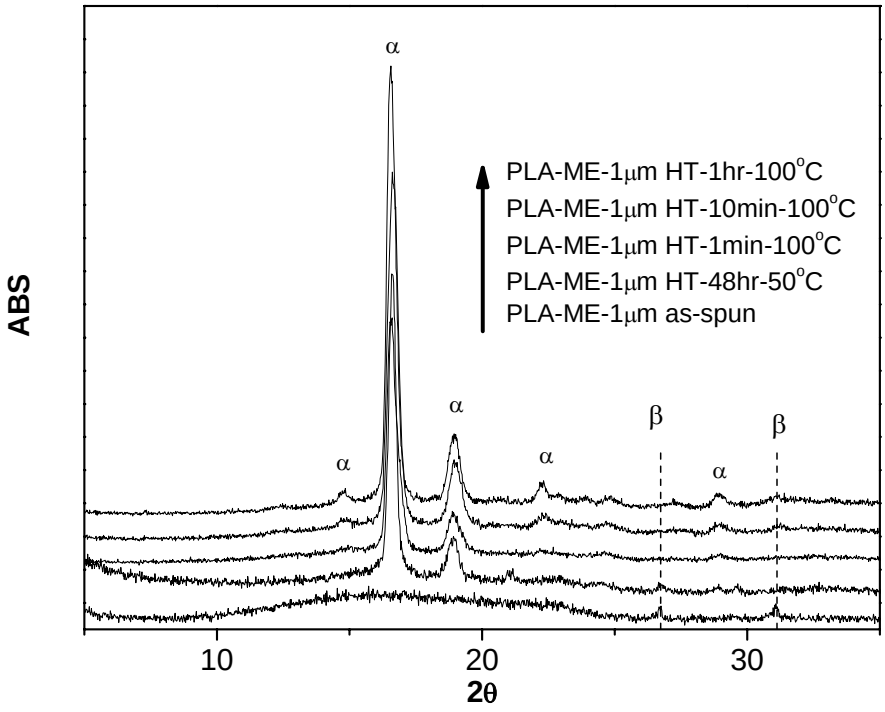

Figure 44 X-Ray diffraction patterns of a series of annealed PLA ME fibers at different conditions

4.8 Mechanical Properties of Melt Electrospun Fibers

The mechanical properties of melt electrospun PLA and its nanocomposite fibers before and after annealing are shown in Table 7. The Young's modulus of the melt electrospun fiber mats is comparable to the solution electrospun fiber mats. However the strength is much lower than that of SE fiber mat. It has been shown in the degradation study, melt electrospun fibers are the degraded PLA fibers. Taking the degradation into account, it is reasonable for melt electrospun fibers to have weaker strength. The annealing can improve the modulus and strength to certain extent. As compensation, annealed fibers are extremely brittle and break at small strain. The effect of nanoclay is not significant in the melt electrospun and it actually decreases the as-spun fiber mechanical properties mostly due to the additional degradation from melt extrusion process prior to the electrospinning.

Table 7 Mechanical properties of melt electrospun PLA and its nanocomposite fibers before and after annealing

	Modulus(Mpa)	Yield Strength(Mpa)	Break Strain
From Melt			
PLA-ME As-spun	13.0	0.38	0.34
PLA-ME Annealed	25.0	0.43	0.07
PLANC1 As-spun	7.7	0.24	0.5
PLANC1 Annealed	27.0	0.72	0.07
From Solution			
PLA-SE As-spun	12.0	0.72	0.27
PLANC1-SE As-spun	13.0	1.49	N/A

4.9 Effect of Nanofibers on Dust Collection Efficiency

To study the effect of nanofibers on dust collection efficiency, the PLA melt has been directly electrospun on to the cellulose filter media. The SEM images of melt electrospun PLA nanofibers on the filter media are shown in Figure 45. The average fiber diameter of is about 800 nm. It should be noted that a good adhesion between the melt-electrospun PLA fibers and the filter media is observed. In fact, some of the electrospun fibers are partially merged to the large cellulose fibers composing the filter media, possibly due to high spinning temperature in the melt electrospinning process.

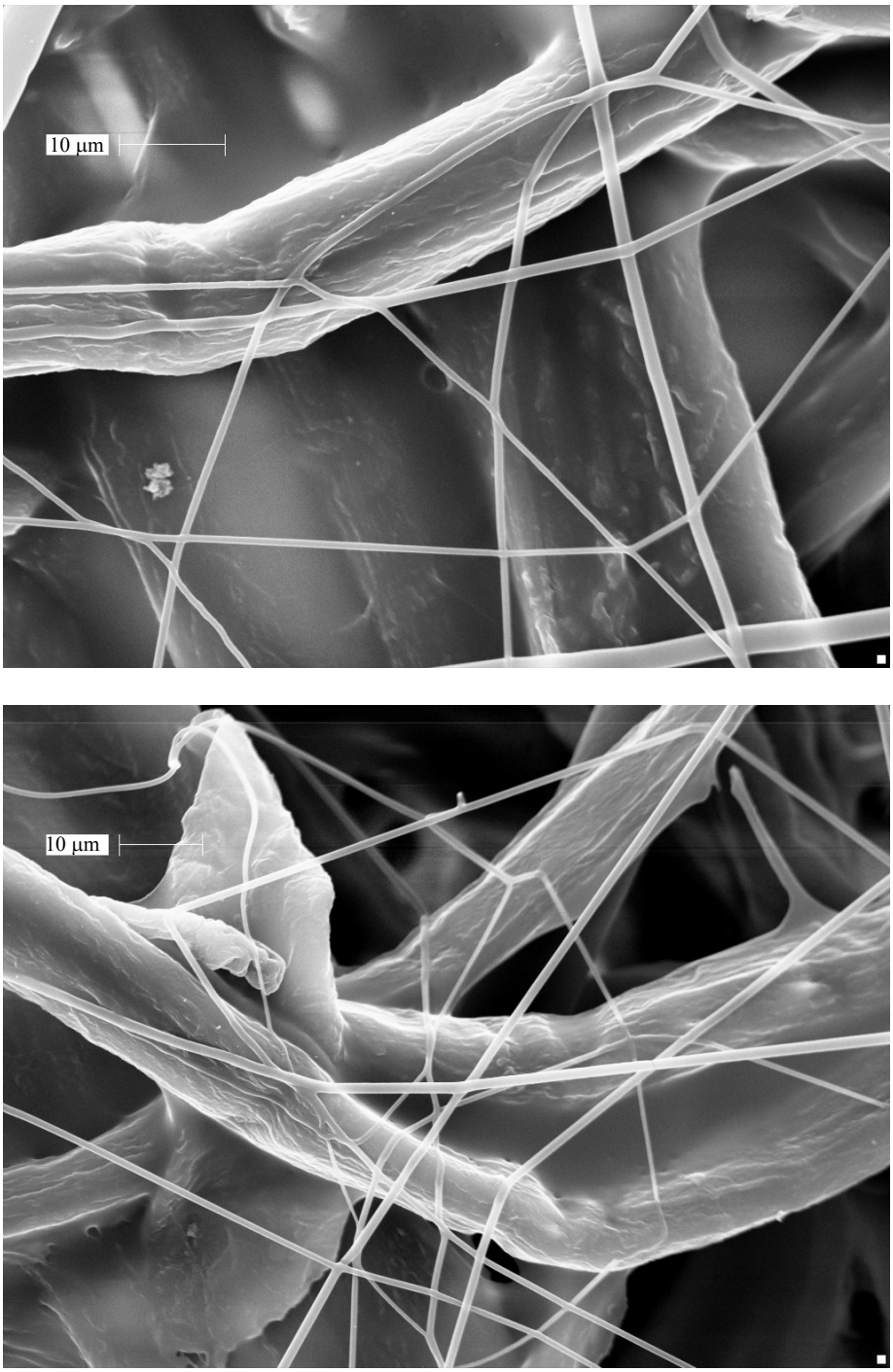

Figure 45 SEM images of melt electrospun PLA fibers collected on filter media

Finally, the collection efficiency of dust particles in air which was measured using a custom-built filtration efficiency tester is shown in Figure 46. Four filters were tested, one containing the standard filter media (12'' x 12"), two containing filter media with sub-micron fibers (0.1 g/ft^2 and 0.25 g/ft^2) and an additional filter media covered with 10 micron sized PLA fibers (0.1 g/ft^2) for comparison. It is observed that all filter media with PLA fibers display a significantly higher collection efficiency of sub-micron sized dust particles with diameters in the range of 0.03 to 1 μm. However the gain in the dust collection efficiency for filter media with 10 micron PLA fibers is coupled with an increase in pressure drop (7.5%) compared to the bare filter media; for the same coverage (0.1 g/ft^2) of sub-micron fibers, the increase in the pressure drop due to additional electrospun fibers is below 3.0%. Hence, obtaining sub-micron scale fibers is crucial to achieving enhanced filtration efficiency without a significant increase in pressure drop. The effect of sub-micron sized fibers on dust collection can be easily illustrated by the higher collection efficiency of dust particles smaller than 0.7 μm (refer to the circled region in Figure 46). Increasing the coverage of sub-micron sized fibers from 0.1 g/ft^2 to 0.25 g/ft^2 drastically increases the collection efficiency, but the percentage increase of pressure drop due to additional coverage of electrospun fibers also rises to 11.1%.

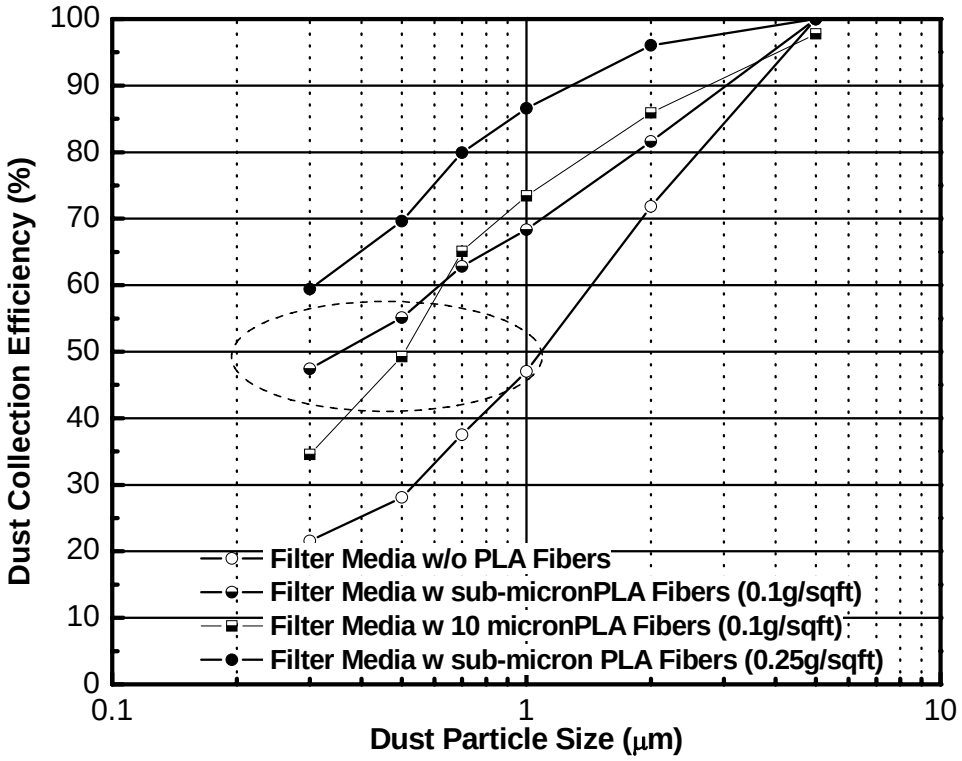

Figure 46 Dust collection efficiency of flat sheet filters with and without PLA nanofibers

CHAPTER 5

EFFECTS OF PEO IN ELECTROSPUN PLA AND PEO BLEND FIBER

Polymer blends constitutes over 30 % of polymer consumption. Since 1960s, numerous synthetic polymer blends have been discovered to achieve certain objectives. In the early years, polymer blending was aimed to achieve higher impact strength. In general polymer blends offer more advantages besides the higher impact strength. The reason of using blending [157] can be categorized into following items:

- Developing materials with a set of desired properties.
- Extending engineering material performance by diluting them with low-cost commercial resins.
- Improving specific properties e.g., impact strength, rigidity, ductility, chemical resistance, barrier properties, abrasion resistance, flammability, gloss, etc.
- Adjusting the material performance to fit customers' specifications at the lowest price.
- Recycling industrial and/or municipal plastics waste.

To achieve a reproducible material performance after blending, compatibility of the blended polymers is usually considered. There are several ways to achieve the compatibility: adding a third-party component which is compatible with both of them; adding a block co-polymer which is compatible with both of them; modifying one species by reaction compounding et al.

Recently, the idea of blending has been applied on electrospun fibers. Bognitzki and co-workers [75] electrospun fibers from PLA and PVP blend. After selectively etching out the one of the components, porous fibers with only PLA or PVP were obtained. Norris et al. [158] fabricated conductive electrospun fibers from polyaniline

and PEO blend and found that the conductivity of the blend fibers was slightly lower than the cast film due to the porous structures and non-woven nature. Chitosan with PEO blend fibers were electrospun by several researcher groups [159-161]. Tunable optical properties of MEH-PPV/PFO and MEH-PPV/PHT electrospun fibers were achieved by adjusting the blending ratio by Babel et al [162]. Recent study by Cha and co-workers [163] investigated the mechanical behavior of polysulfone and polyurethane electrospun fibers and found that with increasing amount of the blended polyurethane, mechanical properties, such as Young's modulus and yield strength increased by up to 80%.

PLA is a bio-degradable material and has potential applications in biomedical field. However, the glass transition temperature is around 55^{o}C which makes PLA hard and brittle at room temperature. Although as a fiber format, the flexibility has been improved but more can be done to improve the mechanical performance of PLA fibers. Multi-component systems have been design to solve the problem. PLA and starch were blended with a reactive agent during the extrusion process by adding a catalytic amount of some reactants (peroxides, anhydrides). The mechanical properties of the so-obtained reactive blends improved significantly because of the good compatibility and the cross-linking or coupling reactions between multi-components [164].

PEO has a low Tg and could improve the mechanical properties of PLA without sacrificing the bio-compatibility. However, for PLA and PEO blend system, few studies can be found in literature although people have been studying their block co-polymers extensively and intensively. Similar to PEO, poly(propylene glycol) is long known to be a good plasticizer and increase the crystallinity of PLA. Results of recent study [165] on PPG and PLA system revealed that high content of PPG caused the phase separation and blend sample crystallized when deformed while with low content

of PPG, crazing was observed. Sheth and co-workers [166] studied the crystallization behavior and mechanical properties of PLA and PEG blends and found for PEG content below 50%, the crystallization of PEG was suppressed and any blend system showed lower tensile strength. Additionally, they found the degradability of PLA was improved by adding any amount of PEG. However adding organoclays into the PLA and PEG blend by melt compounding showed an increase in the tensile strength [167].

For electrospun fibers, not only will the blending composition affect the properties of the material, but also processing such as blending method and electrospinning conditions will have effects on the morphologies, structures and properties. In this chapter, effects of PEO on the blend cast, electrospun fibers from both solution and melt will be studied and discussed. The nanoclay effects will briefly be discussed.

5.1 Experiments

5.1.1 Solution Electrospinning

PLA and PEO blend solutions were prepared in two methods in a similar way to preparation of PLA and nanoclay solutions describe in chapter 3. PLA and PEO blend resins were prepared using melt extrusion at the composition of 3 wt%, 10 wt% and 50 wt%. Solutions with concentrations of 10 and 15 wt% PLA-PEO in chloroform were made for each extruded blend. 0.1 wt% lithium chloride was also added into the 10 wt% of PLA-10PEO solutions to study the effect of conductivity on solution electrospun fibers. Similarly, solutions of PLA-PEO in chloroform were prepared by dissolving the resins directly in solvent at room temperature, creating an ad hoc mixture in solution rather than a melt-extruded blend.

The conductivity of the solutions was measured prior to electrospinning via a conductivity meter (VWR Scientific). After the solutions were ready, solution electrospinning was first carried out with typical condition at Q=0.01 ml/min, D=15

cm, V=15-20 kV with 27 gauge needle at room temperature. The reason why two different kinds of voltages were used will be explained in later section. The conditions are listed in Table 8.

Table 8 Electrospinning conditions for PLA-PEO solutions

Solution	Voltage (kV)	Flow Rate (mL/min)	Collector Dist. (cm)
Extruded Blend	15	0.01	15
Direct Blend	20	0.01	15

Morphology of the as-spun fibers was examined by SEM. Thermal properties were characterized by DSC and crystal structures were investigated using XRD. Mechanical properties were measured by an Instron tensile testing instrument. As-spun fibers were annealed at 65^{o}C for 18 hrs and then at 120^{o}C for 1 hr. XRD data were collected after each annealing. As-spun 50 wt% PEO fibers were soaked in a solvent mixture with 70 water : 30 ethanol for two days to dissolve the PEO. The morphology of the etched fibers was observed by SEM.

5.1.2 Melt Electrospinning

Melt electrospinning was conducted at the conditions similar to pure PLA. PLA and PEO blend resins were loaded into a 5mL syringe and after melting the resin for ½ hour, electrospinning was started. The drastic difference between them is that the splaying or whipping for PLA-PEO jet is more vigorous and dramatic. This phenomenon could be caused by the higher charge density induced by PEO and thus could lead to smaller fibers. In the melt electrospinning, T_1 was fixed at 200^{o}C and T_2 was varied with two different temperatures: 225^{o}C and 255^{o}C to study the effect of

needle temperature on fiber morphology and structures. T3 was varied with two different temperatures: 25^{o}C and 70^{o}C. Voltage (V) was kept at 15 kV and flow rate (Q) was set at 0.005 mL/min all the time. Collecting distance (d) was always 7.5 cm.

The collected fibers were characterized in the aspects of thermal properties, structural properties and mechanical properties. PLA-10PEO melt electrospun (ME) fibers were also directly spun onto cellulose fiber mat and filtration efficiency test was carried out.

5.1.3 Cast Films

Cast films were also prepared by two methods. Those cast films for mechanical test were considerably thick and were prepared by evaporating chloroform slowly from dilute (3-5 wt%) solutions of PLA-PEO in a flat, level Teflon mold (2''x2''). These films were created from both extruded and direct blend solutions for each composition. The other type of cast films for etching experiments was made using sliding casting in which a small drop of solution on a glass substrate was slid flat using another glass slide. These thin cast films were then put into HPLC water for at least 24 hours for extracting PEO component out. SEM was employed to examine the film morphologies. Fourier transform infrared spectroscopy (Mattson Model 5020) was used to compare cast films and fibers from extruded and direct blends. Structural studies were performed using XRD and polarizing optical microscopy (Olympus Japan BX51).

5.2 Effects of PEO on PLA-PEO Solution Electrospun Fibers

5.2.1 Conductivities of PLA-PEO Solutions

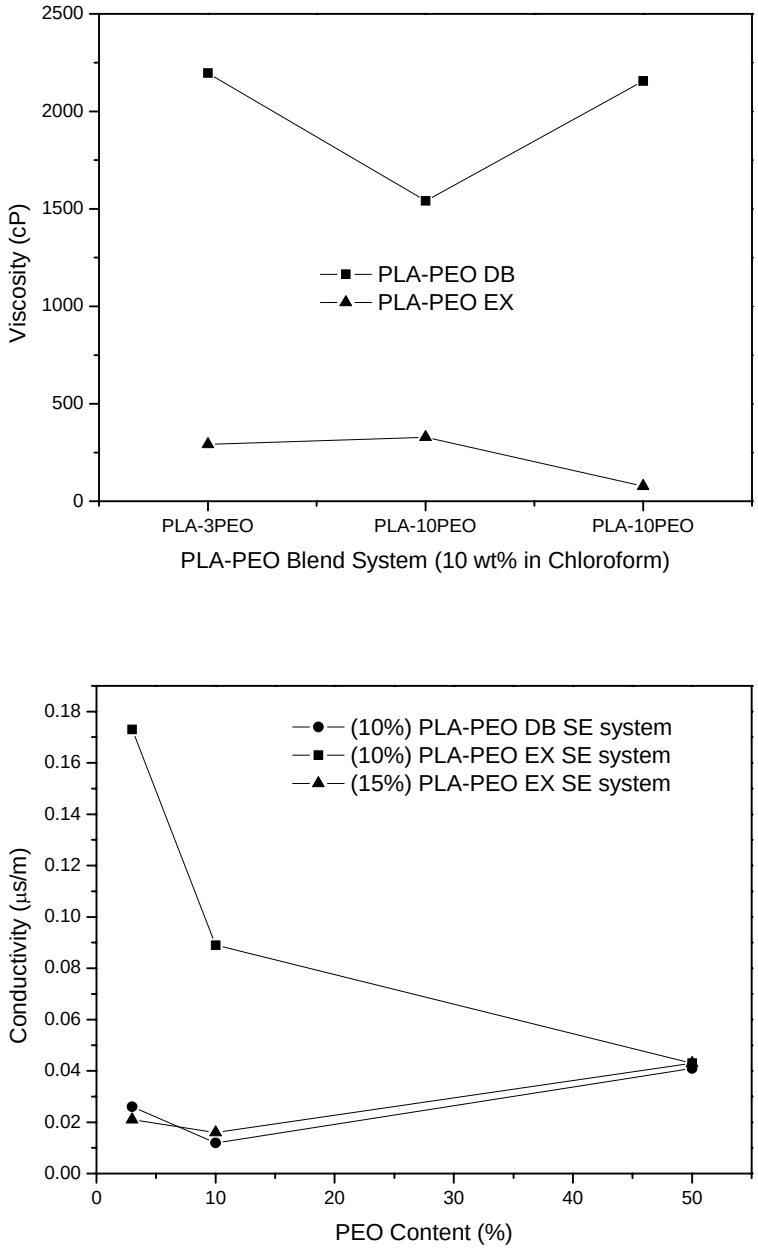

Figure 47 Conductivities and viscosities of PLA-PEO blend solutions with different concentrations

Electrospinning experiments revealed that electrospinning of extrusion-blended solutions went better than that of direct blended solutions at the concentration of 15 wt%. To find out the underlying causes, two properties of the solutions were investigated: viscosity and conductivity (Figure 47). Viscosity of extrusion-blended solution is lower than the viscosity of direct blend counterpart possibly due to the degradation in the melt extrusion process. Conductivity of PLA-PEO solutions is not only related to the blending method but also related to the solution concentration and PEO content. The conductivity of 10 wt% extrusion-blended solutions is nearly one order of magnitude higher than that of 10 wt% direct blended solutions at the PEO composition of 3 wt%. Comparing the viscosity, the difference is also one order of magnitude. The discrepancy diminishes as the PEO concentration increases and the trend lines of conductivity converge at PLA-50PEO. In addition, 15 wt% extrusion-blended solutions and 10 wt% direct-blended solutions show quite similar trend in the conductivity-concentration curve: first decrease and then increase comparing the constant decreasing conductivity of solutions.

In fact, conductivity and viscosity are dependent. As we know, conductivity (s) of an electrolyte given by $s = n\ q\ \mu$ depends upon the carrier concentration (n) and mobility (μ). The mobility is inversely related to the viscosity (η) of the electrolyte as $\mu = q/6\pi r\eta$. By adding additional polymers, two counteracting factors play in a roll. The inversed linear relationship between conductivity and viscosity is demonstrated at low PEO content smaller than 10 wt% for 10 wt% solutions. With PLA and PEO blending ratio of 1 to 1, significant phase separation appears and the charge carrier effect is more prominent thus the conductivity rises.

5.2.2 Fiber Morphology

Fiber morphology depends on the processing conditions and solution properties such as concentration and conductivity. The viscosity and conductivity of PLA-PEO solutions are determined by not only the solution concentration but also the blending methods as described in the previous section.

Morphologies of as-spun fibers of PLA-PEO were examined by SEM (Figure 48). Overall speaking, fibers from 10 wt% direct blend solutions are more homogeneous than those from extruded blend solutions due to the higher viscosity. Nevertheless, all the solutions produce fibers with bi-modal distributions of size. It is unclear what causes the bi-modal distribution.

For the 10 wt% extruded blend solutions, higher conductivity and low viscosity contribute to the non-uniformity. Slightly increases viscosity by adding PEO from 3 wt% to 10 wt% results in smoother fibers. And then viscosity decreases significantly at 50 wt% of PEO. As a consequence, bead-string morphology appears. Conductivity decrease also contributes. The formation of beads is influenced by three factors: repulsive force from charges; surface tension causing bead formation; viscoelasticity maintaining the continuity of the jet. Results on electrospun PEO fibers from PEO in water solution by Reneker et al. [19] showed that by suppressing the surface tension beadless fibers could be produced such as increasing the solution viscosity or conductivity. Higher conductivity shows that solution carries more charges and repulsive force is stronger in the jet which causes fewer beads. For the 10 wt% direct blend PLA-PEO solutions, viscosity is higher which makes the solution more viscoelastic thus generates smoother fibers.

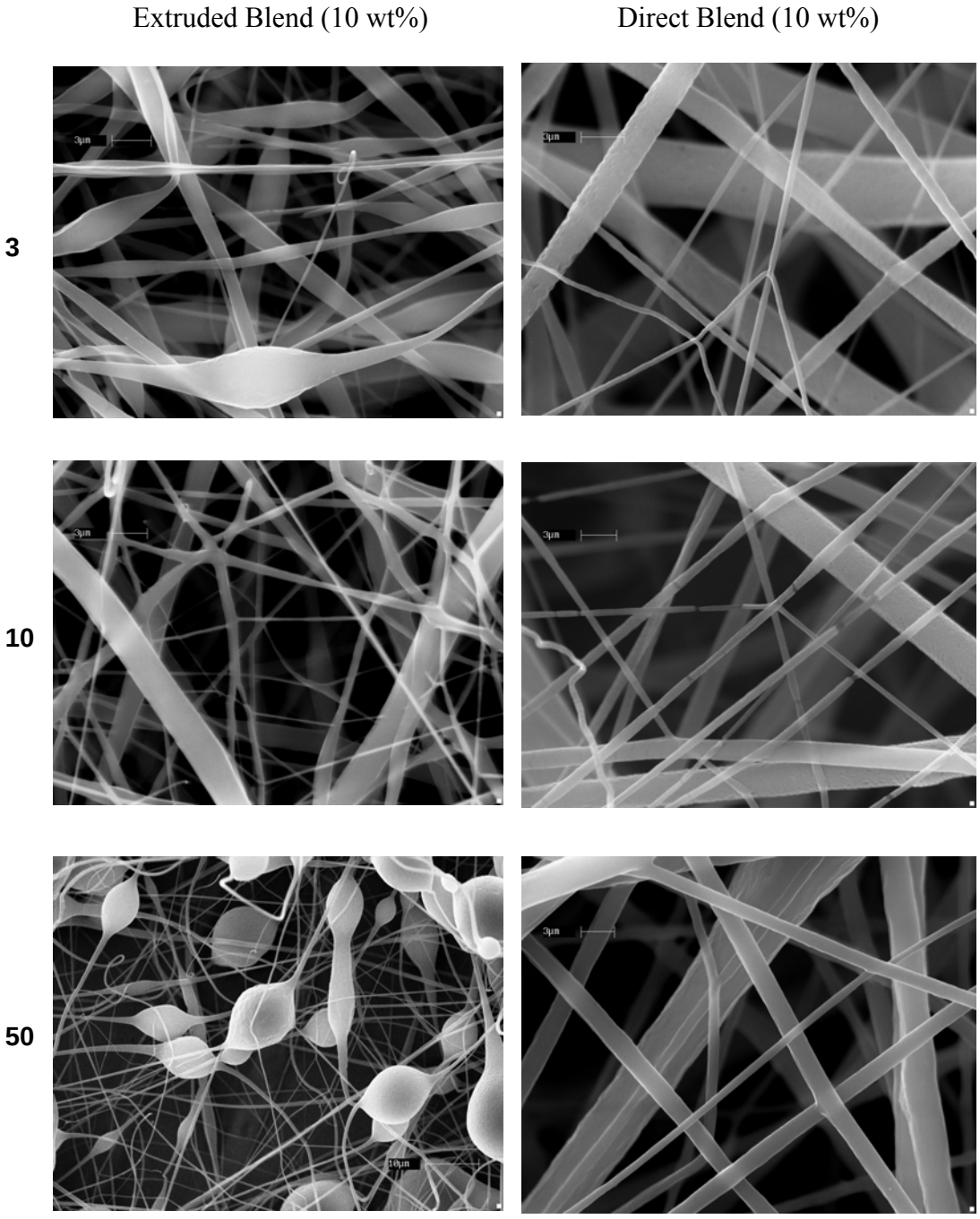

Figure 48 As-spun fibers from 10 wt% extruded blend (left) and direct blend (right) PLA-PEO solutions

Adding a small amount of an ionic salt such as LiCl increases the conductivity of the solution dramatically and evens the charge distribution. When 0.1 wt% LiCl was introduced to a 10 wt% (10 wt% PEO) extruded blend solution, the conductivity increased nearly fourfold from 0.089 μs/m to 0.332 μs/m. The resulting fibers (Figure 49) are noticeably more homogeneous. Fiber diameter for solution without lithium chloride has a wide distribution with bi-modal profile: one around 300 nm and one around 2 μm. The distribution for solution with lithium chloride is much more concentrated near 500 nm.

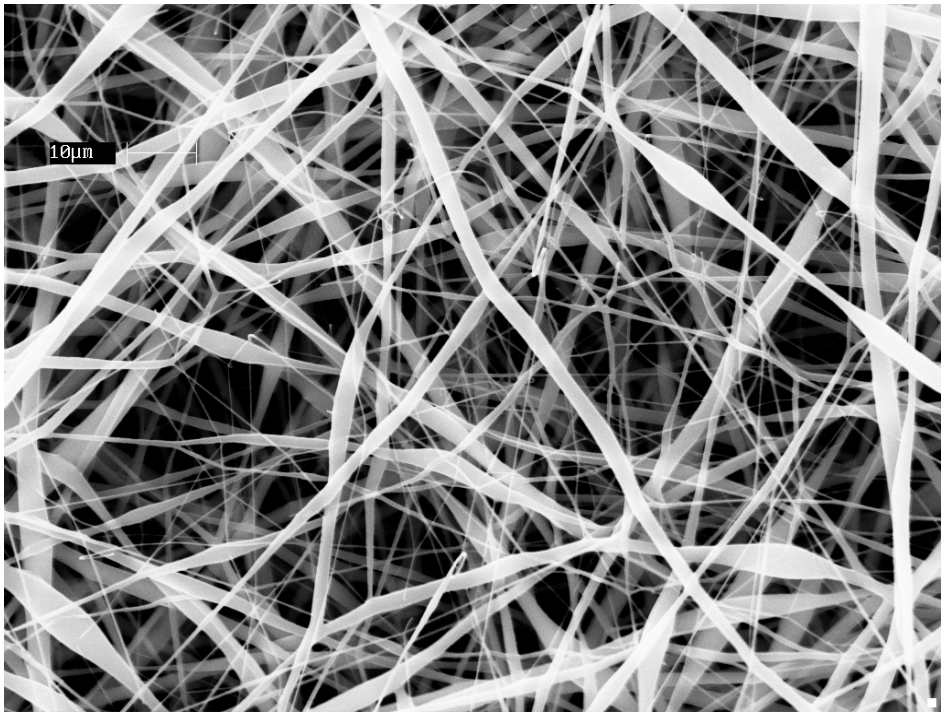

Figure 49 SEM and fiber size distribution of as-spun PLA-10PEO fibers from 10 wt% solutions with and without lithium chloride

Figure 49 (Continued)

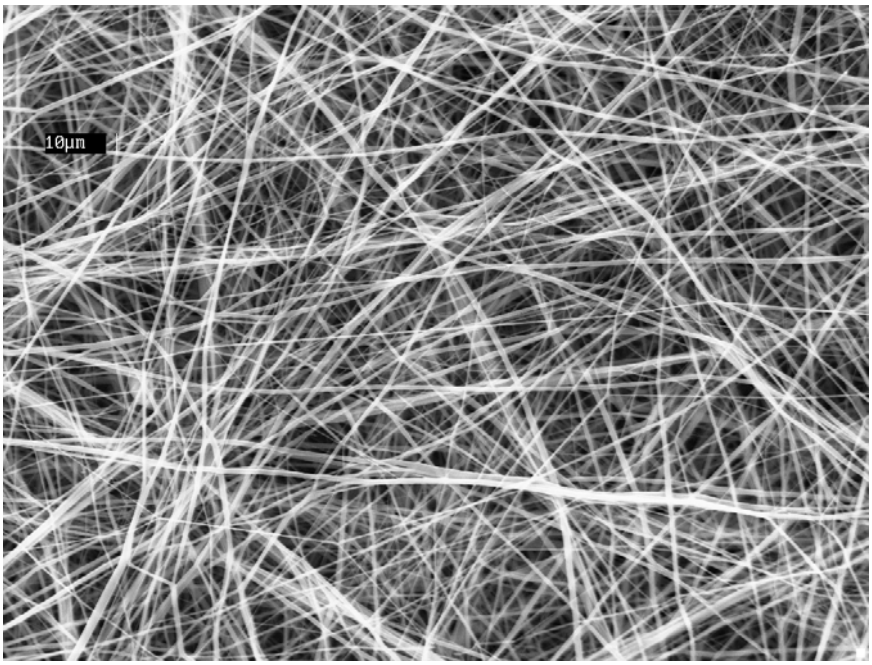

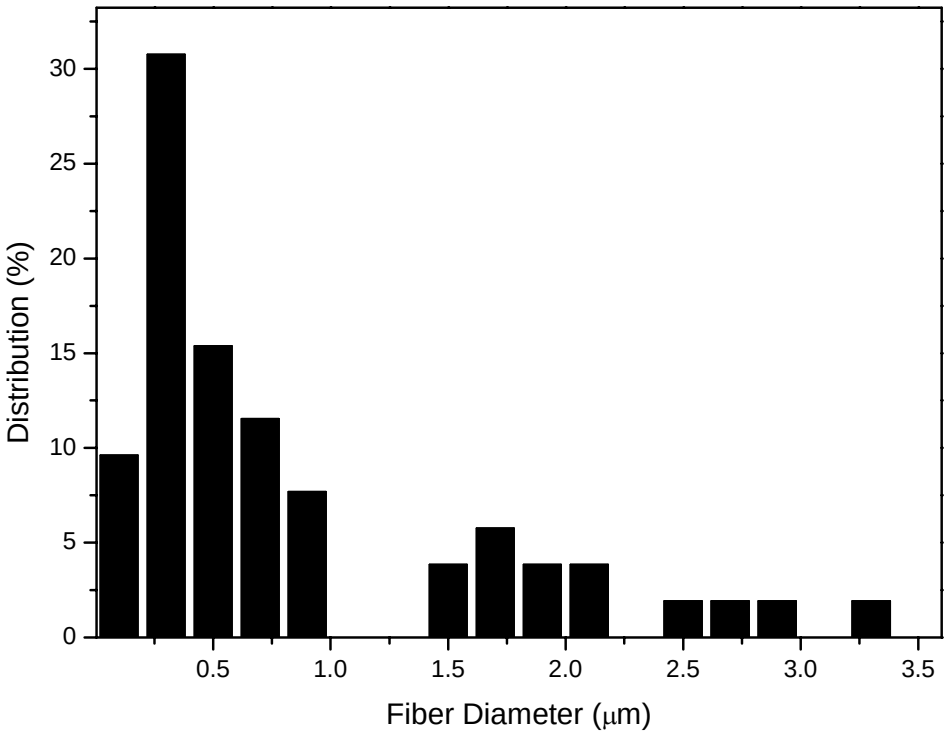

Figure 49 (Continued)

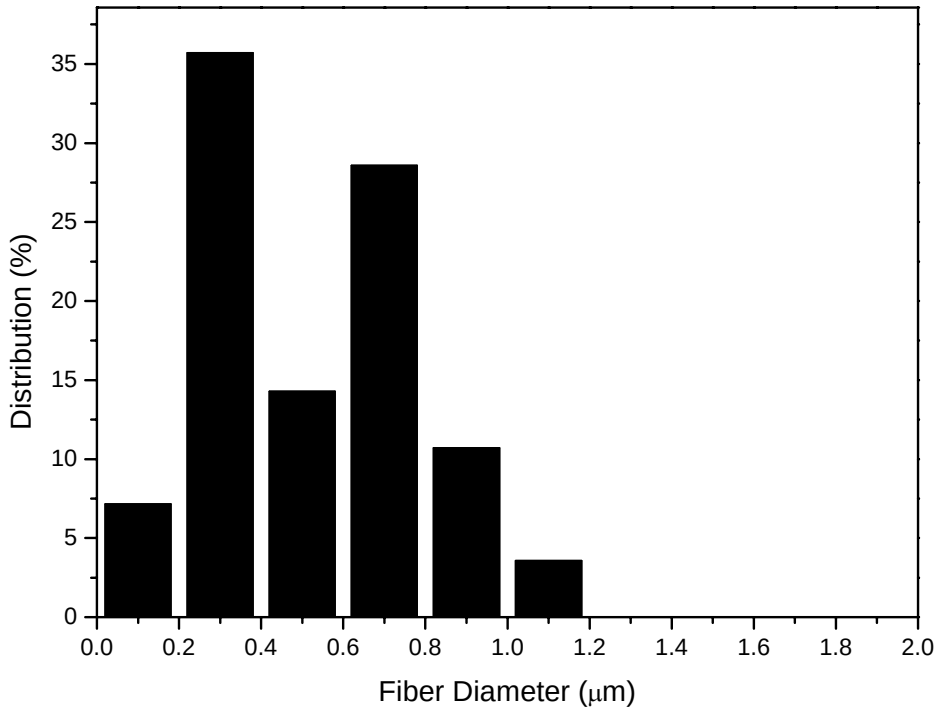

5.2.3 Fiber Morphology after Etching out PEO

By selectively removing one component in the polymer blend, porous morphology is achieved. It also serves as a tool to investigate the distribution and interaction between PEO with PLA by examining pore shape and size. In addition, effect of deformation on fiber morphologies and structures can also be demonstrated. In PLA nanocomposite, we have observed strong alignment of nanoclays along the fiber axis due to the strong deformation during electrospinning. And in self-assembling polymers, electrospun fibers show some stretched structures caused by the deformation.

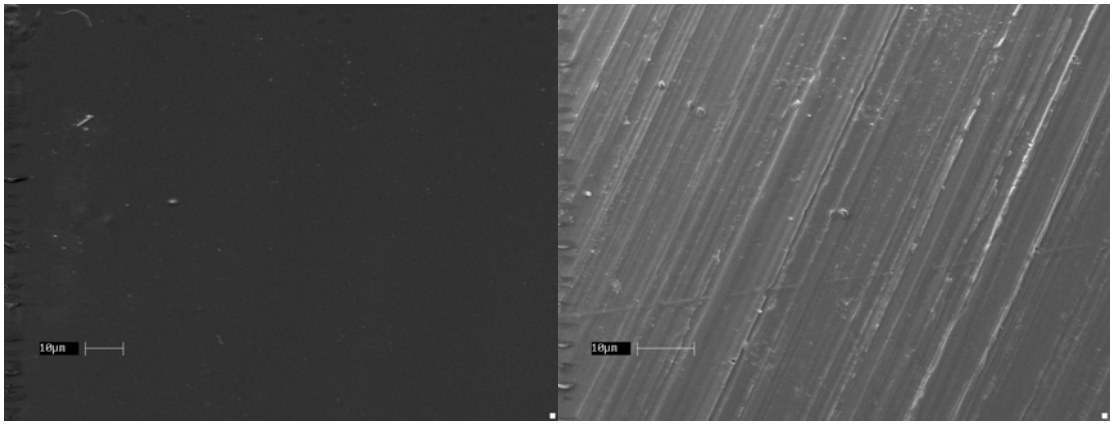

PLA-3PEO-DB PLA-3PEO-EX

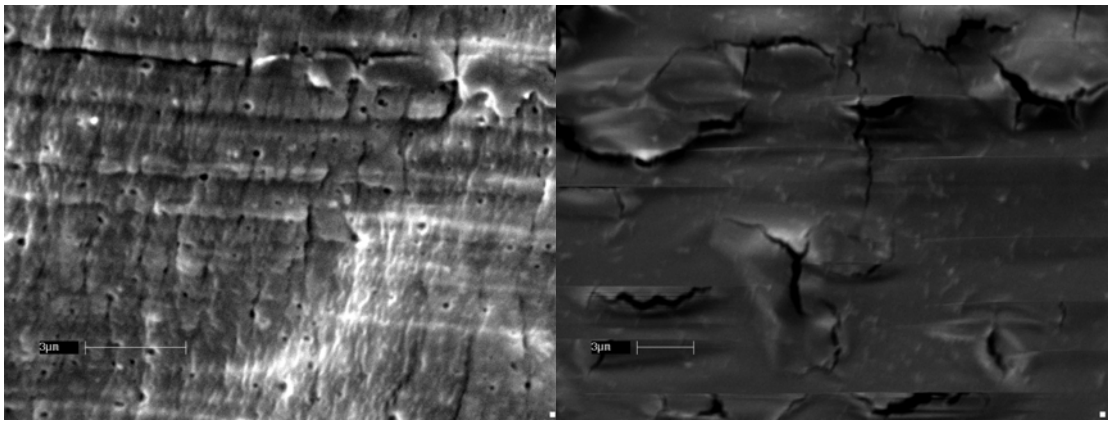

PLA-10PEO-DB PLA-10PEO-EX

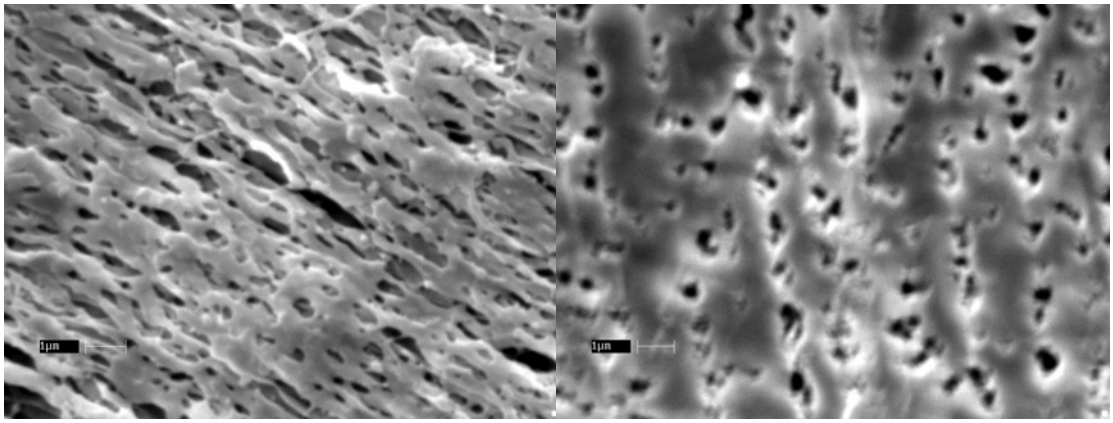

PLA-50PEO-DB PLA-50PEO-EX

Figure 50 Surface morphologies of etched PLA-PEO cast films at different composition

The morphologies of cast films after etching are revealed in Figure 50. The left row of images is etched cast films of direct blends and the right is extrusion blended. As the images indicate, there is no pore for both PLA-3PEO-DB and PLA-10PEO-EX cast film, a few pores in PLA-10PEO-DB film and no pore in PLA-10PEO-EX film. It also suggests that PEO is soluble in PLA at low compositions and 10 wt% is about the boundary between a good mixture and phase separated mixture. Due to the higher degree of homogeneity of extrusion blend and partial degradation, PEO exhibits more solubility in PLA thus no pore is observed in the picture for PLA-10PEO-EX cast film. Pores in PLA-50PEO-DB and PLA-50PEO-EX films have similar size and distribution around 300 nm. The only difference is the pore numbers. As described above, degraded PEO in extrusion blend has more solubility in PLA.

For the etched PLA-3PEO blend fibers, there is no significant change in surface morphology. PLA-10PEO fibers are selected to compare with their cast films. The morphologies are shown in Figure 51. It is found that pores in etched direct blend fibers are elongated along the fiber direction with the aspect ratio about 400 nm : 80 nm. While in extruded blend fibers pores are more regular-shaped with circular opening smaller than 60 nm in diameter and the density of the pores are significantly higher. These surface morphologies indicate that PEO domains in direct blend fibers are larger than in extruded blend fibers. The smaller domain size is possibly due to the break-up of large domains during melt extrusion. Solutions made from extrusion blend are more homogeneous than the direct blend.

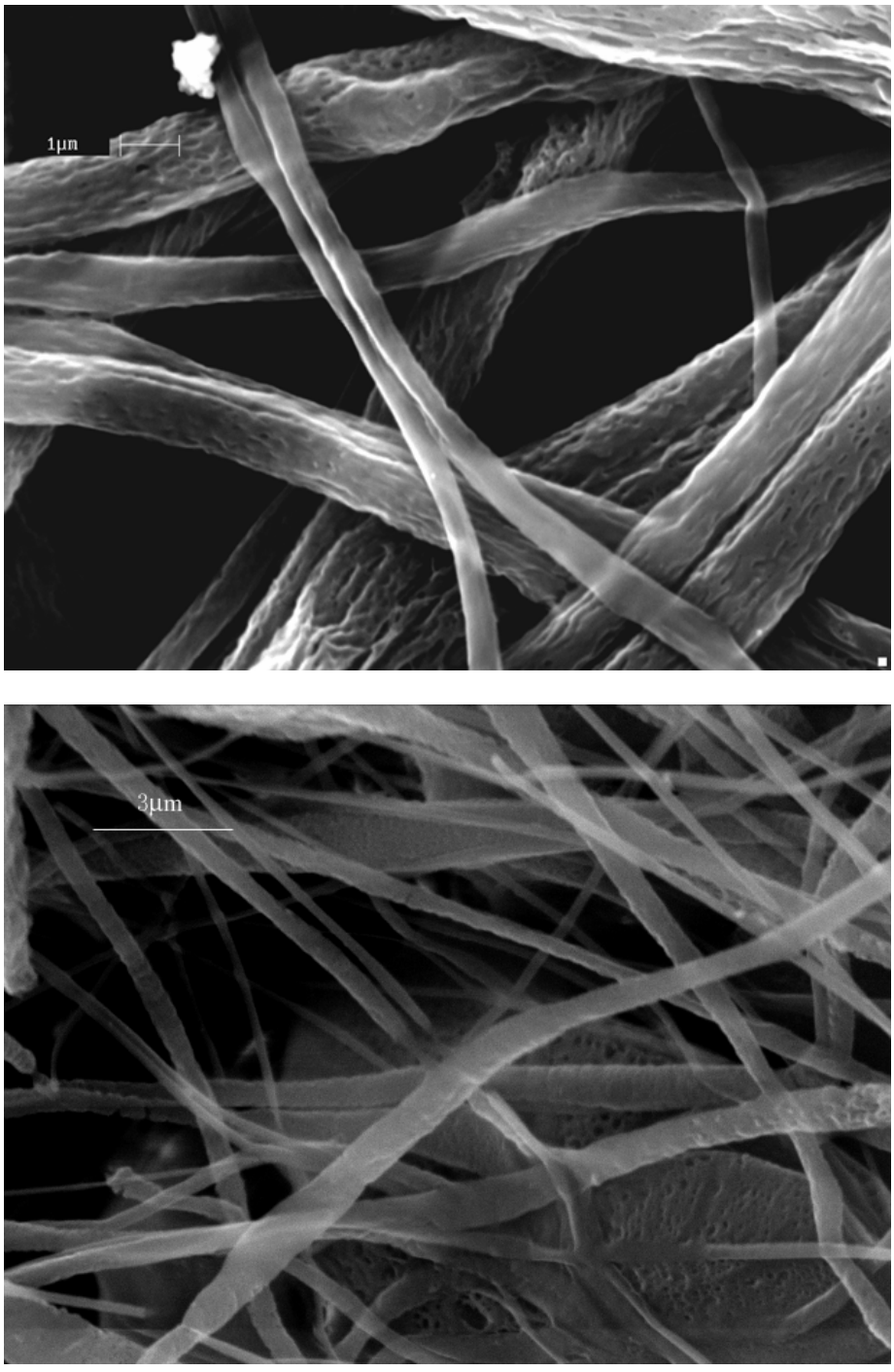

Figure 51 Fiber morphologies of PLA-10PEO fibers after removing PEO

5.2.4 Models for Cast Films and Fibers from Extrusion Blends

Based on the etching results, it is clear that distribution of PEO in PLA in direct blend cast film and fiber is not affected greatly by electrospinning except the elongated shape. We will put our focus on comparison between cast films and fibers from extrusion blend. EX cast films present bigger PEO domains and fibers show smaller PEO domains if there is any. Our model also proposes that PEO molecules interact with PLA molecules more strongly due to the smaller domain size (Figure 52). Possible chemical change is not detected in our FTIR studies. The size and homogeneity of the dispersed domains as well as the interaction between the embedding and matrix is crucial to the structure and property of the blends. For example, the nucleation and crystallization is closely related to the size and distribution.

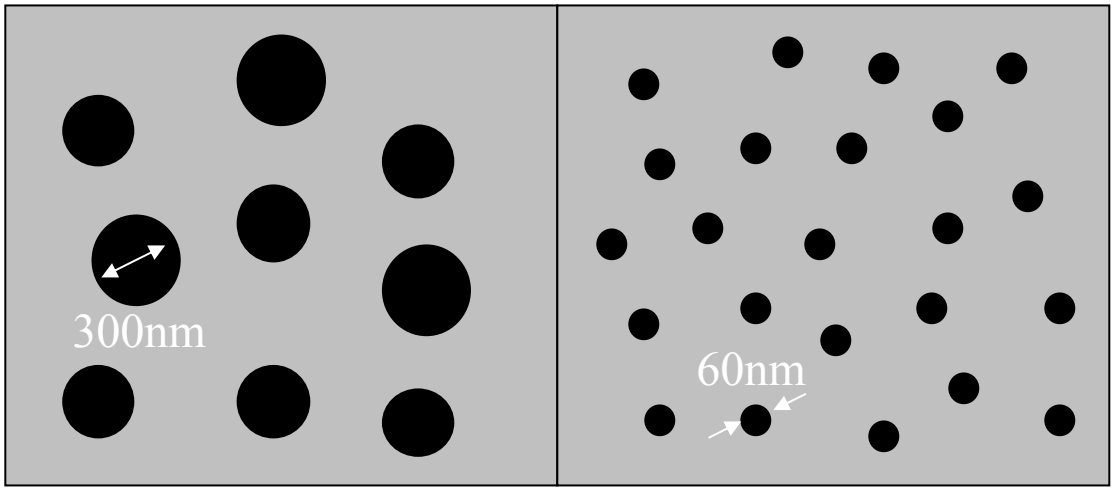

Figure 52 Distribution of PEO in PLA-10PEO-EX cast film (left) and fiber (right)

The major reason for the difference of PEO domain size in cast films and fibers can be split into two factors: the short residence time of the solution jet and fast

solidification during electrospinning. The typical residence time of the jet is at millisecond scale. To phase separate, polymer chains require enough relaxation time which is typically longer than the residence time in electrospinning. Due to the fast solidification, the mobility of polymer chains also decreases. Besides these, shearing flow and confinement effect may contribute to the formation of smaller PEO domain size.

5.2.5 Thermal Properties of PLA-PEO Solution Electrospun Fibers

Thermal properties of PEO and PLA are very different individually since PEO with molecular weight of 100,000 has a melting point of 66^{o}C and glass transition temperature is about -65^{o}C. Blending PEO with PLA not only lowers the glass transition temperature but also lower the melting temperature of PLA. These changes are shown in Figure 53 and Figure 54. Figure 53 compares the thermal properties of cast films from PLA-PEO direct blend and extruded blend and Figure 54 shows the comparison between PLA-PEO direct blend fibers and extruded blend fibers.

The complication of the DSC includes the overlap of melting temperature of PEO and glass transition temperature of PLA. So we will mostly focus on the melting behavior of PLA. For cast films, melting temperature depression is observable for both direct blend and extruded blend. PLA-50PEO cast film shows phase separation and additional melting peak at 58^{o}C assigned to PEO melting appears. The behavior of melting temperature depression of both PLA and PEO suggests the miscibility of the components and extruded blend cast film shows stronger intra-molecular interactions suggested by the greater depression of melting temperature [168]. Studies by Nijenhuis and co-worker [169] showed that the phase separation took place when PEO content was above 20 wt%. Close examining the DSC curve of PLA-10PEO, we can find that there is a small melting peak of PEO which suggests that at this PEO

concentration, phase separation already initiates. The lowering of PEO melting temperature in the blend is partially caused by the degradation of PEO. On the other hand, imperfect crystallization is anther possible reason according to several researchers [166, 168, 170] who also observed such behavior and claimed that PEO crystals were trapped in the PLA spherulites when crystallizing.

Same thermal depression behavior is observed regarding the as-spun fibers. But the transition is much more insignificant. The general crystallinity of as-spun fibers is smaller than the corresponding cast films which is due to the fast solidification during the electrospinning process. Another noticeable point of interest is the cold crystallization peak. The cold crystallization peak for pure PLA fibers is broad and at relatively higher temperature (100^{o}C). As PEO increases in the blend from 0 to 10 wt%, this peak shifts towards lower temperature and becomes sharper and sharper which suggests that introducing low amount of PEO into PLA can cause more deformation and thus lower cold crystallization peak. And this deformation is due to the higher conductivity of the blend system. PEO in the extruded blend shows stronger influence on the cold crystallization peak in the aspect of peak width and strength. PEO molecules in the extruded blend fibers exist in smaller domains as shown in the etching studies in previous section. In addition, it is believed that PEO in extruded blend fibers interacts more with PLA molecules and thus more deformation is undertaken. However, when PEO separates with PLA in phase at 50 wt%, PEO content shows the contrary effect on cold crystallization behavior: the peak disappears completely.

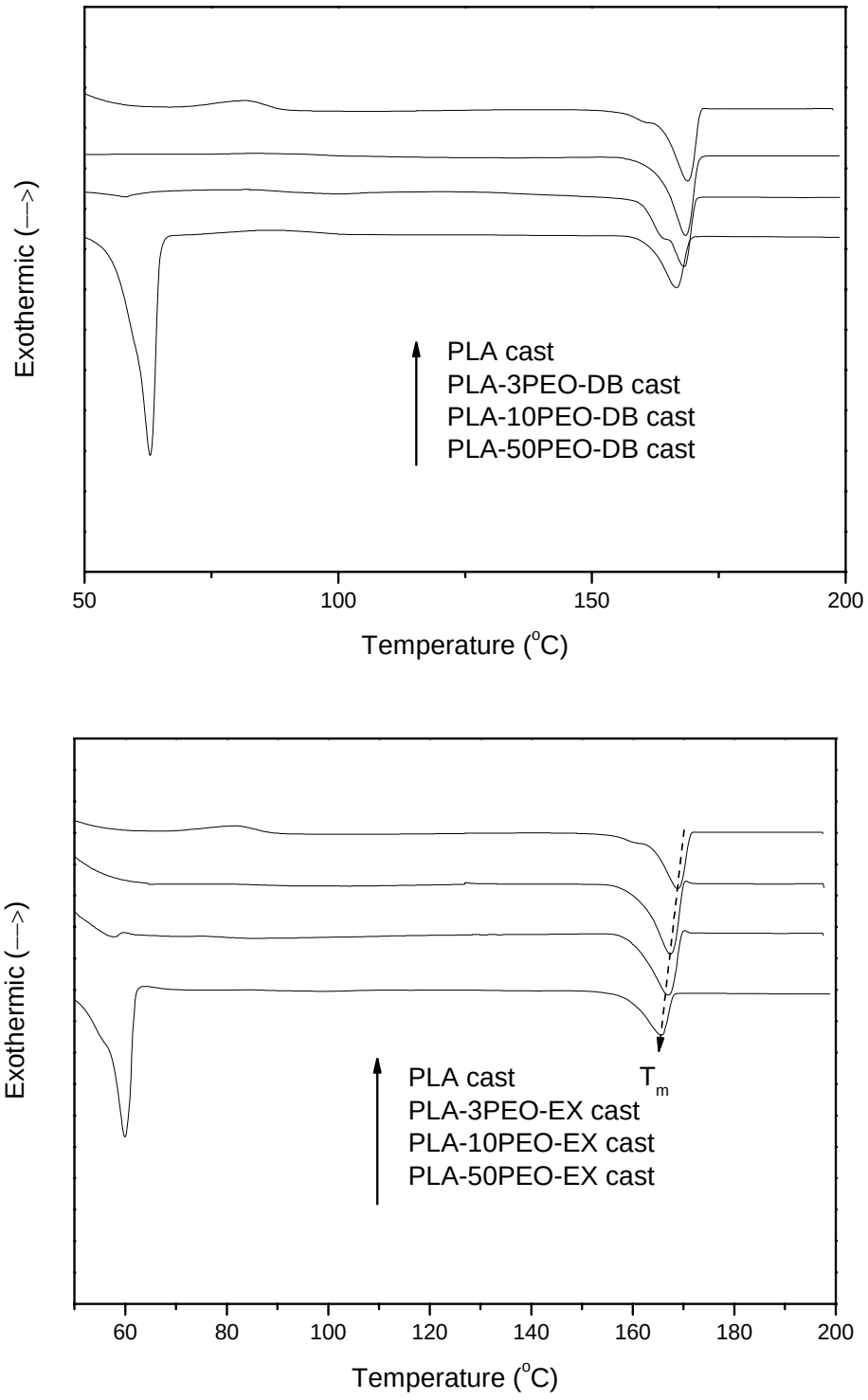

Figure 53 DSC of cast films of PLA-PEO direct blend and PLA-PEO extruded blend

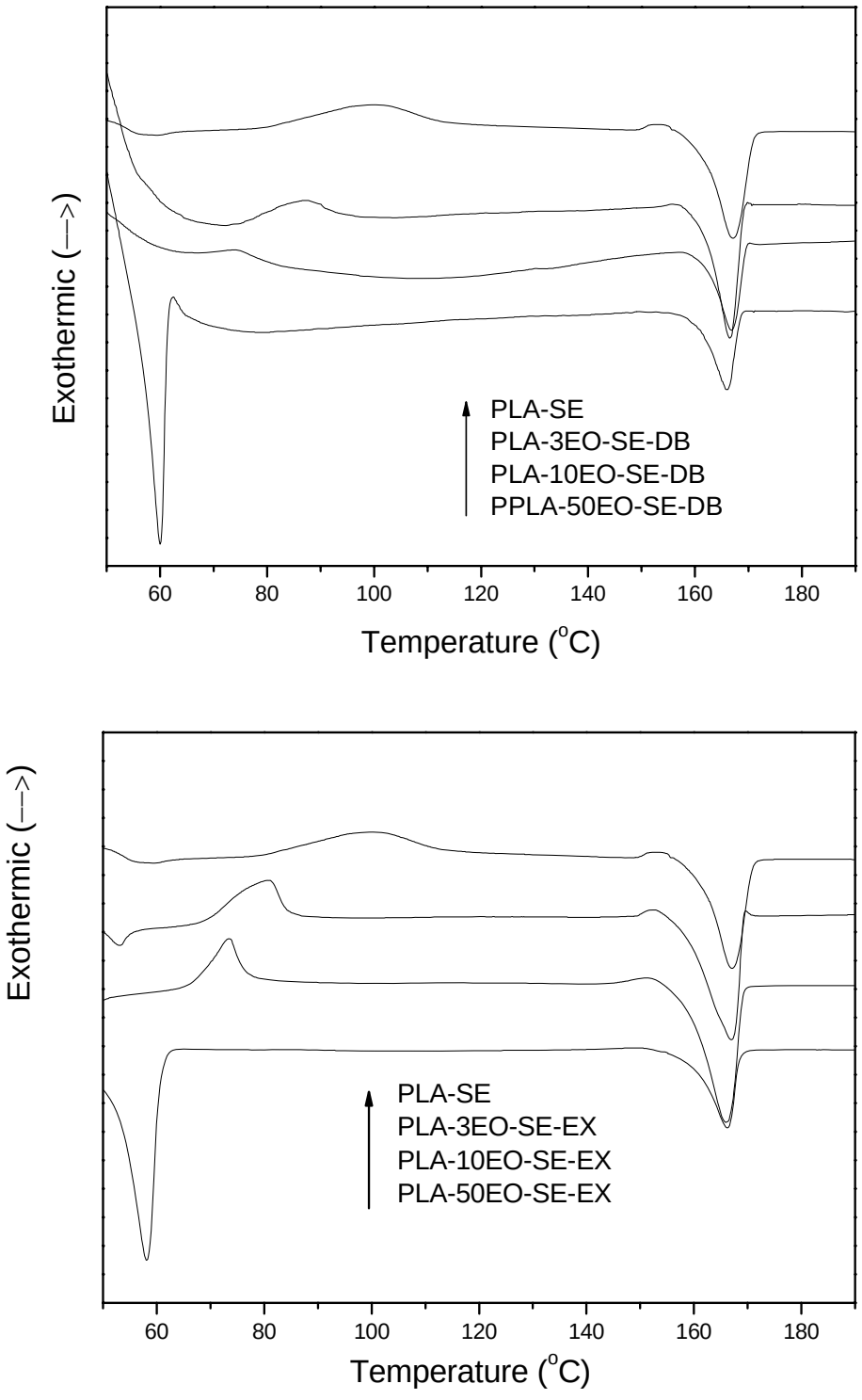

Figure 54 DSC of a) solution electrospun fibers of PLA-PEO direct blend and b) PLA-PEO extruded blend

Table 9 Thermal properties of PLA-PEO cast films and as-spun fibers

	Tm of PLA (^{o}C)	*Tcold* (^{o}C)	χ (%) of PLA
Direct Blend Cast Films			
PLA	168.8	82.2	29.7%
PLA-3PEO	168.5	92.8	31.1%
PLA-10PEO	168.1	83.6	21.9%
PLA-50PEO	166.6	85.7	9.3%
Extruded Blend Cast Films			
PLA-3PEO	167.5	81.8	41.5%
PLA-10PEO	166.9	N/A	37.4%
PLA-50PEO	165.5	N/A	25.8%
Direct Blend Fibers			
PLA	167.1	100.0	N/A
PLA-3PEO	166.5	87.0	N/A
PLA-10PEO	166.7	74.4	N/A
PLA-50PEO	165.9	N/A	N/A
Extruded Blend Fibers			
PLA-3PEO	167.0	80.9	N/A
PLA-10PEO	165.9	73.4	N/A
PLA-50PEO	166.2	N/A	N/A

The melting peaks and the crystallinity in the cast films and fibers are listed in Table 9. Crystallinity of as-spun fibers is not accurate since the cold crystallization peak partially overlaps with melting peak of PEO. Besides the changes of the melting

temperature and cold crystallization temperature, crystallinity of PLA in the blend is also affected by PEO existence. For cast films, 3 wt% PEO in PLA reaches the maximum crystallinity. As to the fibers, the crystallinity of PLA reaches the peak at 10 wt% PEO and decreases slightly after 10 wt% PEO. For PLA-50PEO, PEO crystallinity is an important factor regarding the mechanical behavior and crystal structure which we will discuss in the following sections. The total crystallinity of the cast films and fibers will directly determine the mechanical properties described later.

5.2.6 Effects of PEO on Crystal Structures of PLA-PEO Fibers

It has been shown that the electrospinning processing is an extra factor in determining the crystal structures of as-spun fibers. Due to the strong deformation and fast solidification, meta-stable crystal structures are often found in as-spun fibers. It is more complicated now since there is an additional player in the game. Pure PEO has monoclinic crystal structure in the regular crystallization and PEO is miscible with PLA below 10 wt%. Phase separation has been detected using DSC analysis at 50 wt%. Morphologies of polymer blend constantly change when the composition changes. In some cases, for instance, PET and PVA blends, lamellar morphology can be achieved at the right condition. But in most cases, spheres appear in the blends.

XRD studies of PLA-PEO can reveal the effect of PEO on crystal structures of the blend system. Figure 55 displays the XRD patterns of PLA-PEO cast films from both direct blend and extruded blend. It is interesting to find that the general trend of the peak change is different for direct blend and extruded blend cast films. For direct blend cast films. Small amount such as 3 wt% of PEO acts as nucleating agent thus greatly enhances the crystallization behavior and above 3 wt%, PLA peak at 16.7^{o} shrinks as PEO concentration increases, which in other word can be interpreted as crystallization is suppressed by the addition of PEO after its concentration is above 3

wt%. However, the decrease of PLA crystallinity is not significant for the extruded blend cast films. The crystallinity for PLA-3PEO-EX for reaches saturated crystallinity and extra PEO deters the crystallization of PLA slightly due to mobility decrease of PLA molecules.

For cast films of PLA-3PEO and PLA-10PEO formed from both blends, no PEO crystal peak is present which suggests there are no PEO crystals in the blends after the solvent evaporates. It is because at low concentration of PEO, PEO is a minor phase and surrounded by PLA molecules. Chance for them to crystallize is negligible. When PLA crystallizes, PEO molecules are trapped in the amorphous region of the blends. For these two cast films, the difference lies in the distribution of the PEO micro-domains and the interaction between PEO and PLA. Due to weaker interaction between PEO and PLA, network in the chloroform solution is more likely to form during evaporation and reduce the mobility of PLA molecules thus hinders the crystallization of PLA. And this effect is more prominent when PEO content increases over 3 wt%.

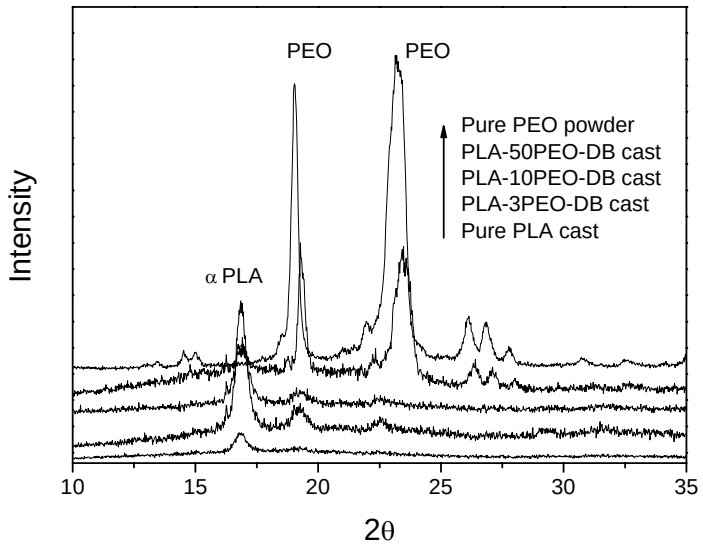

Figure 55 XRD patterns of PLA-PEO cast films from both direct blend and extruded blend

Figure 55 (Continued)

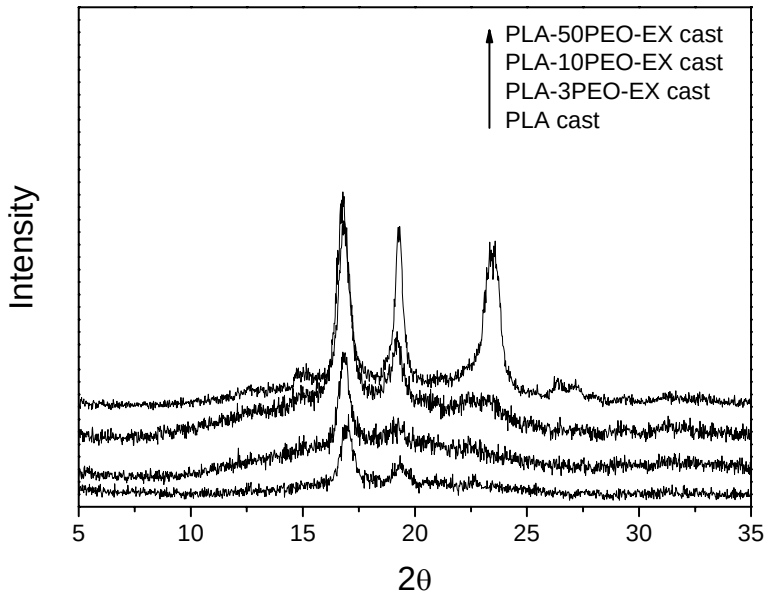

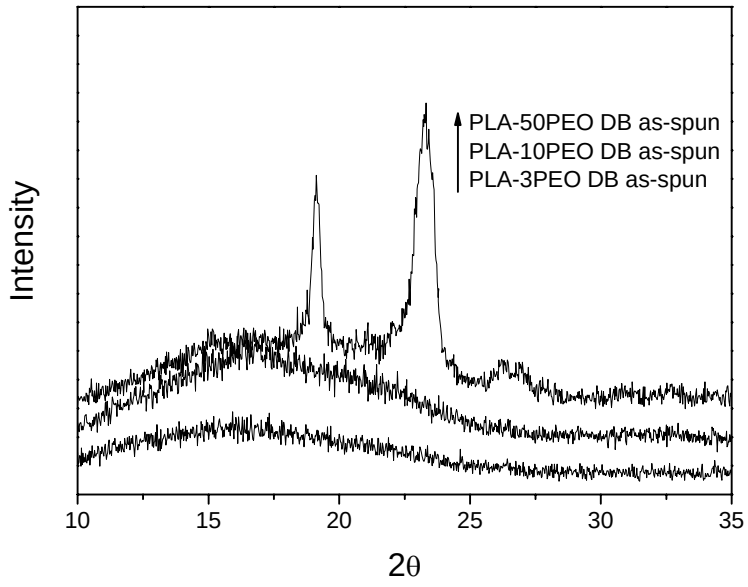

Figure 56 XRD patterns of PLA-PEO as-spun fibers from both direct blend and extruded blend

Figure 56 (Continued)

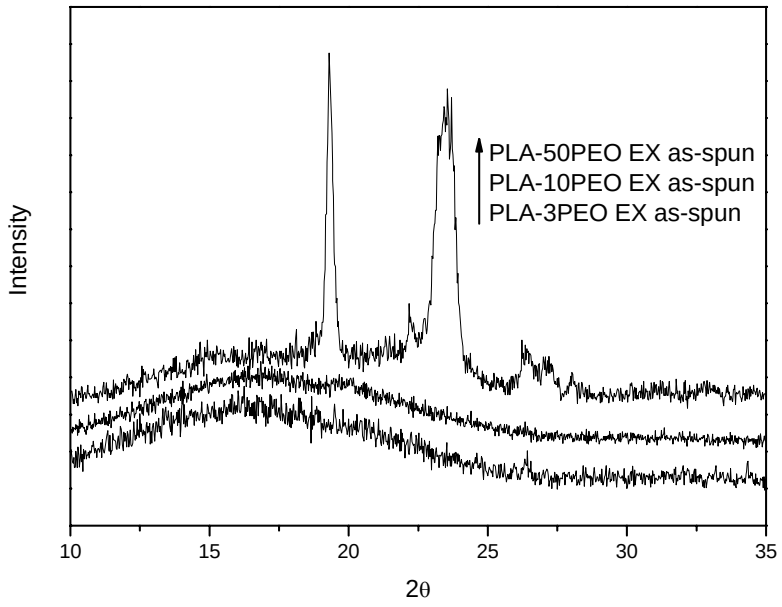

XRD patterns of as-spun fibers from both direct blend and extruded blend are shown in Figure 56. For PLA-3PEO and PLA-10PEO as-spun fibers, there is no apparent PLA crystal peaks available though the small amount of crystals could exist in the fibers as indicated in DSC. For the composition of PLA-50PEO, only strong PEO peaks protrude out of the amorphous halo. Due to the fast solvent evaporation, effect of PEO on crystallization of PLA is suppressed. So we annealed the as-spun fibers to let PLA crystallize and XRD scan was done for analysis (Figure 57). In the annealing test, direct blend fibers and extruded fibers exhibit same behavior so only direct blend fibers are shown in Figure 57.

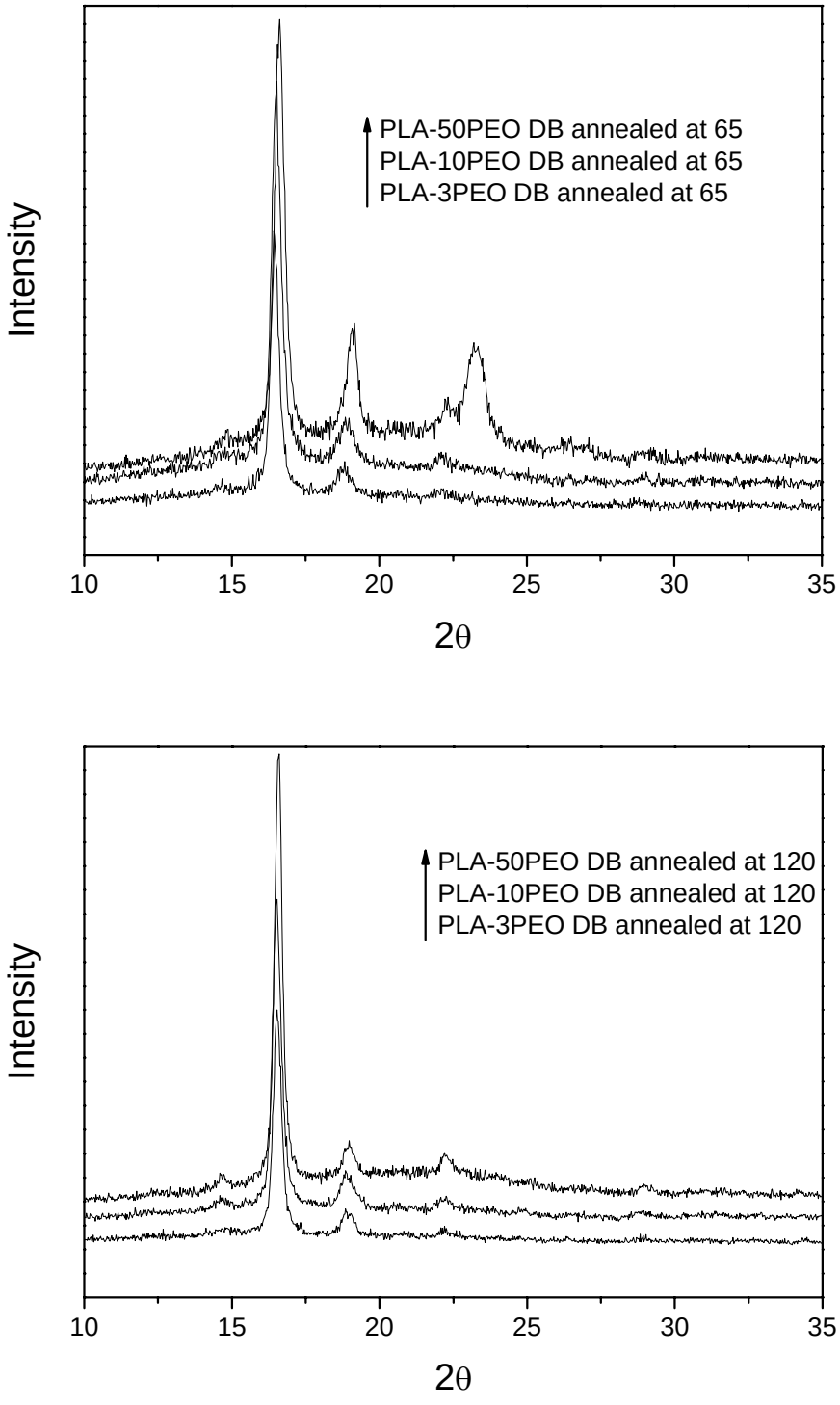

Figure 57 XRD patterns of PLA-PEO direct blend fibers annealed at 65°C and 120°C

The reason why 65^{o}C was picked for annealing temperature is that this temperature is below the melting temperature of PEO while above the glass transition temperature of PLA. So we expect to see that strong PLA peaks showing up due to the cold crystallization while PEO peak remains. According to Figure 57, we observed the same phenomena as expected. After annealing at 120^{o}C for 1 hr, PEO crystals all melt and since PLA has a glass transition temperature above the crystallization temperature of PEO which is at 40^{o}C according to DSC data, PEO molecules are frozen in the amorphous region of PLA and no crystallinity forms after cooling down. That is why the PEO peaks disappear.

5.2.7 Mechanical Properties of PLA-PEO Cast Films and Fibers

One of the most important motivations for this study is to find a way to create fibers with better mechanical strength since we found that pure melt electrospun PLA fibers are too weak to apply to filtration application. Due to the high glass transition temperature, melt electrospun PLA fibers are brittle. PEO as a plasticizer or elasticizer has been long known for industries and academics. Blending PEO in the PLA as observed can reduce the glass transition temperature thus help improve the flexibility of the fibers. For solution electrospun fibers, we expect the same function of PEO in the blends.

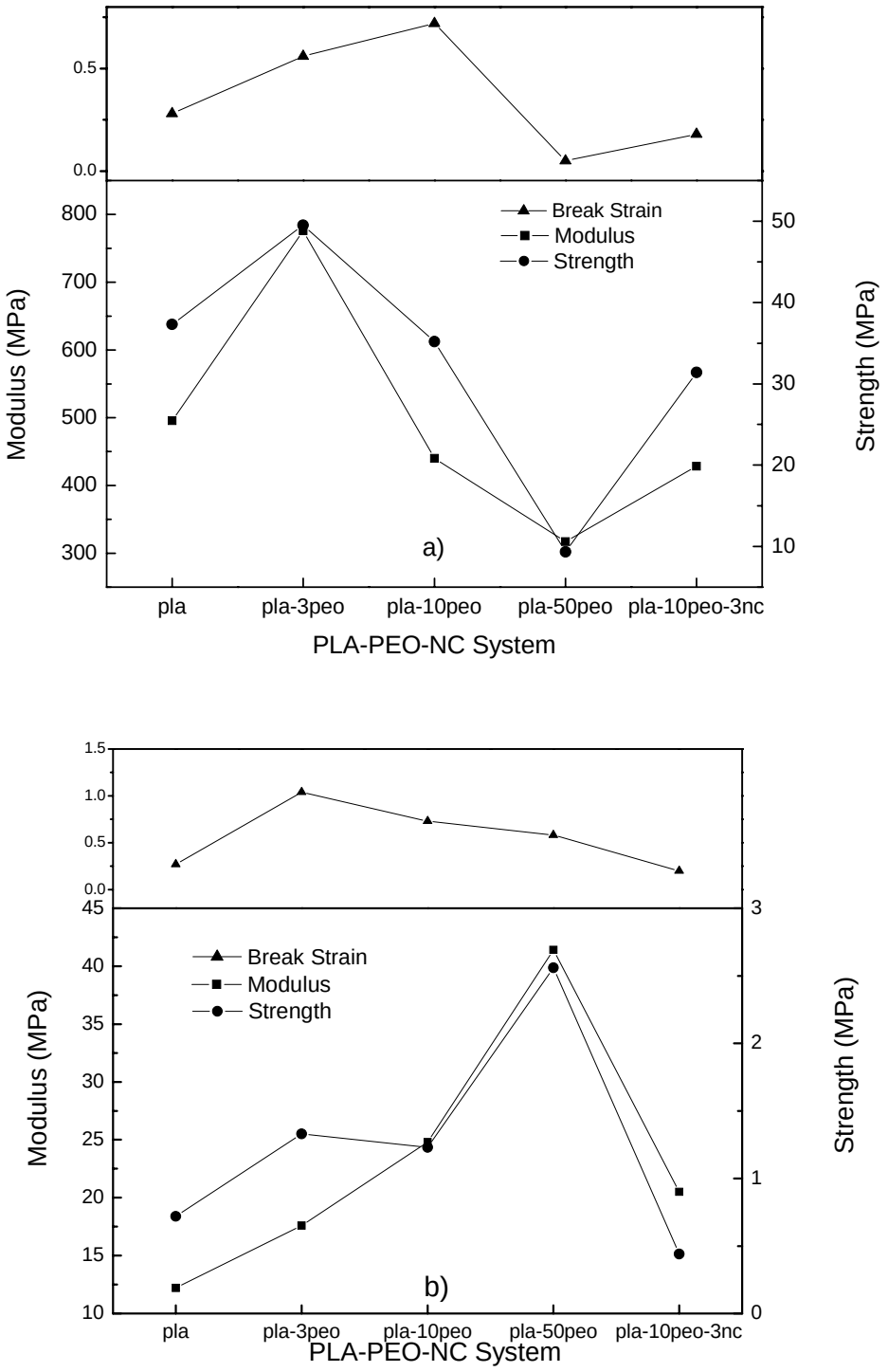

Figure 58 Mechanical properties of PLA-PEO-NC cast system and solution electrospun system from extrusion blend

Figure 58 demonstrates the effects of PEO on the elastic modulus, yield strength and break strain of the cast films and solution electrospun fibers from extrusion blend. It is surprising that the trend of the mechanical property change is different for the cast film system and electrospun fiber system. Modulus and yield strength are maximized when 3 wt% of PEO is added into PLA. However at blending ratio of 1:1 for the electrospun fibers, these two values reach their maximum. The inherent causes for these two different trend lines lie on the crystallinity (Figure 59). For the cast films, 3 wt% of PEO acts as nucleating agent and increases the crystallinity of the cast film from 29.7% to 41.5% resulting in great improvement in mechanical properties. And then phase separation creates large amount of defects in the cast films when PEO is above 3 wt% which leads to the decrease in mechanical strength. In the fiber system, electrospinning as a dynamic process which introduces deformation in the system homogenizes the distribution of PEO domain and breaks down the domain size. The rapid solidification prevents the early agglomeration of large PEO domains in the fibers and thus suppresses the adverse effect of extra PEO addition. In the meantime, the nucleating effect of PEO prevails. So there are at least two counteract effects in the system when adding PEO: the nucleating effect and defects created by the grain boundary or else. Which effect prevails will determine the mechanical property enhancement or detriment.

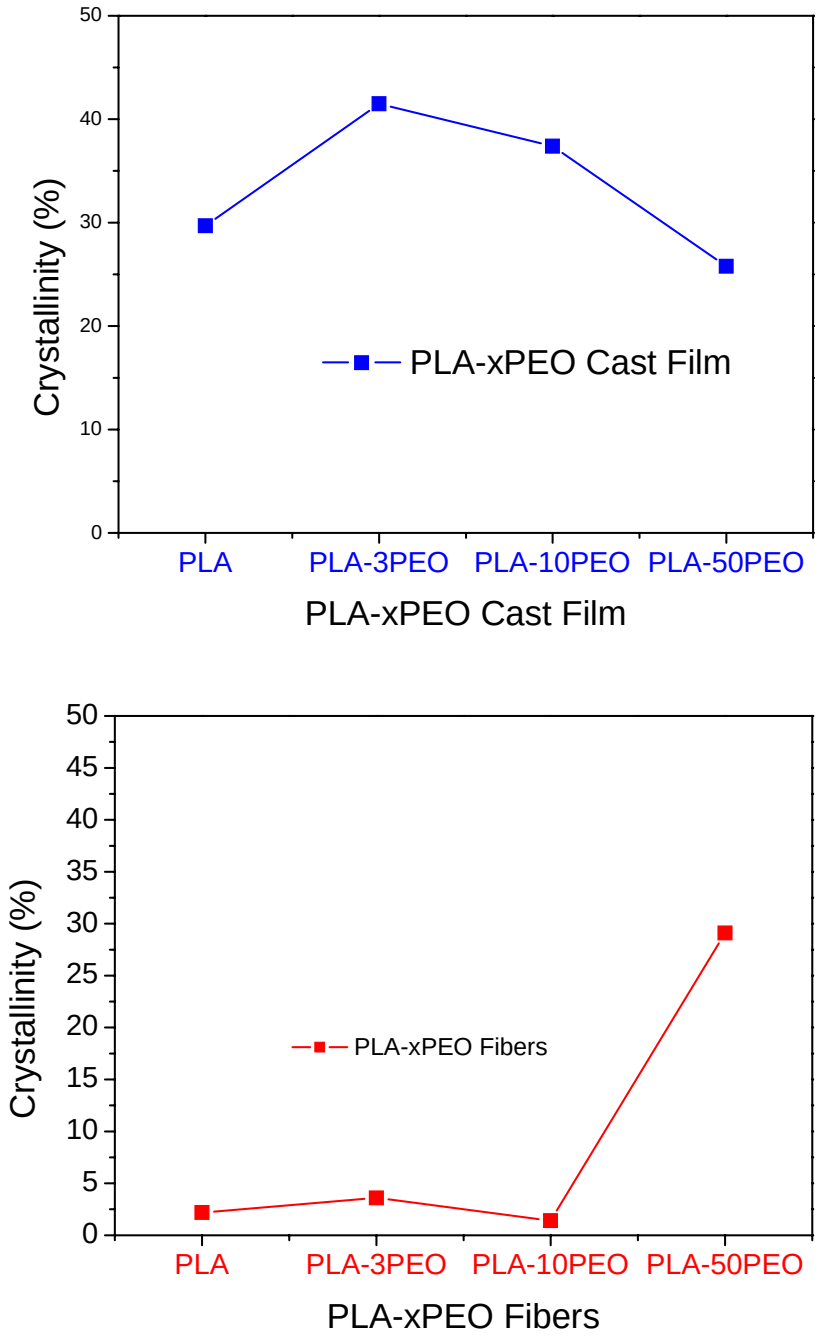

Figure 59 Effect of PEO on the crystallinity of PLA-PEO-EX cast films and fibers

To summarize the effect of PEO on the mechanical properties of both cast films and solution electrospun fibers, mechanical data are tabularized as Table 10.

Table 10 Mechanical properties of PLA-PEO-NC cast film and fibers from solutions

	Modulus (Mpa)	Strength(Mpa)	Breaking Strain
Cast Films from Extrusion Blend			
pla	495.4	37.3	0.28
pla-3peo	775.7	49.5	0.56
pla-10peo	440.3	35.2	0.72
pla-50peo	317.1	9.35	0.05
pla-10peo-3nc	428.4	31.4	0.18
Solution Electrospun Fibers from Extrusion Blend			
pla	12.2	0.72	0.27
pla-3peo	17.6	1.33	1.04
pla-10peo	24.8	1.23	0.73
pla-50peo	41.4	2.56	0.58
pla-10peo-3nc	20.5	0.44	0.20

5.3 Results of Melt Electrospun PLA-PEO Fibers

5.3.1 Rheology of PLA-PEO Melts

The dynamic shear viscosity of PLA-PEO-EX depending on variant shear frequency is shown in Figure 60. The general trend of the shear viscosity change when adding PEO is illustrated in Figure 58b. Adding even a small amount of PEO into PLA significantly reduces the shear viscosity of PLA-PEO blends thus enables

possible melt electrospinning. The decreasing in shear viscosity is the result of plasticization effect attributed to PEO. And there is no significant shear thinning observed for all compositions.

As discussed in the melt electrospinning of pure PLA, shear viscosity is just one factor to consider in melt electrospinning. Viscoelasticity of the melt is a critical factor to achieve sub-micron sized fibers. To acquire information on the viscoelasticity of the melts, loss modulus over storage modulus is plotted against shear frequency (Figure 60c). Across the frequency span, viscous behavior dominates the elastic behavior for all the compositions. The addition of PEO presents two different influences on the viscoelasticity of the melts. At low frequency below 10 s^{-1}, PEO strengthens the elastic property more while at high frequency increases the viscous property more. During melt electrospinning, shear rate is comparable to the low frequency thus addition of PEO enhances the elastic behavior of the melts and may count-act the positive effect of boosts in melt conductivity brought by PEO.

Elongational viscosity is another factor to take into account and is critical to obtaining small size fibers without breaking the jet. In this study, we did not characterize the elongational viscosity of the melt and should be done in the future work.

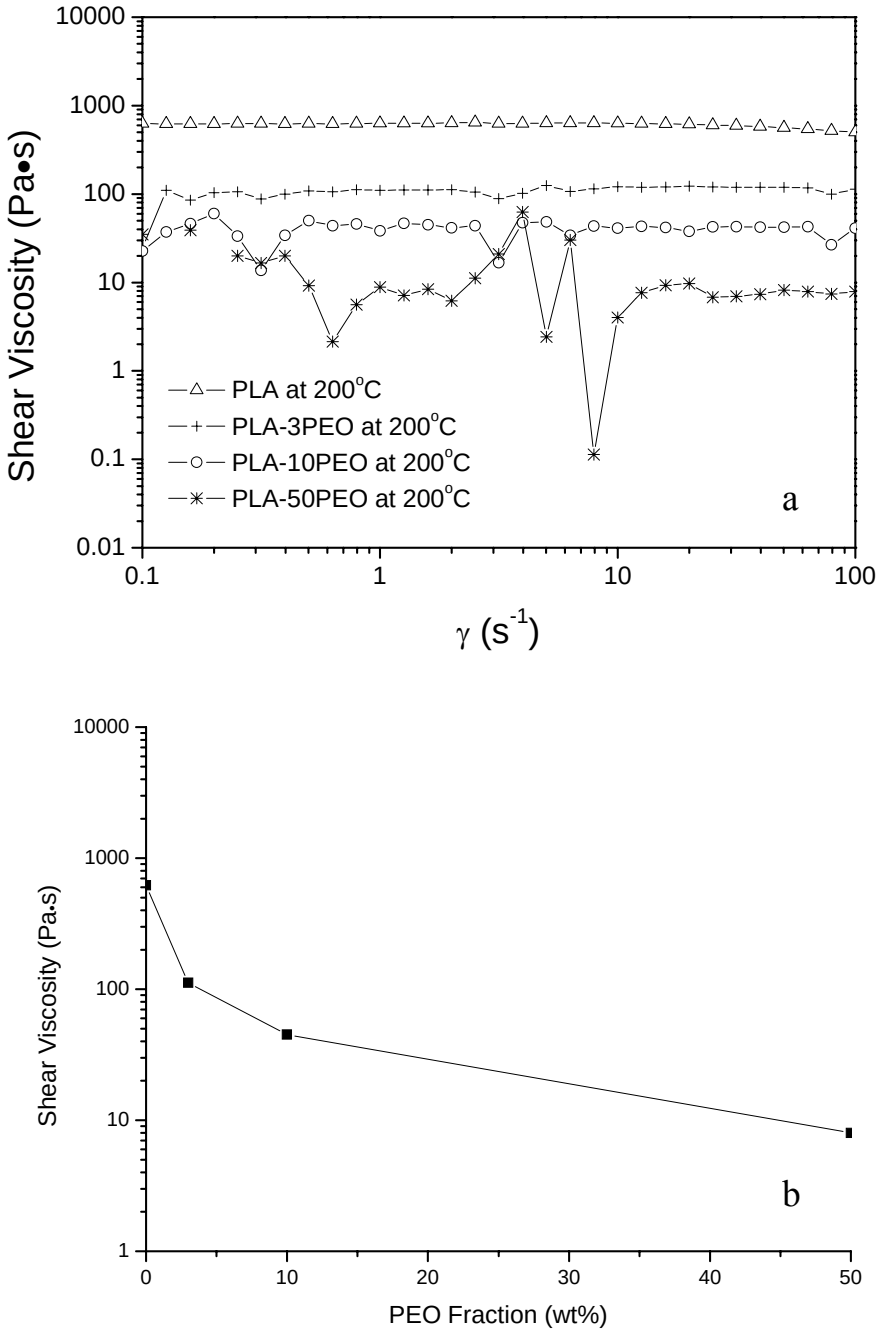

Figure 60 Dynamic shear viscosity of PLA-PEO-EX as a function of a) temperature and b) composition; c) viscoelastic property of PLA-PEO-EX at 200°C

Figure 60 (Continued)

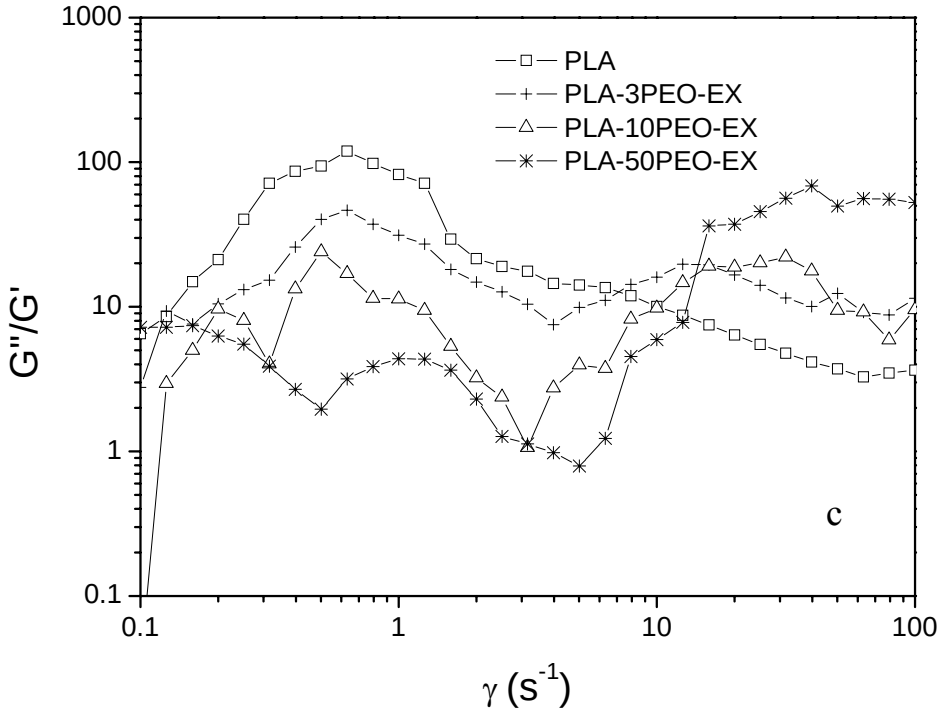

5.3.2 Effect of Processing Conditions and PEO on Fiber Morphology

In regard to the effect of processing conditions on fiber morphology, we will focus the effect of nozzle temperature as most of the effects are similar to the melt electrospinning of pure PLA. Figure 61 shows PLA-3PEO-EX and PLA-50PEO-EX fibers from melt electrospinning at 225°C and 255°C. The images clearly manifest that increasing nozzle temperature (*T2*) reduces the fiber diameters for both PLA-30PEO-EX and PLA-50PEO-EX. Nonetheless, the reduction percentage is higher for PLA-3PEO-EX, which could be caused by the different viscoelasticity behavior of the melts.

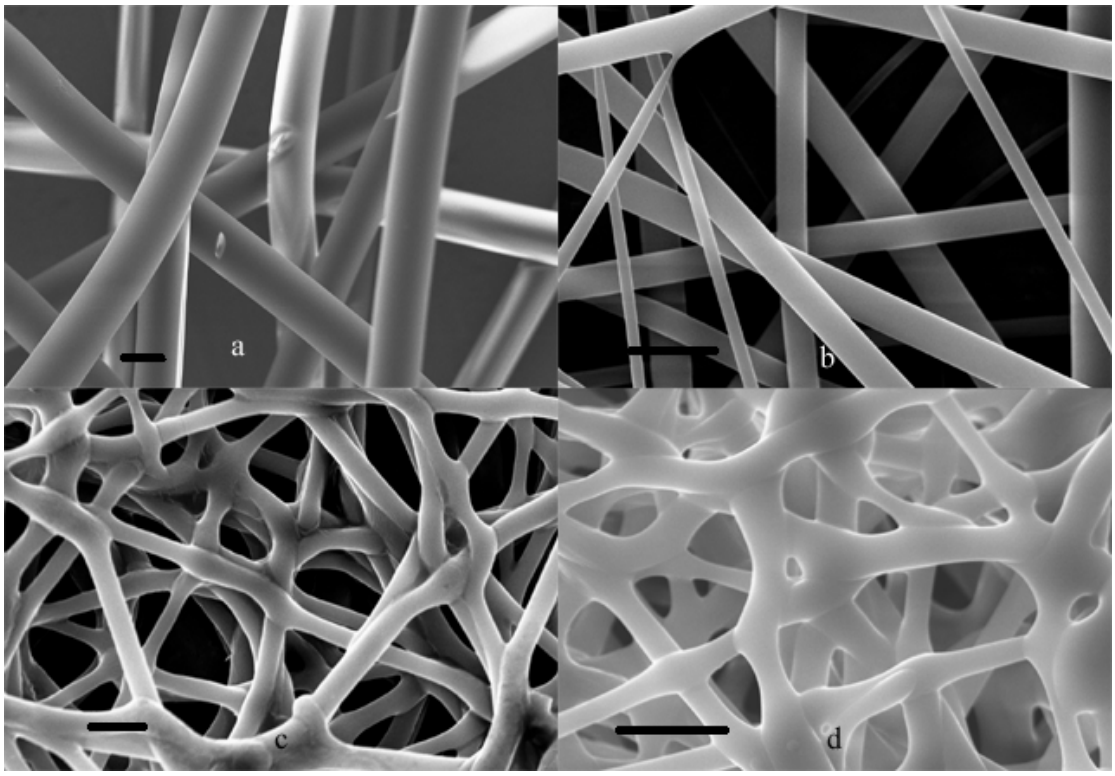

Figure 61 SEM micrographs of a, b) PLA-3PEO-EX and c, d) PLA-50PEO-EX fibers from melt electrospinning at 225^{o}C (left) and 255^{o}C (right); scale bar: 10 μm

Effect of PEO on fiber morphology is shown in Figure 62. The processing conditions were: T1=200^{o}C; T2=255 ^{o}C; T3=T4=25 ^{o}C; Q=0.005ml/min; V=15kV; D=7.5cm and Dnozzle=0.21mm. The as-spun fibers of all compositions exhibit similar diameter ranging from 1-3 μm. The bigger sized fibers result from the higher viscoelasticity of the blend melts. The surface morphology of PLA-3PEO-EX and PLA-10PEO-EX fibers is the same as pure PLA fibers: smooth and round-shaped. For PLA-50PEO-EX fibers, the morphology is distinctive with the other two. Fibers tend to melt together at the joint, which is due to the high content of PEO. The melt jet is not fully quenched during the flight and causes PEO domains to melt together.

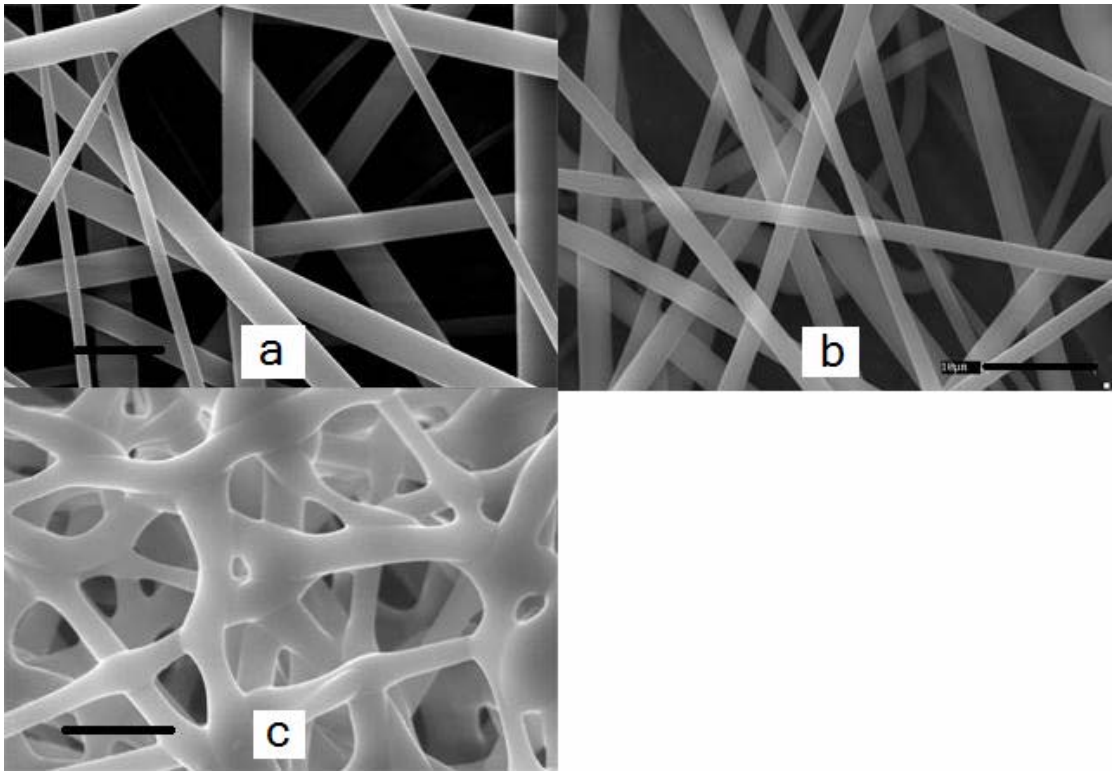

Figure 62 SEM micrographs of PLA-3PEO-EX, PLA-10PEO-EX and PLA-50PEO-EX fibers from melt electrospinning at the same condition

5.3.3 Thermal Properties of Melt Electrospun PLA-PEO Fibers

The thermal properties of fibers are studied to track the thermal history and mechanical history of the fibers as we did in the previous chapters. The DSC scan curves of melt electrospun PLA-3PEO-EX and PLA-50PEO-EX fibers are shown in Figure 63. These fibers were electrospun at two different nozzle temperatures: 225^{o}C and 255^{o}C. All curves exhibits some characteristic features: a cold crystallization peak and a melting peak of PLA although PLA-3PEO shows an additional melting peak of imperfect α crystals and PLA-50PEO shows the melting peak of PEO at around 57^{o}C. At nozzle temperature of 255^{o}C, PLA-3PEO fibers only exhibit small amount of

crystallinity (8%) which is slightly higher than the melt electrospun PLA fibers. Large presence of PEO (50 wt%) suppresses the cold crystallization of PLA but it does increase the crystallinity of PLA from 8.0% to 20.4%.

Besides the existence of PEO, nozzle temperature is another factor to affect the thermal properties of fibers. After comparing the two sets of curves, we conclude that at low nozzle temperature not only is the melting temperature and cold crystallization temperature of PLA lower than at high nozzle temperature, but also the crystallinity is smaller. The possible reason is that with the high nozzle temperature, fibers require longer time to fully cool down and molecules have more time to crystallize or crystallize into more perfect structures.

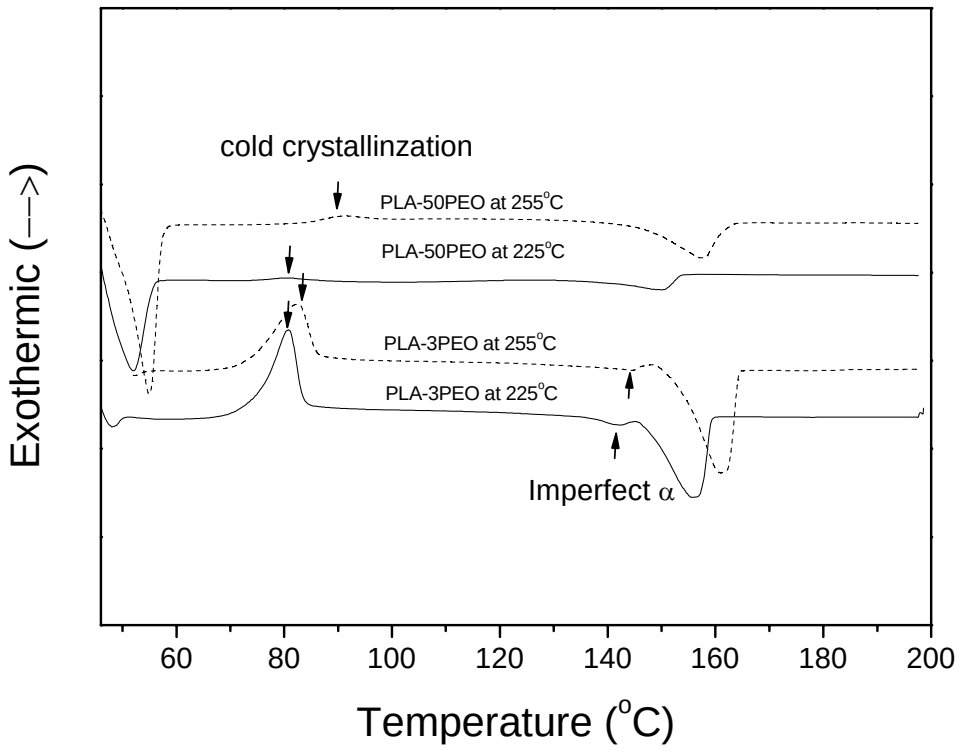

Figure 63 First scan curve of DSC thermogram of PLA-3PEO-EX and PLA-50PEO-EX from melt electrospinning at two different nozzle temperatures: 225°C and 255°C

5.3.4 Structural Characteristics of Melt Electrospun Fibers

As indicated in the solution electrospun PLA-PEO fibers, fast solidification during electrospinning prevents the crystal structure from formation, especially for the slow crystallizable polymers. The relaxation time is much longer for PLA than the residence time in which molecules can reorganize. Adding small amount of PEO does not change the characteristic time of crystallization thus amorphous morphological structure will be observed which is manifested in Figure 64.

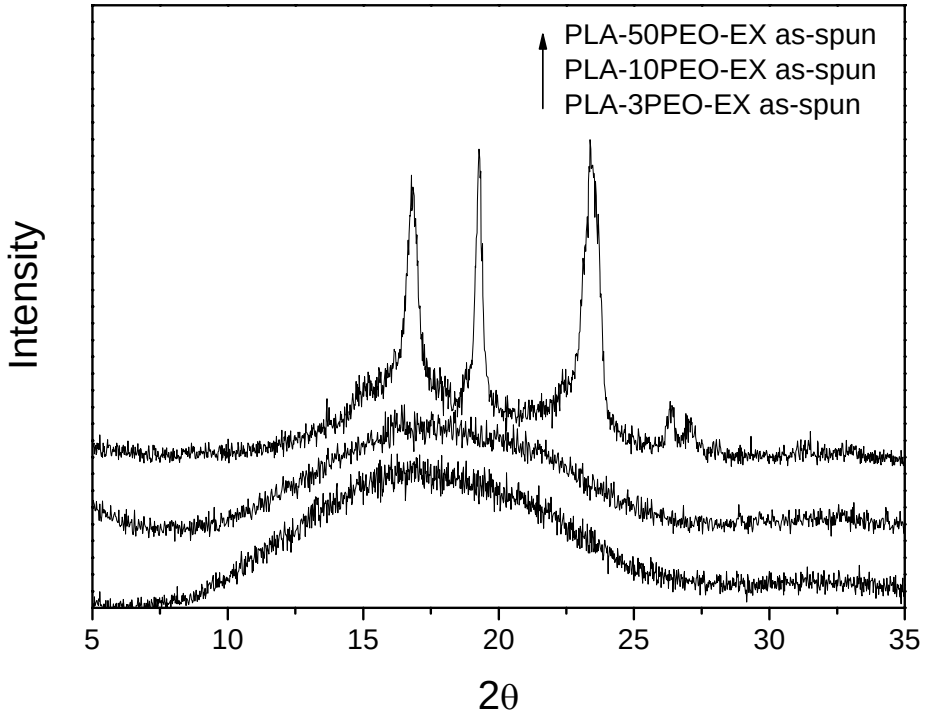

Figure 64 XRD patterns of melt electrospun PLA-PEO-EX fibers at all compositions

For PLA-3PEO and PLA-10PEO fibers, there is a strong amorphous halo present and only a tiny peak at 28^{o} assigned to α structure is observable. The PLA-50PEO fibers show strong α peak at 16.7^{o} and typical PEO crystal peaks are detected. This is a very interesting phenomenon since during solution electrospinning there is no strong PLA peaks at 16.7^{o}. We attribute this phenomenon to concomitant crystallization. Due to the strong entanglement and interaction between PLA and PEO molecules, the organization and crystallization of PEO creates free space and provides additional energy for the oriented structures of PLA to crystallize. The interaction between two species is critical in this case. Park and co-workers studied the crystallization behavior of PLA and poly(butylenes succinate) and found that there was PLA crystal peaks observed with existing PBS peaks [171].

5.3.5 Mechanical Properties of the Blend Fibers

The improvement of mechanical properties by blending PEO into PLA is already shown in solution electrospun fibers. PLA-50PEO-EX fibers from solution electrospinning display the strongest properties. However in melt electrospinning, due to the strong adhesion between PLA-50PEO fibers shown in morphological studies. The comparison is not meaningful in regard to the fiber strength. As an example, PLA-10PEO fiber mats were tested and the data is listed in Table 11.

Compared to the pure PLA from melt electrospinning, the modulus is improved by 130% and the yield strength is increased by over 26%. However the break strain is not superior to the pure PLA fibers with a moderate decrease.

Table 11 Comparison between the mechanical properties of PLA and PLA-10PEO-EX fibers from melt electrospinning at the same condition

	Young's Modulus(MPa)	Yield Strength(MPa)	Break Strain
PLA	18.0	0.38	0.34
PLA-10PEO	30.0	0.54	0.17

5.3.6 Application of PLA-PEO Blend Fibers on Filter Media

Cellulose filter media covered with 0.1g/sqft PLA-10PEO fibers were prepared using rotational collector. The morphology of fibers on the filter media is shown in Figure 65. The average fiber diameter is 2.6 μm with relative small deviation. The obtained fibers have good adhesion with each other.

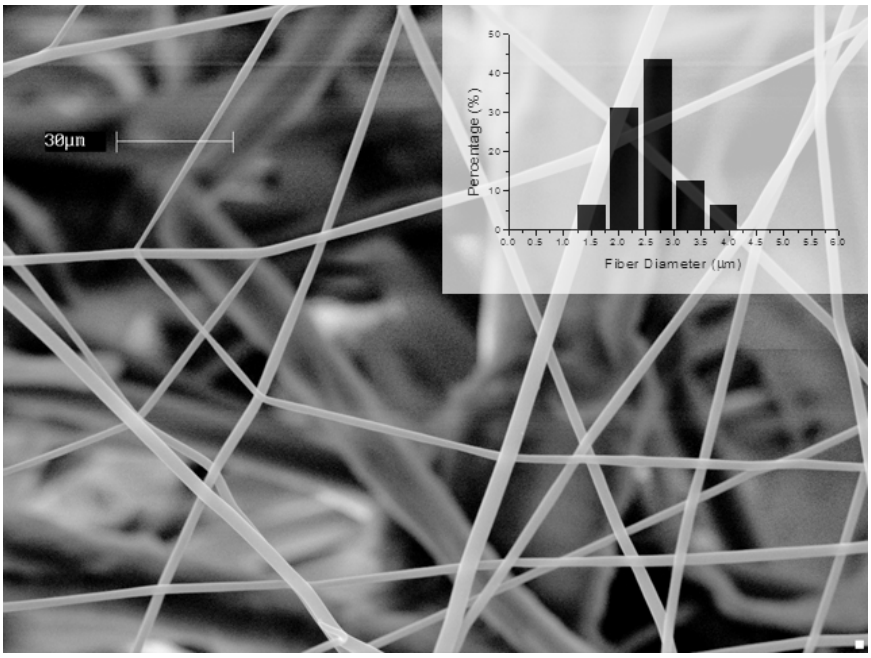

Figure 65 SEM micrograph of PLA-10PEO fibers on filter media

The filtration efficiency of the filter media covered with 0.1g/sqft of PLA-10PEO is shown in Figure 66. At dust particle size above 700nm, the filtration efficiency is comparable among all the filter media. When dust particles size goes below that, the advantage of using sub-micron fibers appears. With decreasing fiber size, the filtration efficiency increases from 34.5% to 38.2% and finally reaches 47.4%.

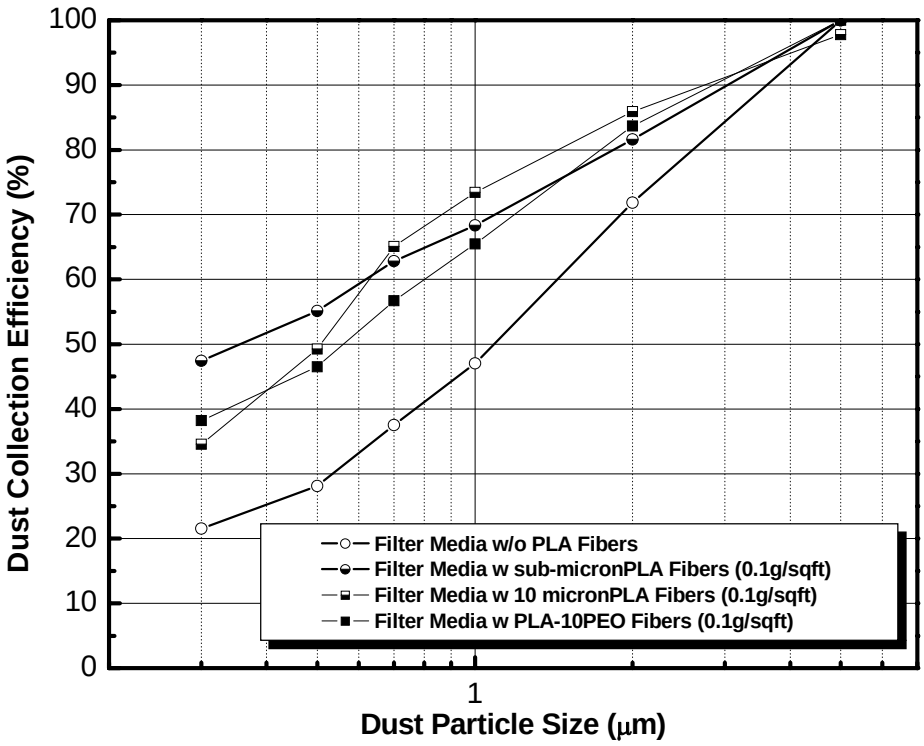

Figure 66 Filtration efficiency of filter media covered with 0.1g/sqft of 10 μm PLA fibers, sub-micron PLA fibers and 2.6 μm PLA-10PEO fibers

CHAPTER 6

SUB-MICRON SCALE POLYPROPYLENE FIBERS FROM SOLUTION ELECTROSPINNING AT ELEVATED TEMPERATURE

Polyolefin non-woven fibers are to our great interest due to some of their advantageous properties such as hydrophobic feature, good mechanical strength, good chemical resistance, and so on. Gel spun UHMWPE fiber is the strongest fiber among all synthetic fibers. It is approximately fifteen times stronger than steel of the same weight while Kevlar fiber is only five times stronger. Polypropylene fiber is the lightest synthetic fiber and comprises the majority of non-woven polyolefin fibers. In recent years, sub-micron polyolefin fibers are sought to meet the demands in the field of filtration, battery separators and protective coating because of the high surface area to volume ratio.

Electrospinning has been widely studied during the past few years [172, 173]. Over a hundred polymers are reported to be successfully electrospun and jet thinning always causes the deformation of the jet and thus changes the structures of resulting fibers. In addition, the mechanism of jet thinning [34, 36, 146, 148] and the effects of a variety of parameters [16, 26, 145, 173] are investigated for us to better understand the electrospinning process. However, electrospinning of sub-micron polyolefin fibers is still in early stages and only few studies have been published. Larrondo [12-14] was the first reported to apply an electrical field to polyolefin melts to obtain their fiber form, but the instabilities to cause thinning of the jet via the whipping motion had not been explored, leading to the collection of thick (50 micron sized) fibers. Lyons [97, 98] and co-workers systematically studied the effect of processing conditions on electrospinning polypropylene fibers from its melt and found that molecular weight

was the most important factor in obtaining thin fibers. However, parameters such as the temperature in the jet region were yet to be investigated to minimize the fiber diameter as discussed in our previous paper [91].

Recently, exploring the possibility of producing superhydrophobic fiber mats through electrospinning has been intensively carried out [174-177]. Superhydrophobic materials are of great interest for anti-fouling and self-cleaning surfaces. Researchers [174] in the Rutledge group studied the superhydrophobicity of poly (styrene-block-dimethylsiloxane) block copolymer fibers and concluded that it is attributed to the combined effects of surface enrichment of siloxane and the surface roughness of the fiber mat. Other researchers such as Singh and co-workers [176] synthesized a novel fluoro-polymer to obtain superhydrophobic film via electrospinning. The wettability of a film depends on the surface energy and surface roughness [178, 179] according to the theory of roughness-induced hydrophobicity developed by Wenzel and Cassie-Baxter. Superhydrophobicity can be produced by generating sub-micron or micron scale roughness on the inherently hydrophobic surface. Electrospinning can exactly produce the roughness at this scale easily and is a promising method to introduce superhydrophobicity to many materials though other methods are sought at the same time. Porous isotactic polypropylene films are prepared by evaporating the solvent from the gel at vacuum environment [180] and superhydrophobicity is observed with a contact angle up to 160^{o}. The surface roughness is determined at 300nm. Combined methods of electrospinning and coating of hydrophobic materials are also reported in several papers. For example, Ma et al. combined the methods of electrospinning and initiated chemical vapor deposition to produce superhydrophobic poly(caprolactone) surface coated with hydrophobic polymerized perfluoroalkyl ethyl methacrylate [175]. Generally speaking, electrospinning is utilized to generate a sub-micron scale roughness and coating of the hydrophobic materials enables the superhydrophobicity.

Electrospinning of polypropylene fibers can be a more straightforward, single-step method to produce superhydrophobicity compared to the methods described above which involves either complicated synthesis of hydrophobic materials or additional coating.

In the current study, we set up an experimental device to carry out the solution electrospinning of polyolefin at elevated temperature since polyolefin does not have proper solvents at room temperature. The effects of spinning parameters--especially nozzle temperature and spinning temperature--on fiber morphology are investigated. The resulting fiber mats are characterized thoroughly and their morphology, thermal properties, structural characteristics and superhydrophobic nature are discussed. Finally, sub-micron polypropylene fibers are directly deposited onto filter media and the enhancement in filtration efficiency for sub-micron scale dust particles is achieved.

6.1 Experiments

The experimental setup used in melt electrospinning was employed in our electrospinning experiments at elevated temperature. Polyolefin solution is kept in a reservoir at relatively low temperature enough to maintain the solution, while nozzle temperature is adjusted to obtain the optimal spinning viscosity. Spinning region temperature controls the solidification of the jet through balancing solvent evaporation and gelling of the jet. Collector temperature controlling is a great addition to regulate the crystallinity of fibers in line by annealing or quenching.

Two isotactic polypropylenes were employed in this study: one (PPMFI) with a molecular weight of 129,000 and polydispersity of 2.8 from Clarcor and the other (PPN) with a molecular weight of 176,000 and polydispersity of 1.8 from Dow Chemical Co. HDPE (GHR 8110) and UHMWPE (GUR 4120) were provided by Ticona, Inc. with a molecular weight of around 800,000 and 2 million respectively.

PPN was exclusively used to study the effect of solution concentration on fiber morphologies. So from now on, all polypropylene indicates PPMFI except where PPN is marked. Variously concentrated PPN, 10 wt% of PPMFI, 10% wt% of HDPE and 1.5wt% of UHMWPE in decalin with 0.5 wt% of antioxidant were prepared separately at 130^{o}C. Each solution was loaded into a 5 mL syringe with an 18-gauge needle and mounted in the spinning setup which had been preheated with T_1 = 130^{o}C, T_2 = 155^{o}C, T_3 = 95^{o}C. Flow rate was set at 0.02 ml/min. T_2 was varied from 140^{o}C to 170^{o}C to study the effect of nozzle temperature. It is worth noting that the needle was connected to a positive power supply and the collector to a negative power supply (Gamma High Voltage) instead of ground in normal cases. The voltage on the needle is noted as *V*+ and collector as *V*- . *V*+ was set from 3 kV to 8 kV and *V*- at -12 kV with the collecting distance *D* at 3 inches. Fibers were collected onto an aluminum plate.

To study the effect of molecular weight on heated solution electrospinning, PP resins were thermally degraded at 235^{o}C for various durations: 5 min, 10min and 30min. The molecular weight was then characterized by HTGPC. 25 wt% degraded polypropylene in decalin solutions were prepared followed by electrospinning experiments using the same procedures described above.

In the filtration efficiency study, a rotational collector with high voltage contact was adopted with a rotational speed at around 10 rpm to homogeneously electrospin PP fibers on filter media.

As-spun fibers were then subjected to various characterizations. Fiber size and surface morphology were determined by a scanning electron microscopy (Leica 440). Thermal properties were analyzed by differential scanning calorimetry (Seiko, DSC 220C) with heating rate at 10^{o}C/min in nitrogen atmosphere until the temperature reached 200^{o}C. Structural studies were performed through XRD (Scintag, Inc. Theta-Theta Diffractometer) in the 2θ range of 5-35^{o}, in steps of 0.02^{o} and a scanning rate of

3 degree per minute. Water contact angle was measured through Contact Angle Analyzer manufactured by Electric Time Co. Inc. The collection efficiency of dust particles in air was measured using a custom-built filtration efficiency tester. Dust particles were counted before and after passing air through the filter media. Air was fed at a rate of 6.9 cfm through each flat-sheet filter and the collection efficiency of dust particles in the size range of 0.03 to 5 μm was measured.

6.2 Processing Conditions and Morphology

Heated solution electrospinning belongs to the category of solution electrospinning in which processing parameters such as solution concentration, flow rate, spinning voltage, spinning temperature and collecting distance play very important role in affecting the electrospinning process and morphologies of consequent fiber.

6.2.1 Effect of Nozzle Temperature

In our polyolefin solution electrospinning at elevated temperature, we found needle temperature and spinning temperature are critical to the success of electrospinning as in melt electrospinning of PLA [91]. They are collectively the same for the control of jet solidification but differ in the mechanism. For melt electrospinning, nozzle temperature is the key to controlling melt viscosity but is limited by the decomposition temperature of polymers [91]. While in solution electrospinning, nozzle temperature is set to an optimal value between solution gelling temperature and solvent boiling temperature. For 10 wt% of PP in decalin solution and T1 below 140^{o}C or above 170^{o}C, there are no fibers obtained because of either fast gelling or fast solvent evaporation. Figure 67 shows the operable temperature window of nozzle temperature and its effect on the average diameter of polypropylene fibers collected at the same conditions. To obtain sub-micron scale fibers, 155^{o}C was found

to be the optimum nozzle temperature. At this temperature, smallest fibers with the least variation were produced.

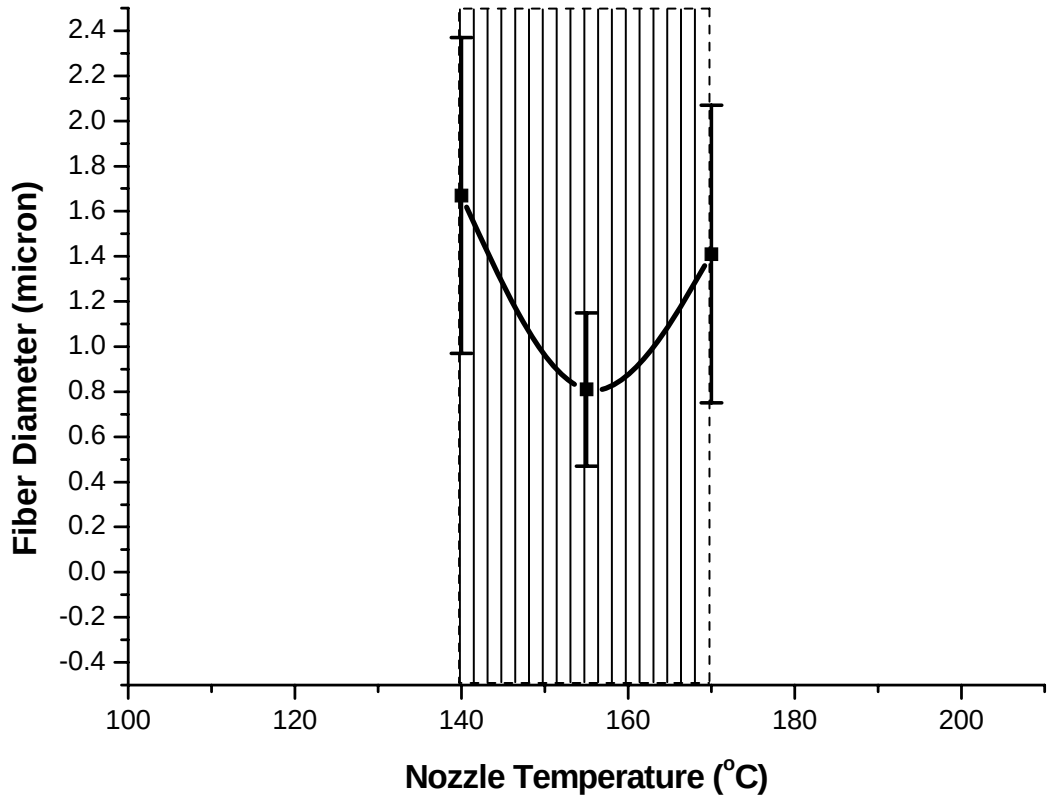

Figure 67 Effect of nozzle temperature on the average diameter of electrospun PP fibers

6.2.2 Effect of Concentration on Fiber Morphologies

Concentration is another important factor which influences fiber morphology, such as formation of beads or smooth fibers. Fibers obtained from 10 wt% solution exhibit both beads and fibers (Figure 68). The size of fibers ranges from 250 nm to 500 nm, while bead diameters are close to 10 μm. As concentration increases, the number of beads decreases and eventually approaches zero. Only at concentrations above 25 wt%

could smooth fibers with relatively large diameter be obtained. Fibers collected from 30 wt% PP in decalin solution have diameter ranging from 3 μm to 20 μm. The concentration not only affects the viscosity of the solution but also controls indirectly the evaporation of the solvent since decalin has a high boiling point at 176°C. An increase in PP content in solutions gradually eliminates the multi-mode distributions of beads and fibers to form homogeneous fibers.

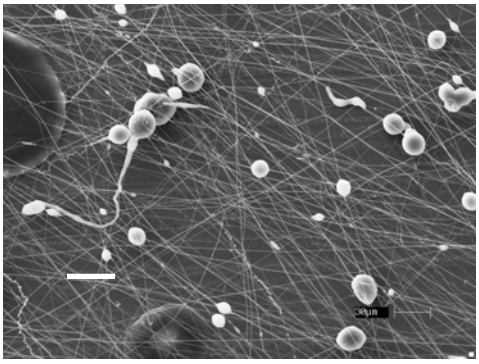

10 wt% PP/decalin

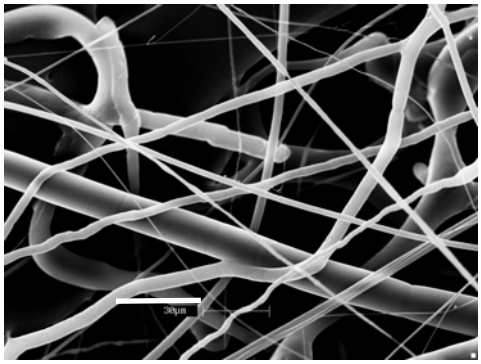

15 wt% PP/decalin

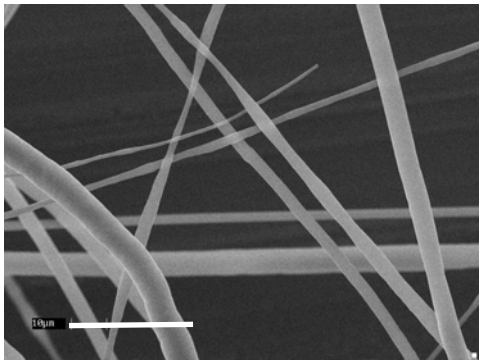

25 wt% PP/decalin

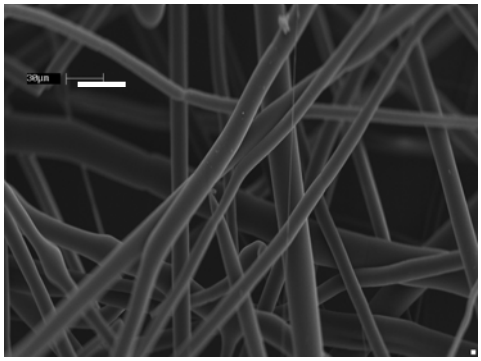

30 wt% PP/decalin

Figure 68 Effect of solution concentration on the morphology of electrospun PP fibers (30 micron scale bar)

6.2.3 Effect of Molecular Weight

The molecular weight of degraded polypropylene is potted against the degradation time and we find that the weight average molecular weight decreases faster than number average molecular weight (Figure 69). In other words, the polydispersity of polypropylene is decreasing as degradation time increases. The number average molecular weight is too small to measure accurately at 30 min and the polydispersity is irrational at this case.

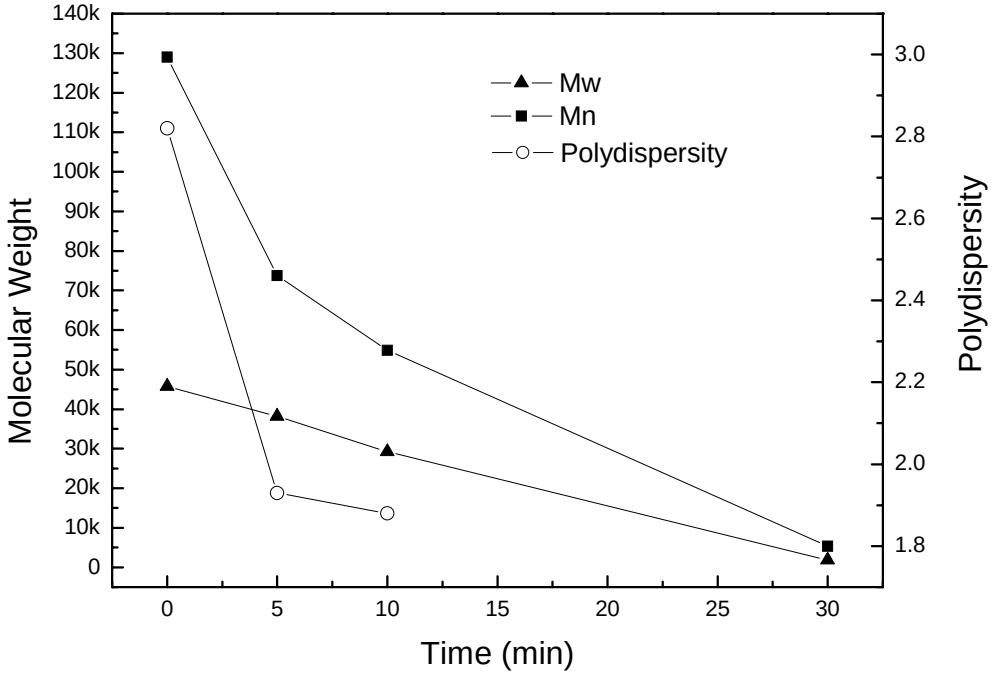

Figure 69 Molecular weight of polypropylene depending on degradation time at 235^{o}C

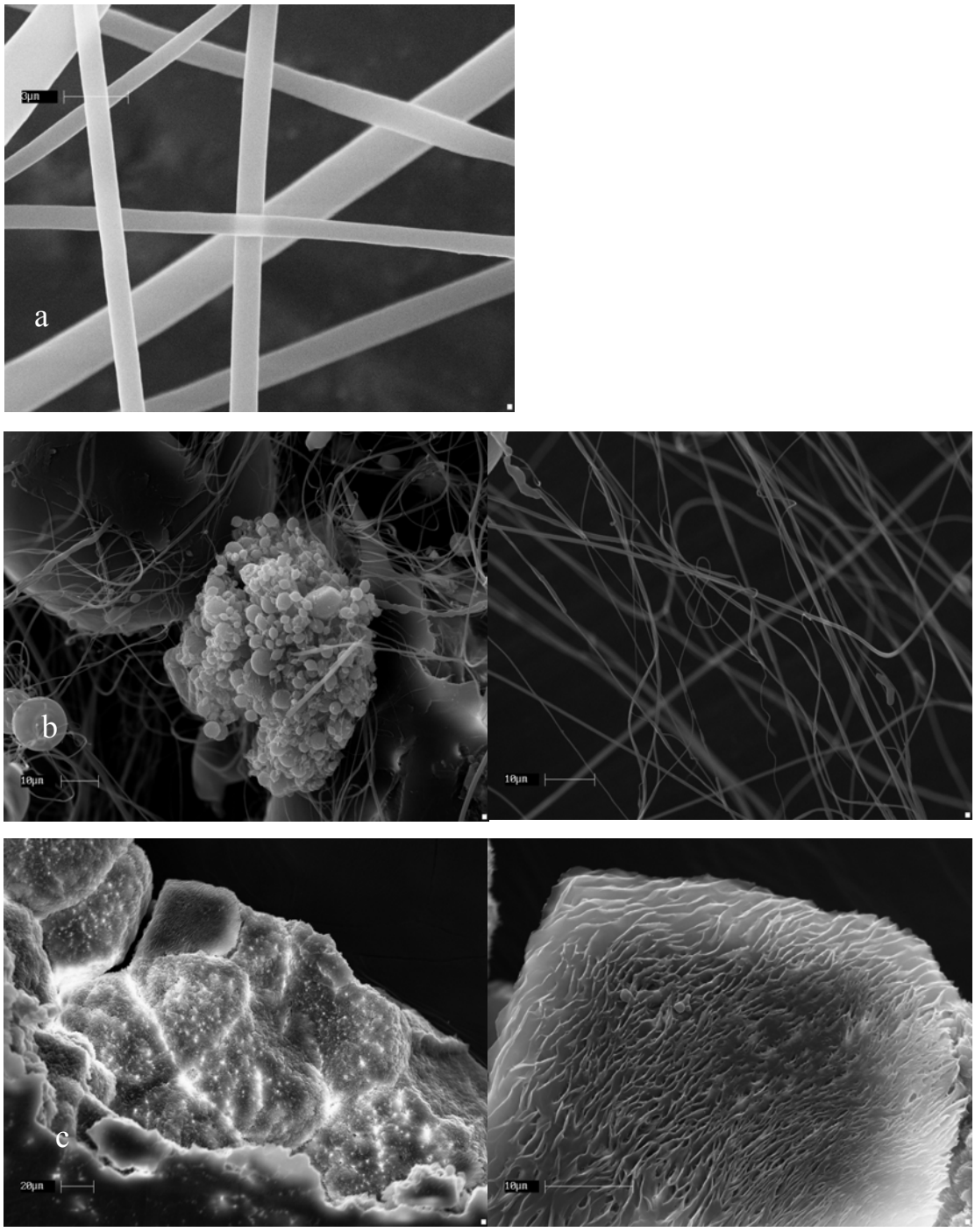

Figure 70 SEM micrographs of degraded polypropylene fibers or droplets: a) 5 mins b) 10 mins c) 30 mins

SEM images of the degraded polypropylene fibers are shown in Figure 70. Continuous fibers can be successfully electrospun from degraded PP for 5min and the fiber size is considerably smaller than those with original molecular weight. For 10min, small fibers with droplet of various sizes are obtained and for 30 min, there is no fiber at all.

6.2.4 Other Parameters

Conductivity is a key parameter in determining the charge density of the solutions, and is thus closely related to the stretching force during electrospinning. Polyolefin/decalin solution has an extremely low conductivity compared to other typical polar solutions which makes the initiation of electrospinning difficult. The combination of positive polarity on the needle and negative polarity on the collector helps the jet eject out of the needle and experience greater stretching force by differentiate the potential of the collector with the grounded heated spinning chamber. Another method to compensate for the low conductivity of solutions is to add highly conductive salt to the solution. Lithium chloride is reported to work well for this purpose [33].

For completeness, SEM images of HDPE and UHMWPE fibers from decalin solutions are shown in Figure 71. From this point on, our studies will be focused only on polypropylene fibers. Detailed studies on HDPE and UHMWPE fibers will be available in forthcoming papers.

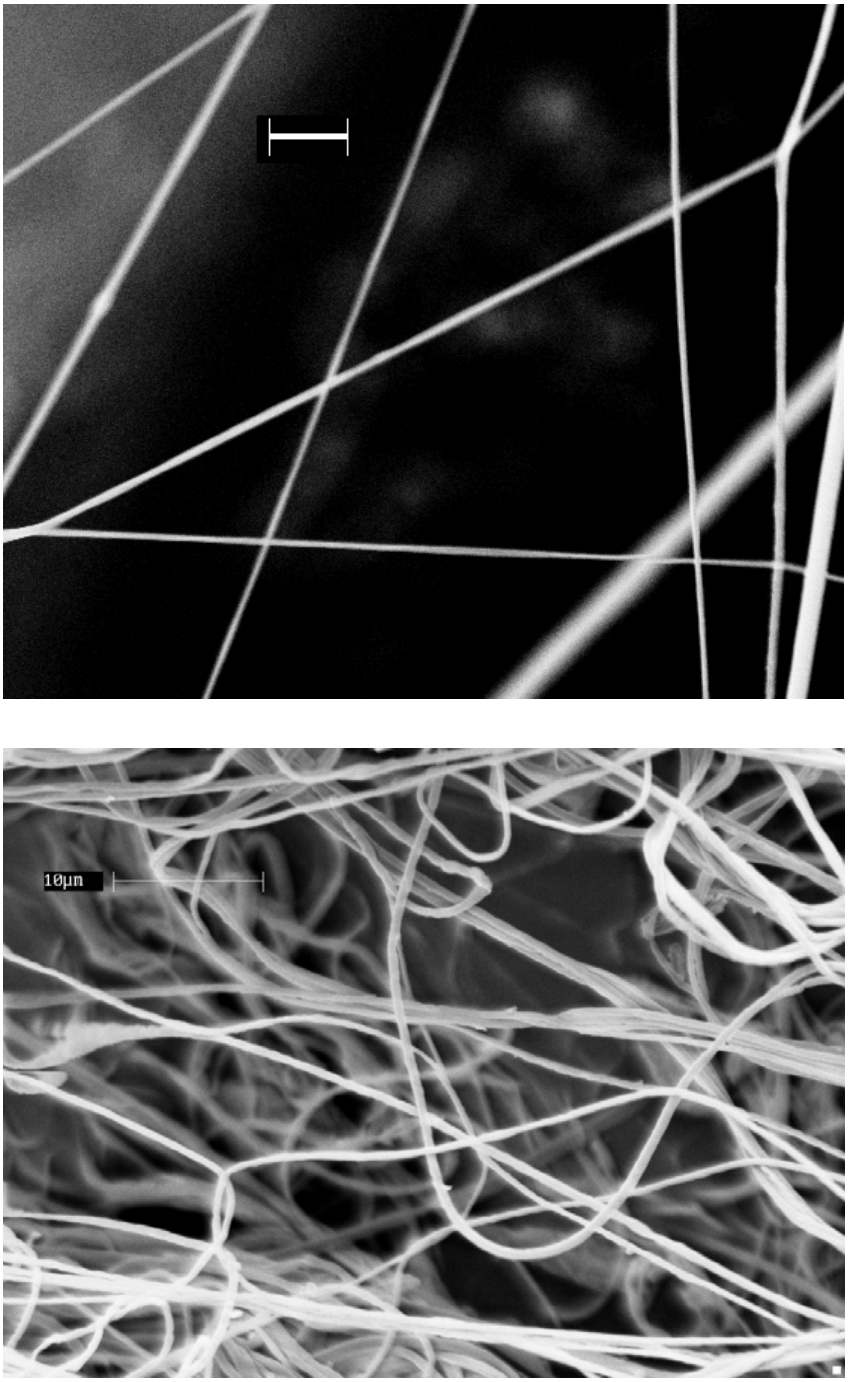

Figure71 SEM images of HDPE and UHMWPE fibers; 10 wt% of HDPE and 1.5wt% of UHMWPE in decalin were used in each case (10 µm scale bar)

6.2.5 Thermal Properties and Crystal Structures

Isotactic polypropylene has three types of crystal structures: α, β and γ crystal form. α structure is thermodynamically the most stable phase and the primary form under normal processing conditions. β crystals are usually obtained by shearing PP melts or through designed crystallization with a special nucleating agent. PP with β crystals exhibits a better impact strength and toughness than in α crystals [181]. γ crystals can be formed during crystallization under high pressure (above 200 MPa) and have not been studied in all aspects.

It has been reported by many authors that electrospun fibers exhibit to some extent meta-stable phases [79, 80, 82] possibly due to two reasons: deformation of the jet and fast solidification (fast solvent evaporation or/and rapid temperature drop). Elongational deformation in electrospinning processes tends to align polymer molecules, and subsequent rapid solidification can freeze the alignment of molecules. Sub-micron sized PP fibers obtained in the current study also exhibit meta-stable β crystals (see Figure 72). For as-received PP resins, there is only one endothermic peak around 162.5^{o}C which is the melting peak for α crystal phase. DSC curves for two different fibers are also shown in the Figure. One is collected with the collector temperature (T4) at 40^{o}C (denoted as PPF-40) and the other is collected at 120^{o}C (PPF-120) with all other conditions the same. As shown in the Figure, for PPF-40, there is a small shoulder with the main endothermic peak at lower temperature around 146.9^{o}C, while the curve for PPF-120 has four distinct peaks. Two are α melting and the other two are β melting peaks. This peak splitting is closely associated with a degree of perfection of the crystals. PPF-40 fibers are collected at a temperature where PP crystallizes really slowly, whereas PPF-120 fibers may have enough thermal energy to recrystallize at 120^{o}C which can cause the splitting [182, 183]. The heat of fusion for pure isotactic polypropylene is taken as 188J/g and the crystallinity

calculated based on this value for PPF-40 is 53.0%. The crystallinity of PPF-120 exceeds 59.4% assuming that the heats of fusion for α and β are the same. It can be explained that part of the deformed structures are frozen in the fibers at 40°C and for PPF-120, the high collecting temperature enables PP molecules with more energy to recrystallize thus increases the total crystallinity of as-spun fibers.

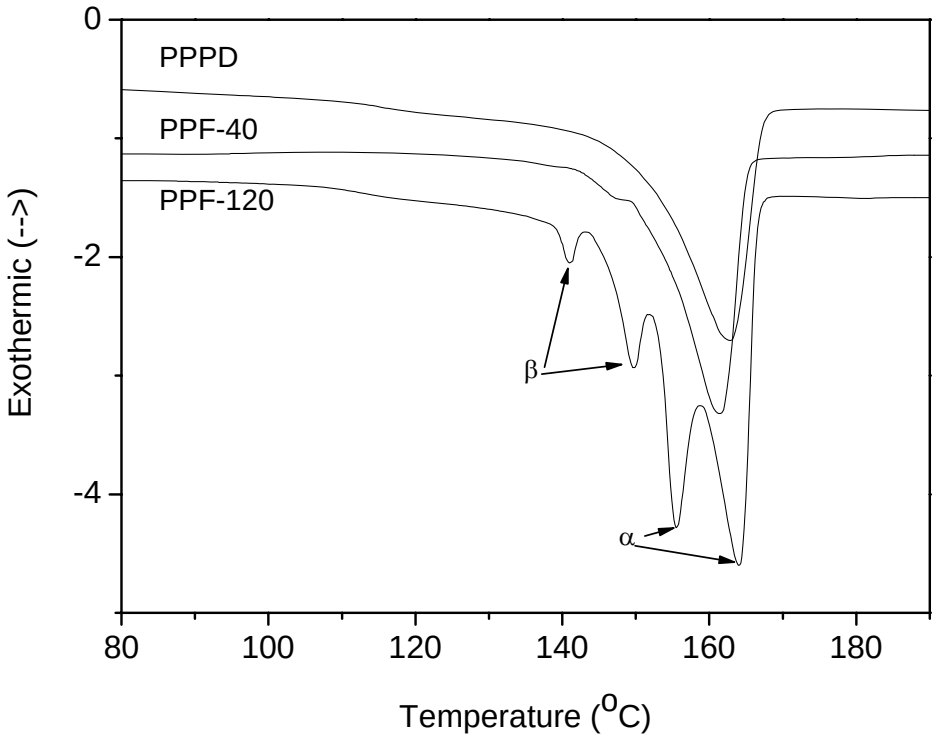

Figure 72 DSC curves for PP resin, PP fibers collected at 40°C and 120°C

These structural changes of PP fibers are further confirmed by the XRD studies (see Figure 73) in which we investigate the relationship between fiber diameter and β content as well as the effect of collecting temperatures. The most distinct change for fibers is the β (300) peak at around 16.2 degrees. After deconvolution of the XRD

curves, we can obtain the detailed phase composition in each fiber system. The β content is estimated based on the calculation of the Turner Jones parameter, k_β, given by [184]

$$k_\beta = I_{\beta(300)} / (I_{\beta(300)} + I_{\alpha(110)} + I_{\alpha(040)} + I_{\alpha(130)})$$

These data are compiled into Table 12. According to the Table, PPF-120 exhibits a higher crystallinity (65.0%) than PPF-40 (53.6%) which agrees with our DSC study. The degree of β content is also larger for PPF-120 (26.9%) than that for PPF-40 (8.1%). It suggests that the frozen elongated structures crystallize into β crystals at 120^{o}C, which is relative stable at this temperature, so no significant transformation from β to α crystals takes place. However, at 40^{o}C, they remain amorphous structures. To confirm the assumption of relating β content to deformed structures, a fiber sample with an average diameter of 10 microns were prepared at 120^{o}C with the same conditions but a higher concentration. The fibers are understood to experience a lower degree of extension. It has a slightly lower crystallinity (63.4%) compared to PPF-120 (65.0%), while the β composition is significantly smaller than PPF-120 (19.0% vs. 26.9%). Therefore, we can conclude that the β composition is due to the strong deformation during the process: the stronger the deformation, the higher the β content.

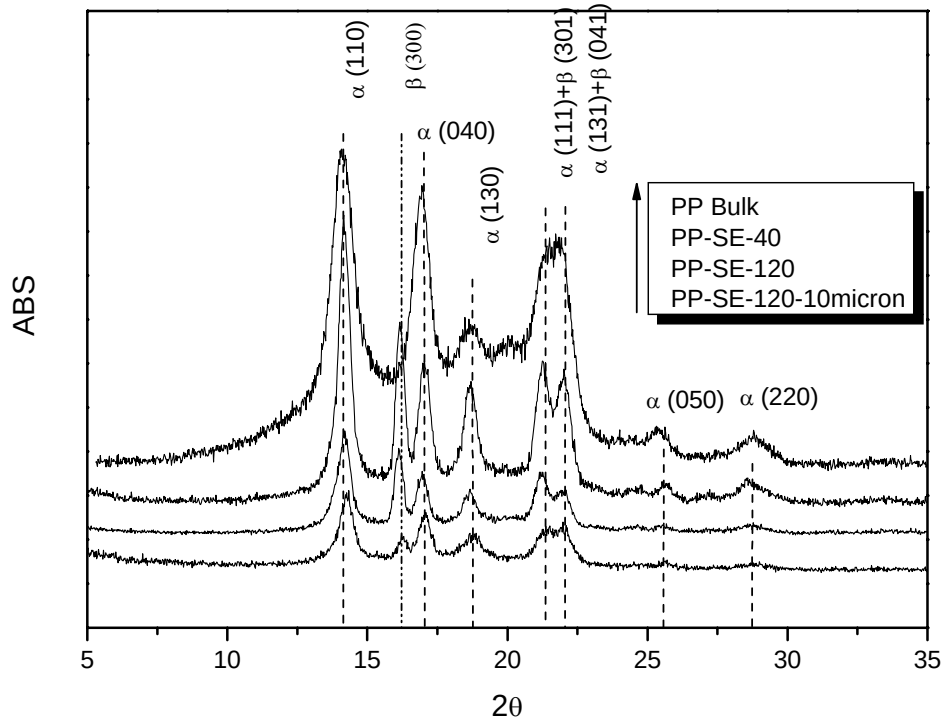

Figure 73 XRD reflection patterns for PP resin, sub-micron PP fibers acquired at 40°C and 120°C and a PP fiber sample with 10 micron size prepared at 120°C

Table 12 Crystallinity and β content of PP resin and fibers

	PP Resin	PPF-40	PPF-120	PPF-120-10micron
Crystallinity (%)	40.2	53.6	65.0	63.4
k_β (%)	0	8.1	26.9	19.0

6.2.6 Hydrophobicity

As mentioned in the Introduction, electrospinning of inherently hydrophobic polypropylene may result in superhydrophobicity. In this study, the water contact angle of three samples are measured: a compression molded PP film, a fiber mat with large fibers of 10 micron scale, and a fiber mat with a mixture of small fibers and beads of sub-micron scale. According to Figure 74, the smooth PP film surface presents a water contact angle of 94^{o}. It is observed that the degree of hydrophobicity is significantly enhanced in our electrospun PP fiber mats. The sub-micron scale fibers even exhibit superhydrophobocity with a water contact angle of 154^{o}. Due to the loose surface morphology, surface plots through AFM are unavailable for the evaluation of surface roughness. However, after examining our fiber mat using SEM (see Figure 75), it is suggested that sub-micron sized fibers have much larger surface area and the number density of fibers is larger for the sub-micron scale fiber mat. And these two factors have great influences on the hydrophobicity of the fiber mat. For PP mats with small fiber size, there are more fibers underlying the water droplet and therefore more repellence can be observed.

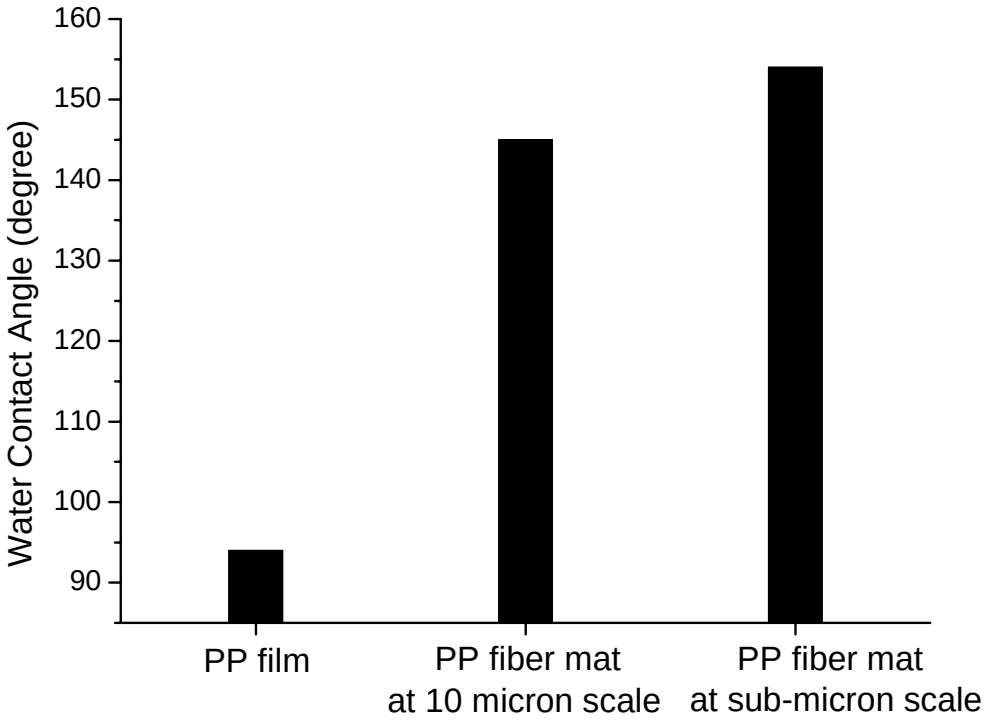

Figure 74 Water contact angle of three different surfaces: compression molded PP film, PP mat of 10 micron scale fibers and PP mat of sub-micron scale fibers

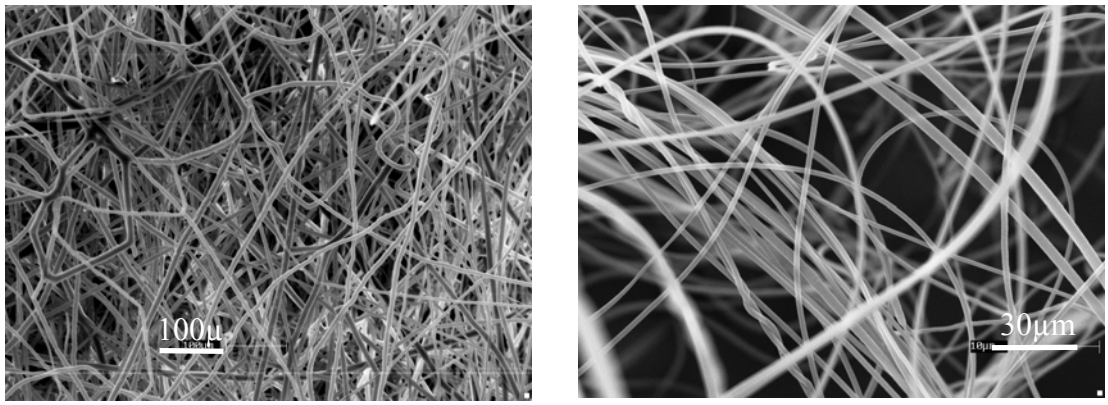

Figure 75 SEM images of mat of 10 micron scale fibers and sub-micron scale fibers, and a water drop on their surfaces

Figure 75 (Continued)

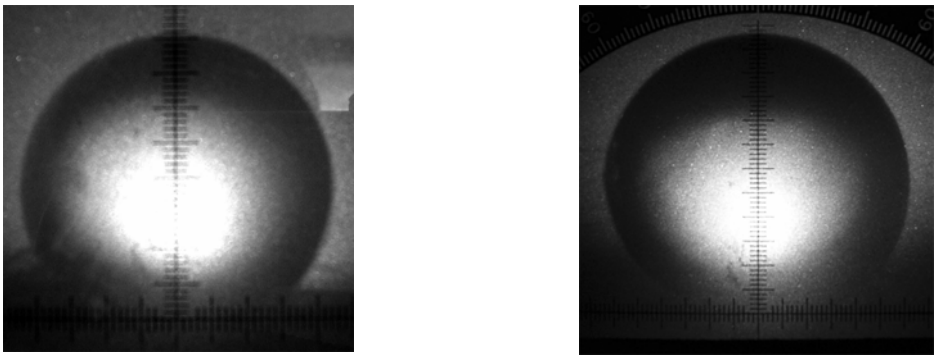

6.2.7 Filtration Efficiency of Sub-micron PP Covered Filter Media

Our final discussion is the filtration efficiency of cellulose filter media covered with PPF-120, shown in Figure 76. The collection efficiency of dust particles in the size range of 0.03 to 5 μm was measured for filter media with and without additional PP fibers. The improvement in the filtration efficiency by laying sub-micron polypropylene fibers on filter media is clearly illustrated in the Figure. It is observed that the enhancement in filtration efficiency due to PP fibers increases with decreasing the dust size.

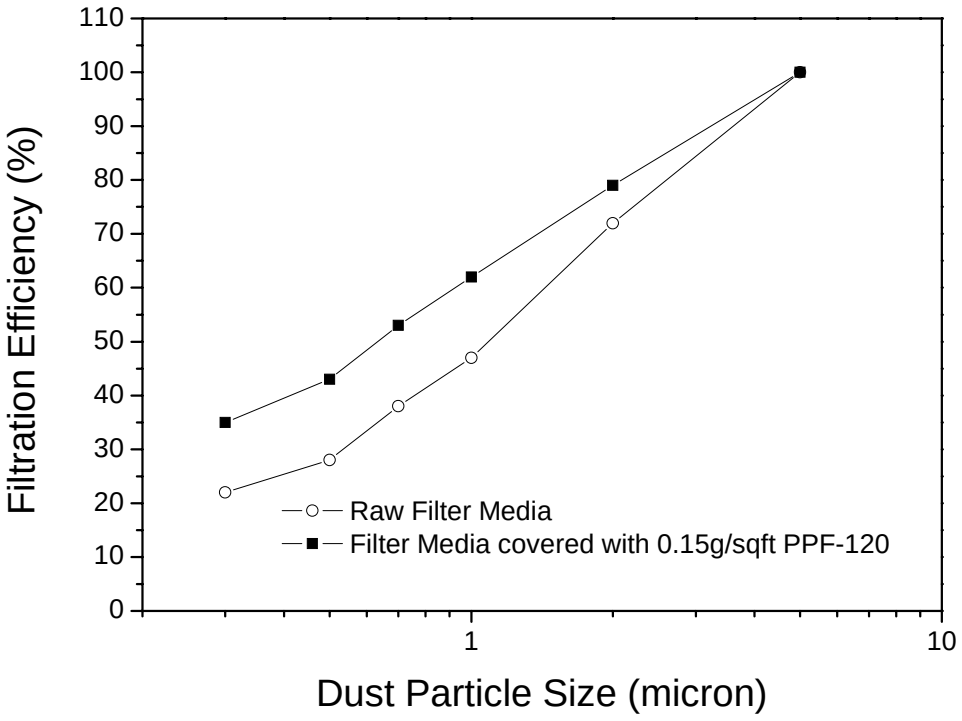

Figure 76 Comparison of filtration efficiency between the raw filter media and the filter media covered with sub-micron PP fibers for different dust particle size

The top view of PP fibers deposited on the filter media is obtained by SEM (Figure 77). The thicker fibers around 10-30 microns in SEM images are cellulose fibers from the base filter media and sub-micron sized electrospun PP fibers on filter media exhibit a uniform distribution in their diameter near 800nm. Although this is believed to be slightly larger than the optimal fiber diameter below 250 nm, we note that the increase in the pressure drop across the filter media with PP fibers was still negligible possibly due to a smaller amount of PP fibers (0.15 g/sqft of filter media).

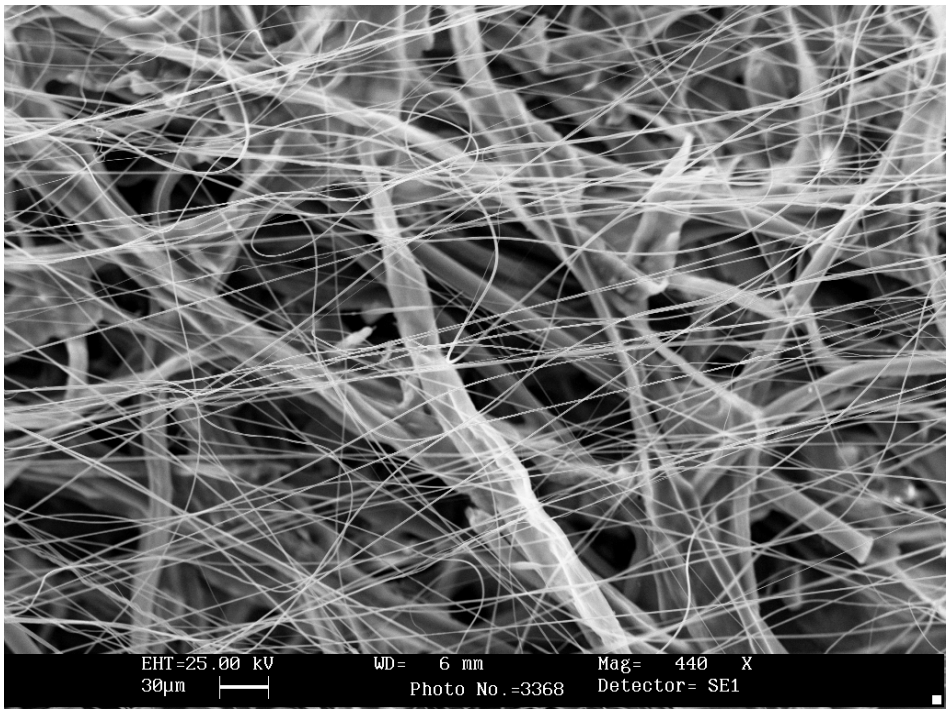

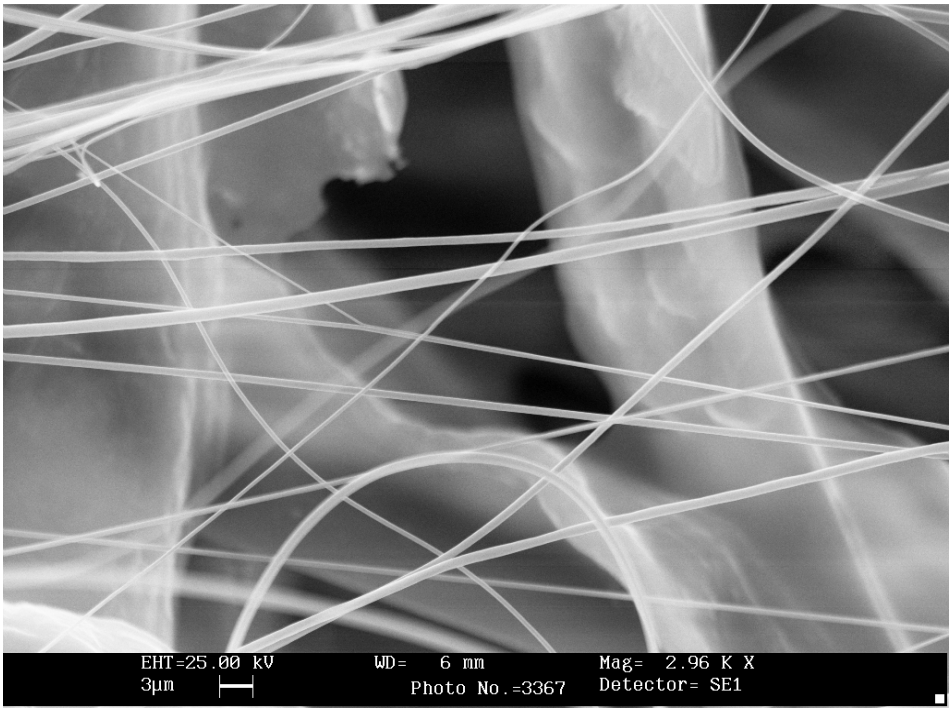

Figure 77 SEM images of filter media covered with PPF-120

CHAPTER 7

CONCLUSIONS

Electrospinning is a versatile tool for producing nano-sized fibers and has been widely studied in many aspects. Over a hundred polymers have been successfully electrospun from their liquid state, mostly solutions. The electrospun fibers are mostly presented as a fiber mat which comprises random oriented nanofibers. These nano-sized fibers have extremely high surface area to volume ratio up to 10,000 m^2/g and useful in a number of applications such as water and air filtration, tissue scaffold and sensor with high sensitivity. In this study, we focused on two polymer categories: biodegradable and biocompatible polylactic acid and widely used polyolefin system.

Polylactic acid is slow crystallizable polymer and during electrospinning crystallization is totally suppressed which eliminates the complications involved. We investigated the effect of processing parameters and inclusion of nanoclay and biocompatible polyethylene oxide on the structures and properties of electrospun fibers. It was found that in solution electrospinning, effects of most of the parameters are similar to the reported results in other papers. Concentration determines the solution viscosity and surface tension which is critical to obtain continuous thin fibers. The addition of highly conductive salt increases the conductivity of solutions and makes the fiber more uniform and bead-free.

We have demonstrated that inclusion of nanoclay enhances the formation of oriented structures in electrospun fibers, which gives rise to substantial cold crystallization between 100^{o}C and 130^{o}C. The intercalated morphologies are preserved during electrospinning. Our results also reveal that electrospinning induces β PLA crystal structure with a fibrillar morphology and the addition of nanoclay enhances the

formation of β crystal structure. This change in molecular structures due to inclusion of nanoclays during electrospinning is shown to significantly increase the mechanical properties of the electrospun fibers and influence the biodegradability. The elastic strength and modulus increases in a non-linear way as the nanoclay concentration increases. 5 wt% is the saturation concentration for nanoclay regarding its effect on the mechanical property of electrospun PLA fibers.

Blending PEO in PLA reduces the glass transition temperature of PLA thus improves the elasticity of PLA. Our studies on the PLA and PEO blend system shows that composition of the blends greatly influences the structures and properties of both their cast films and electrospun fibers. At low concentration (<10 wt%), PLA and PEO are soluble in each other and no significant phase separation is observed. The addition of PEO causes melting temperature depression of PLA. At PEO composition of 50 wt%, phase separation is observed which leads to the strong crystal peak of PEO in XRD studies.

Besides the effects of composition, blending method has significant effects on structures and properties of the blends. The method of direct blending through solutions shows large PEO domain size and poorer domain distribution. On the contrary, extrusion blending creates small and well dispersed PEO domains and it is found to play an important role in controlling the structures and properties as well. In the blend system, effects of PEO comprise two counter-acting sides: boosting crystallization and bringing defects and phase separation. The optimal composition is the point where these two effects are in equilibrium.

The optimal value of the composition is distinctively different for the cast films and electrospun fibers. For the cast films, 3 wt% of PEO in PLA shows the highest PLA crystallinity and thus results in the highest mechanical properties. For

electrospun fibers, 50 wt% of PEO in PLA makes the highest combined crystallinity and shows the strongest mechanical strength.

REFERENCES

1. Huang ZM, Zhang YZ, Kotaki M, Ramakrishna S. Compos. Sci. Technol. 2003, 63, 2223-2253

2. Formhals A. US patent 1,975,504, 1934

3. Formhals A. US patent 2,160,962, 1939

4. Formhals A. US patent, 2,187,306, 1940

5. Formhals A. US patent, 2,323,025, 1943

6. Formhals A. US patent, 2,349,950, 1944

7. Simons HL. US patent 3,280,229, 1966

8. Taylor GI. Proc R Soc London, Series A 1964;280:383

9. Taylor GI. Proc R Soc London, Series A 1966;291:159

10. Taylor GI. Proc R Soc London, Ser A 1969;313:453–475

11. Baumgarten PK. J of Colloid and Interface Science 1971;36:71–79

12. Larrondo L, Manley SJ. J Polym Sci: Polym Phys Ed 1981;19:909-920

13. Larrondo L, Manley SJ. J Polym Sci: Polym Phys Ed 1981;19:921-932

14. Larrondo L, Manley SJ. J Polym Sci: Polym Phys Ed 1981;19:933

15. Srinivasan G, Reneker DH. Polym. Int. 1995 36 (2): 195-201

16. Doshi J, Reneker DH. J. Electrostatics 1995;35 (2-3): 151-160 AUG 1995

17. Reneker DH, Chun I. Nanotechnology 1996;7 (3): 216-223

18. Fong H, Chun I, Reneker DH. Polymer 1999; 40 (16): 4585-4592

19. Reneker DH, Yarin AL, Fong H, et al. J. Appl. Phys. 2000;87 (9): 4531-4547

20. Hou HQ, Reneker DH. Adv. Mater. 2004;16 (1): 69-73

21. Ostermann R, Li D, Yin YD, et al. Nano Lett. 2006;6 (6): 1297-1302

22. Ko F, Gogotsi Y, Ali A, et al. Adv. Mater. 2003; 15 (14): 1161-1165

23. Seoul C, Kim YT, Baek CK. J. Polym. Sci., Part B: Polym. Phys. 2003;41 (13): 1572-1577

24. Sen R, Zhao B, Perea D, et al. Nano Lett. 2004;4 (3): 459-464

25. Fong H, Liu WD, Wang CS, et al. POLYMER 2002 ;43 (3): 775-780

26. Zhou HJ, Kim KW, Giannelis E, et al. ACS SYMPOSIUM SERIES 918: 217-230 2006

27. Ji Y, Li BQ, Ge SR, et al. Langmuir 2006, 22, 1321-1328

28. Mack JJ, Viculis LM, Ali A, et al. Adv. Mater. 2005;17 (1): 77-80

29. Sun ZC, Zussman E, Yarin AL, et al. Adv. Mater. 2003;15 (22):1929-1932

30. Zhang YZ, Huang ZM, Xu XJ, et al. Chem. Mater. 2004 ;16 (18):3406-3409

31. Li D, Babel A, Jenekhe SA, et al. Adv. Mater. 2004;16 (22): 2062-2066

32. Li D, Xia YN. Nano Lett. 2004;4 (5): 933-938

33. Carroll CP, Joo YL. Phys. Fluids 2006;18:053102-14

34. Shin YM, Hohman MM, Brenner MP, et al. Polymer 2001;42 (25): 9955-9967

35. Shin YM, Hohman MM, Brenner MP, et al. Phys Fluids 2001;13: 2201-2220

36. Shin YM, Hohman MM, Brenner MP, et al. Phys Fluids 2001;13: 2221-2236

37. Shin YM, Hohman MM, Brenner MP, et al. Appl. Phys. Lett. 2001;78 (8): 1149-1151

38. Wannatong L, Sirivat A, Supaphol P. Polym. Int. 2004;53 (11): 1851-1859

39. Jarusuwannapoom T, Hongroijanawiwat W, Jitjaicham S, et al. Eur. Polym. J. 2005;41 (3): 409-421

40. Tan SH, Inai R, Kotaki M, et al. Polymer 2005;46 (16): 6128-6134

41. Deitzel JM, Kleinmeyer JD, Hirvonen JK, et al. Polymer 2001;42 (19): 8163-8170

42. Li D, Wang YL, Xia YN. Nano Lett. 2003;3 (8): 1167-1171

43. Sundaray B, Subramanian V, Natarajan TS, et al. Appl. Phys. Lett. 2004;84 (7): 1222-1224

44. Theron A, Zussman E, Yarin AL. Nanotechnology 2001;12 (3): 384-390

45. Xu CY, Inai R, Kotaki M, et al. Biomaterials 2004;25 (5): 877-886

46. Dalton PD, Klee D, Moller M. Polymer 2005;46 (3): 611-614

47. Smit E, Buttner U, Sanderson RD. Polymer 200546 (8): 2419-2423

48. Kim HS, Kim K, Jin HJ, et al. Macromol. Symposia 2005;224: 145-154

49. Kim KW, Lee KH, Khil MS, et al. Fibers Polym. 2004;5 (2): 122-127

50. Reneker DH, Kataphinan W, Theron A, et al. Polymer 2002 ;43 (25): 6785-6794

51. Bognitzki M, Frese T, Wendorff JH, et al. Abstr. Paper Am. Chem. Soc. 2000;219: 173-PMSE Part 2

52. You Y, Min BM, Lee SJ, et al. J. Appl. Polym. Sci. 2005;95 (2): 193-200

53. Fang X and Reneker DH. J. Macromol. Sci.-Phys. B 1997;36: 169-173

54. Jin HJ, Chen J, Karageorgiou V, Altman GH, and Kaplan DL. Biomaterials 2004;25: 1039-1047

55. Wnek GE, Carr ME, Simpson DG and Bowlin GL. Nano. Lett. 2003;3:213-216

56. Jiang HL, Fang DF, Hsiao BS, Chu B, and Chen WL. Biomacromolecules 2004;5: 326-333

57. Matthews JA, Wnek GE, Simpson DG, et al. Biomacromol. 2002;3 (2): 232-238

58. Yoshimoto H, Shin YM, Terai H, et al. Biomaterials 2003;24 (12): 2077-2082

59. Lee SW, Belcher AM. Nano Lett. 2004;4 (3): 387-390

60. Sundaray B, Subramanian V, Natarajan TS, et al. Appl. Phys. Lett. 2006;88 (14): Art. No. 143114

61. Ge JJ, Hou HQ, Li Q, et al. JACS 2004;126 (48): 15754-15761

62. Ra EJ, An KH, Kim KK, et al. Chem. Phys. Lett. 2005;413 (1-3): 188-193

63. Lee KH, Kim HY, Ryu YJ, et al. J. Polym. Sci., Part B: Polym. Phys. 2003;41 (11): 1256-1262

64. Kim K, Yu M, Zong XH, et al. Biomaterials 2003 ;24 (27): 4977-4985

65. Drew C, Wang XY, Bruno FF, et al. Compos. Interfaces 2005 ;11 (8-9): 711-724

66. Han GY, Guo B, Zhang LW, et al. Adv. Mater. 2006;18 (13): 1709-1712

67. Wang YZ, Yang QB, Shan GY, et al. Mater. Lett. 2005;59 (24-25): 3046-3049

68. Wang Y, Serrano S, Santiago-Aviles JJ. Synth. Met. 2003;138 (3): 423-427

69. Kim C, Yang KS. Appl. Phys. Lett. 2003;83 (6): 1216-1218

70. Choi SS, Chu B, Lee SG, et al. J. Sol-Gel Sci. Technol. 2004;30 (3): 215-221

71. Dai HQ, Gong J, Kim H, et al. Nanotechnology 2002;13 (5): 674-677

72. Li D, Xia YN. Nano Lett. 2003 ;3 (4): 555-560

73. Son WK, Cho D, Park WH. Nanotechnology 2006;17 (2): 439-443

74. Lee DY, Kim BY, Lee SJ, et al. J. Kor. Phys. Soc. 2006;48 (6): 1686-1690

75. Bognitzki M, Frese T, Steinhart M, et al. Polym. Eng. Sci. 2001 ;41 (6): 982-989

76. Zong XH, Ran SF, Fang DF, et al. Polymer 2003 ;44 (17): 4959-4967

77. Buchko CJ, Chen LC, Shen Y, et al. Polymer 1999 ;40 (26): 7397-740

78. Buchko CJ, Kozloff KM, Martin DC. Biomaterials 2001 ;22 (11): 1289-1300

79. Zeng J, Chen X, Liang Q, Xu X, Jing X Macromol. Biosci. 2004;4:1118-1125

80. Inai R, Kotaki M, Ramakrishna M J. Polym. Sci. Part B: Polym. Phys. 2005;43:3205-3212

81. Gao K, Hu XG, Dai CS, et al. Mater. Sci. Eng., B -Solid State Mat. Adv. Technol. 2006;131 (1-3): 100-105

82. Dersch R, Liu TQ, Schaper AK, Greiner A, Wendroff JH. J. Polym. Sci. Part A: Polym. Chem. 2003;41: 545-553

83. Zong XH, Kim KS, Chu B et. al. Polymer 2002;43: 403-4412

84. Shin K, Xiang HQ, Moon SI, et al. Science 2004; 306 (5693): 76-76

85. Ruotsalainen T, Turku J, Heikkila P, et al. Adv. Mater. 2005;17 (8): 1048-1052

86. Kalra V, Kakad PA, Mendez S, et al. Macromolecule 2006;39 (16): 5453-5457

87. Huang CB, Chen SL, Reneker DH, et al. Adv. Mater. 2006;18 (5): 668-671

88. Kim J-S, Reneker DH. Polymer Composites 1999;20(1):124–31

89. Graham K, Ouyang M, Grafe T, et al. Fifteenth Annual Technical Conference & Expo of the American Filtration & Separations Society, Gavelston, Texas 2002

90. Shin C, Chase GG, Reneker DH. Colloids Surf., A Physicochem. Eng. Aspects 2005;262 (1-3): 211-215

91. Zhou HJ, Green TB, Joo YL. Polymer 2006; 47 (21): 7497-7505

92. Li WJ, Laurencin CT, Caterson EJ, et al. J. Biomed. Mater. Res. 2002;60 (4): 613-621

93. Ji Y, Ghosh K, Shu XZ, et al. Biomaterials 2006 ;27 (20): 3782-3792

94. Jia HF, Zhu GY, Vugrinovich B, et al. Biotechnol. Progr. 2002 ;18 (5): 1027-1032

95. Wang XY, Lee SH, Ku BC, et al. 2002 ; J. Macromol. Sci., Pure Appl. Chem. 2002;A39 (10): 1241-1249

96. Wang XY, Drew C, Lee SH, et al. Nano Lett. 2002;2 (11): 1273-1275

97. Lyons J, Li C, Ko F. Polymer 2004;45(22):7597-7603

98. Lyons J. PhD Dissertation, Drexel University, 2004

99. Kim JS, Lee DS. Polymer. J. 2000; 32: 616-618

100. Lee S, Obendorf SK. J. Appl. Polym. Sci. 2006;102 (4): 3430-3437

101. Dalton PD, Klinkhammer K, Salber J, et al. Biomacromolecules 2006;7 (3): 686-690

102. Ichikawa M, Sugimoto M, Hatada K, et al. Kobunshi Ronbunshu 1995 ;52 (3): 134-140

103. Antoniadis SJ, Samara CT, Theodorou DN. Macromolecules 1999;32 (25): 8635-8644

104. Jones TD, Chaffin KA, Bates FS, et al. Macromolecules 2002;35 (13): 5061-5068

105. Liao TY, Adanur S, Drean JY. Textile Res. J. 1997;67 (10): 753-760

106. Lee SH, Tekmen C, Sigmund WM. Mater. Sci. Eng. A-Struct. Mater. Prop. Microstruct. Process. 2005;398 (1-2): 77-81

107. Tan EPS, Lim CT. Appl. Phys. Lett. 2004;84 (9): 1603-1605

108. Inai R, Kotaki M, Ramakrishna S. Nanotechnology 2005;16 (2): 208-213

109. Vasanthakumari R, Pennings AJ. Polymer 1983;24 (2): 175-178

110. Krikorian V, Pochan DJ. Macromolecules 2004 ;37 (17): 6480-6491

111. Di Lorenzo ML. Eur. Polym. J. 2005;41 (3): 569-575

112. Yasuniwa M, Tsubakihara S, Iura K, et al. Polymer 47 (21): 7554-7563 2006;47 (21): 7554-7563

113. Ogata N, Jimenez G, Kawai H, Ogihara T J. Polym. Sci. Part B: Polym. Phys. 1997, 35, 389-396

114. Ray SS, Maiti P, Okamoto M, Yamada K, Ueda K. Macromolecules 2002, 35, 3104-3110

115. Yang F, Ou YC, Yu ZZ. J. Appl. Polym. Sci. 1998, 69, 355-361

116. Ray SS, Yamada K, Okamoto M, Ueda K. Polymer 2003, 44, 857-866

117. Ray SS, Okamoto M. Macromol. Rapid Commun. 2003, 24, 815-840

118. Ray SS, Yamada K, Okamoto M, Ueda K. Nano Lett. 2002, 2, 1093-1096

119. Groitzsch D, Fahrbach E. US patent 4,618,524, 1986

120. Luu YK, Kim K, Hsiao BS, Chu B, Hadjiargyrou M. J. Controlled Release 2003, 89, 341-353

121. Kim K, Yu MK, et al. Biomaterials 2003, 24, 4977-4985

122. Zeng J, Xu XY, Jing XB, et al. J. Controlled Release 2003, 92, 227-231

123. Kenawy ER, Bowlin GL, Wnek GE, et al. J. Controlled Release 2002, 81, 57-64

124. Shao CL, Kim HY, Park SJ, et al. Mater. Lett. 2003, 57, 1579-1584

125. Gong J, Li XD, Kim HY, et al. J. Appl. Polym. Sci. 2003 ,89, 1573-1578

126. Fong H, Liu WD, Wang CS, Vaia RA. Polymer 2002, 43, 775-780

127. Hoosteen W, Postema AR, Penning AJ, Brinke GT, Zugenmaier P. Macromolecules 1990, 23, 634-642

128. Koombhongse S, Liu WX, Reneker DH. J. Polym. Sci. Part B: Polym. Phys. 2001;39 (21): 2598-2606

129. Huang CB, Chen SL, Lai CL, et al. Nanotechnology 17 (6): 1558-1563

130. Casper CL, Stephens JS, Tassi NG, et al. Macromolecules 37 (2): 573-578

131. Eling B, Gogolewski S, Pennings AJ. Polymer 1982, 23, 1587-1593

132. Sawai D, Takahashi K, Imamura T, Nakamura K, Kanamoto T, Hyon SH. J. Polym. Sci. Part B: Polym. Phys. 2002, 40, 95-104

133. Migliaresi CD, Cohn D, De Lollis A, Fambri L. J. Appl. Polym. Sci. 1991, 43, 83-95

134. Nam JY, Ray SS, Okamoto M. Macromolecules 2003, 36, 7126-7131

135. Ke YC, Yang ZB, Zhu CF. J. Appl. Polym. Sci. 2002, 85, 2677-2691

136. Pluta M, Galeski A, Alexandre M, Paul MA, Dubois P. J. Appl. Polym. Sci. 2002, 86, 1497-1506

137. Stephens JS, Chase DB, Rabolt JF. Macromolecules 2004, 37, 877-881

138. Lehermeier HJ, Dorgan JR. Polym. Eng. Sci. 2001;41:2172-2184

139. Cooper-White JJ, Mackay ME. J. Polym. Sci. Part B: Polym. Phys. 1999;37:1803-1814

140. Dorgan JR, Janzen J, Clayton MP. J. Rheol 2005 49:607-619

141. Wachsen O, Platkowski K, Reichert KH. Polym. Degrad. Stabil. 1997;57:87-94

142. Södergård A, Näsman JH. Polym. Degrad. Stabil. 1994;46:25-30

143. Jamshidi K, Hyon SH, Ikada Y. Polymer 1988;29:2229-2234

144. Zong XH, Kim K. Polymer 2002;43:4403-4412

145. Jun Z, Hou H, Schaper A, Wendorff, JH, Greiner A. e-Polymers 2003;9:1-9

146. Shin YM, Hohman MM, Brenner MP, Rutledge GC. Appl. Phys. Lett. 2001;78:1149-1151

147. Shin YM, Hohman MM, Brenner MP, Rutledge GC. Polymer 2001;42:9955-9967

148. Fridrikh SV, Yu JH, Brenner MP, Rutledge GC. Phys. Rev. Lett. 2003;90: 1445021-1445024

149. Hohman MM, Shin M, Rutledge G, Brenner MP. Phys. Fluids 1997;13:2221-2236

150. Zhang CX, Yuan XY, Wu LL, et al. Eur. Polym. J. 2005;41(3): 423-432

151. Tan SH, Inai R, Kotaki M, et al. Polymer 2005;46 (16): 6128-6134

152. Deitzel JM, Kleinmeyer J, Harris D, et al. Polymer 2001;42 (1): 261-272

153. Krishnappa RVN, Desai K, Sung CM. J. Mater. Sci. 2003;38 (11): 2357-2365

154. Schindler A, Harper D. J. Polym. Sci. 1979;17: 2593-2599

155. Yasuniwa M, Tsubakihara H, Sugimoto Y, Nakafuku C. J. Polym. Sci. Part B: Polym. Phys. 2004;42:25-32

156. Cicero JA, Dorgan JR. J. Polym. Environ. 2001;9:1-10

157. Ultracki LA. ‘Commercial Polymer Blends’ Chapman & Hall, London, UK 1998

158. Norris ID, Shaker MM, Ko FK, et al. Synth. Met. 2000;114 (2): 109-114

159. Duan B, Dong CH, Yuan XY, et al. J. Biomater. Sci. - Polym. Ed. 2004;15 (6): 797-811

160. Spasova M, Manolova N, Paneva D, et al. E-Polymers 2004;Art. No. 056

161. Bhattarai N, Edmondson D, Veiseh O, et al. Biomaterials 2005;26 (31): 6176-6184

162. Babel A, Li D, Xia YN, et al. Macromolecules 2005 ;38 (11): 4705-4711

163. Cha DI, Kim KW, Chu GH, et al. Macromol. Res. 2006;14 (3): 331-337

164. Jun CL. J. Polym. Environ. 2000;8: 33–37

165. Kulinski Z, Piorkowska E, Gadzinowska K, et al. Biomacromol. 2006;7 (7): 2128-2135

166. Sheth M, Kumar RA, Dave V, et al. J. Appl. Polym. Sci. 1997;66 (8): 1495-1505

167. Tanoue S, Hasook A, Iemoto Y, et al. Polym. Compos. 2006 ;27 (3): 256-263

168. Lai WC, Liau WB, Lin TT. Polymer 2004 ;45 (9): 3073-3080

169. Nijenhuis AJ, Colstee E, Grijpma DW, et al. Polymer 1996 ;37 (26): 5849-5857

170. Hu Y, Hu YS, Topolkaraev V, et al. Polymer 2003 ;44 (19): 5681-5689

171. Park JW, Im SS. J. Polym. Sci. Part B: Polym. Phys. 2002 ;40 (17): 1931-1939

172. Dzenis Y Science 2004; 304:1917-1919

173. Sukigara S, Gandhi M, Ayutsede J, et al. Polymer 2003;44:5721-5727

174. Ma ML, Hill RM, Lowery JL, et al. Langmuir 2005;21:5549-5554

175. Ma ML, Mao Y, Gupta M, et al. Macromolecules 2005;38:9742-9748

176. Singh A, Steely L, Allcock HR. Langmuir 2005;21:11604-11607

177. Acatay K; Simsek E, Yang CO, Menceloglu YZ. Angew. Chem. Int. Ed. 2004;43: 5210-5213

178. Wenzel RN. Surface roughness and contact angle. Industrial Engineering Chemistry 1936;28: 988-994

179. Cassie ABD, Baxter S Wettability of porous surfaces. Transactions of Faraday Society 1944;40: 546-551

180. Erbil HY, Demirel AL, Avc Y, Mert O Science 2003;28:1377-1380

181. Karger-Kocsis J, Mouzakis DE, Ehrenstein GW, Varga J. J. Appl. Polym. Sci. 1999;73:1205-1214

182. Zhu X, Yan D, Tan S, et al. J. Appl. Polym. Sci. 2000 ;77:168-170

183. Torre J, Cortazar M, Gomez M et al. J Polym Sci Part B : Polym Phys 2004 ;42:1949-1959

184. Turner Jones A et al. Macromol. Chem. 1964;75:134